

Structural analysis of sandwich beams composed of reinforced concrete faces and a foamed concrete core

Citation for published version (APA):

Salet, T. A. M. (1990). *Structural analysis of sandwich beams composed of reinforced concrete faces and a foamed concrete core*. [Phd Thesis 1 (Research TU/e / Graduation TU/e), Built Environment]. Technische Universiteit Eindhoven. <https://doi.org/10.6100/IR335204>

DOI:

[10.6100/IR335204](https://doi.org/10.6100/IR335204)

Document status and date:

Published: 01/01/1990

Document Version:

Publisher's PDF, also known as Version of Record (includes final page, issue and volume numbers)

Please check the document version of this publication:

- A submitted manuscript is the version of the article upon submission and before peer-review. There can be important differences between the submitted version and the official published version of record. People interested in the research are advised to contact the author for the final version of the publication, or visit the DOI to the publisher's website.
- The final author version and the galley proof are versions of the publication after peer review.
- The final published version features the final layout of the paper including the volume, issue and page numbers.

[Link to publication](#)

General rights

Copyright and moral rights for the publications made accessible in the public portal are retained by the authors and/or other copyright owners and it is a condition of accessing publications that users recognise and abide by the legal requirements associated with these rights.

- Users may download and print one copy of any publication from the public portal for the purpose of private study or research.
- You may not further distribute the material or use it for any profit-making activity or commercial gain
- You may freely distribute the URL identifying the publication in the public portal.

If the publication is distributed under the terms of Article 25fa of the Dutch Copyright Act, indicated by the "Taverne" license above, please follow below link for the End User Agreement:

www.tue.nl/taverne

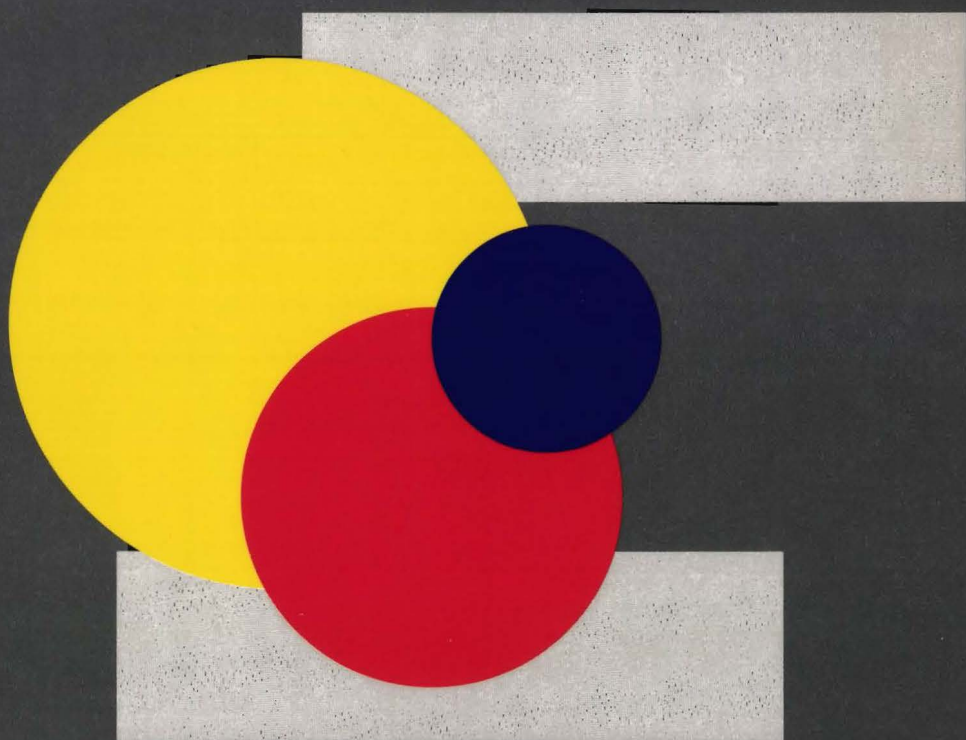
Take down policy

If you believe that this document breaches copyright please contact us at:

openaccess@tue.nl

providing details and we will investigate your claim.

**STRUCTURAL ANALYSIS OF SANDWICH BEAMS
COMPOSED OF REINFORCED CONCRETE FACES
AND A FOAMED CONCRETE CORE.**



THEO A.M. SALET

**STRUCTURAL ANALYSIS OF SANDWICH BEAMS
COMPOSED OF REINFORCED CONCRETE FACES
AND A FOAMED CONCRETE CORE**

CIP-DATA KONINKLIJKE BIBLIOTHEEK, DEN HAAG

Salet, Theodorus Arnoldus Maria

Structural analysis of sandwich beams composed of reinforced concrete faces and a foamed concrete core /

Theodorus Arnoldus Maria Salet. - [S.l. : s.n.]. - Ill.

Thesis Eindhoven. - With summary in Dutch.

ISBN 90-9003527-3

SISO 694.5 UDC 624.07.012(043.3)

Subject heading: sandwich beam/foamed concrete

Copyright © T.A.M. Salet, 1990

Printed by: Vereniging Nederlandse Cementindustrie (VNC)

**STRUCTURAL ANALYSIS OF SANDWICH BEAMS
COMPOSED OF REINFORCED CONCRETE FACES
AND A FOAMED CONCRETE CORE**

PROEFSCHRIFT

ter verkrijging van de graad van doctor aan de
Technische Universiteit Eindhoven, op gezag van
de Rector Magnificus, prof.ir. M. Tels, voor
een commissie aangewezen door het College van
Dekanen in het openbaar te verdedigen op
vrijdag 31 augustus 1990 te 14.00 uur

door

THEODORUS ARNOLDUS MARIA SALET

geboren te Nijmegen

Dit proefschrift is goedgekeurd door de promotoren

prof. dr. ir. G. Scherpbier

en

prof. dr. -ing. H.W. Reinhardt

copromotor

ir. W.J.J. Huisman

Acknowledgement

Bij het verschijnen van dit proefschrift wil ik al diegenen bedanken die hebben bijgedragen aan de uitvoering en de afronding van dit werk en voor de vriendschap en steun die ik in de loop der jaren heb ondervonden. Enkele personen wil ik met naam noemen vanwege hun bijzondere inzet.

De (voormalige) doctoraal studenten Simon Hamerlink en Eric Vianen. De technische staf van het Pieter van Musschenbroek laboratorium in de personen van Sip Overdijk, Jeff Neggens, Johan van den Oever, Dick Toussaint en Huub Donders.

Het secretariaat BKO met in het bijzonder Muriel Alblas. Henk Soen, afdeling technologische adviezen van Mebin

Dank ook aan Mebin en VNC voor de verzorging van de uitgave van dit proefschrift.

CONTENTS

Notations

| | |
|--|----|
| 1. Introduction | |
| 1.1. Subject | 1 |
| 1.2. Aim of the study | 3 |
| 1.3. Research strategy | 3 |
| 2. Finite difference analysis of sandwich beams | |
| 2.1. Introduction | 5 |
| 2.2. Basic differential equations for deflection and shear | |
| 2.2.1. General | 6 |
| 2.2.2. Basic assumptions | 7 |
| 2.2.3. Displacement-strain relations | 7 |
| 2.2.4. Stress-strain relations | 9 |
| 2.2.5. Equations of equilibrium | 9 |
| 2.2.6. The coupled differential equations | 10 |
| 2.2.7. The uncoupled differential equations | 11 |
| 2.3. Finite difference solution procedure | |
| 2.3.1. General | 12 |
| 2.3.2. Deflection | 12 |
| 2.3.3. Strains | 15 |
| 2.3.4. Stresses | 17 |
| 2.4. Flow-chart | 17 |
| 2.5. Numerical examples | |
| 2.5.1. Comparison between the extended differential equations, the common theory of bending and the common sandwich theory | 18 |
| 2.5.2. Convergence of the numerical solution procedure | 20 |
| 2.6. Conclusions | 23 |
| 3. Inhomogeneity and physical nonlinearity | |
| 3.1. Introduction | 25 |
| 3.2. Inhomogeneity and material nonlinearity | |
| 3.2.1. Inhomogeneity | 25 |
| 3.2.2. Material nonlinearity | 25 |
| 3.2.3. General flow-chart of the numerical calculation of the short-term behaviour | 29 |

| | |
|---|----|
| 3.3. Structural nonlinearity due to cracking of the reinforced concrete face loaded in tension | |
| 3.3.1. General | 30 |
| 3.3.2. Smearred-out crack analysis | 30 |
| 3.3.3. Discrete crack analysis | 32 |
| 3.3.4. Flow-chart of the discrete crack analysis | 40 |
| 3.4. Numerical examples | |
| 3.4.1. The stiffness of a reinforced concrete bar subjected to a constant tensile load | 41 |
| 3.4.2. The stiffness of a reinforced concrete bar subjected to a sinusoidally distributed tensile load | 42 |
| 3.5. Conclusions | 45 |
| | |
| 4. Nonlinearity due to creep and shrinkage | |
| 4.1. Introduction | 47 |
| 4.2. Principle of the relaxation model (RM) | 49 |
| 4.3. Elaboration of the relaxation model for sandwich beams | 54 |
| 4.4. Numerical examples | |
| 4.4.1. Reinforced concrete bar loaded in permanent compression | 57 |
| 4.4.2. The influence of the shear stiffness of the core on the effects of time-dependent strains induced by the faces | 59 |
| 4.4.3. Creep of the core under sustained shear load | 61 |
| 4.5. Flow-chart | 65 |
| 4.6. Discussion and conclusions | 66 |
| | |
| 5. Failure criteria | |
| 5.1. Introduction | 67 |
| 5.2. Ultimate bending moment | 67 |
| 5.3. Ultimate shear load | 68 |
| 5.4. Horizontal slip of the reinforced concrete face loaded in tension | 68 |
| 5.5. Discussion and conclusions | 72 |

| | |
|---|-----|
| 6. Experimental research into the structural properties of the foamed concrete core, concrete facing and reinforcement | |
| 6.1. Introduction | 73 |
| 6.2. Foamed concrete | |
| 6.2.1. Mix proportion and manufacture | 74 |
| 6.2.2. Compression tests | 75 |
| 6.2.3. Torsion tests | 76 |
| 6.2.4. Tensile tests | 80 |
| 6.2.5. Failure criterion for shear and normal load | 81 |
| 6.2.6. Creep and shrinkage tests | 82 |
| 6.3. Concrete | |
| 6.3.1. Mix proportions | 87 |
| 6.3.2. Compression tests and tension tests | 87 |
| 6.3.3. Creep and shrinkage tests | 89 |
| 6.4. Reinforcement | 90 |
| 6.5. Summary of the test results | 91 |
| 6.6. Discussion and conclusions | 93 |
| 7. Experimental research and verification of the numerical model | |
| 7.1. Introduction | 95 |
| 7.2. Characteristics and manufacture of specimen | 97 |
| 7.3. Short-term tests | |
| 7.3.1. Test performance | 99 |
| 7.3.2. Test results and discussion | 100 |
| 7.4. Long-term tests | |
| 7.4.1. Test performance | 112 |
| 7.4.2. Test results | 113 |
| 7.5. Discussion and conclusions | 117 |
| 8. Structural parameters | |
| 8.1. Introduction | 121 |
| 8.2. Numerical results | 125 |
| 8.3. Conclusions | 129 |
| 9. Summary and conclusions | 131 |

APPENDICES

| | | |
|------|--|-----|
| A2-1 | Elaboration of the equations [2.13a] and [2.13b] | 137 |
| A2-2 | Elaboration of the equations [2.15a] and [2.15b] | 139 |
| A3-1 | Numerical modelling of the shear connectors | 140 |
| A4-1 | Application of the relaxation method to creep of the core under sustained shear load | 141 |
| A6-1 | Elaboration of the torsion test | 142 |
| A7-1 | Four point bending tests on small concrete sandwich beams composed of concrete facing and a foamed concrete core | 143 |
| A7-2 | Details of the crack patterns | 148 |

References

Samenvatting

Curriculum Vitae

NOTATIONS

Upper case letters

| | |
|------------------|--|
| E | Young's modulus |
| G | shear modulus |
| L | span of the beam or length of the bar |
| I | second moment of area |
| T | total cross-sectional shear force |
| M | total cross-sectional bending moment |
| M_t | torsional moment |
| M_s | Steiner part of the bending moment |
| N | total cross-sectional normal load |
| A | cross-sectional area |
| B | bending stiffness |
| B_s | bending stiffness corresponding to the Steiner part of the bending moment |
| K | shear stiffness |
| $N(x)$ | tensile load distribution |
| N | tensile force |
| ΔL | elongation of the reinforced bar |
| $\Delta\Delta N$ | increment of the tensile load along a small part Δx of the transfer length |
| ΔN | increment of the tensile load after the initiation of a crack |
| L_t | transfer length |

Lower case letters

| | |
|----|---|
| w | deflection of the beam |
| u | deformation in the direction of the length of the beam |
| h | layer thickness |
| zp | distance between the centre-line and the reference-line |
| z | distance from a centre-line of a layer to a location within the same layer |
| n | number of pivotal points along the length of the beam |
| m | number of fibres in each layer |
| j | index of a segment |
| i | index of a fibre |
| a | distance between the reference-line of the beam and the centre-lines of a layer |
| t | time |

| | |
|---|------------|
| r | radius |
| b | beam width |
| h | height |

Greek letters

| | |
|-------------------------|---|
| ϵ | normal and/or bending strain |
| γ | shear strain |
| σ | normal and/or bending stress |
| τ | shear stress |
| $\Delta\tau$ | bond stress increment in the transfer zone |
| Δx | length of a small part of the transfer zone |
| α | distribution factor |
| $\Delta\Delta u$ and | increase of the relative displacement between the reinforcement and concrete |
| $\Delta\Delta u_r$ | increase of the elongation of the reinforced bar caused by the initiation of a crack |
| $\Delta\Delta u_{co}$ | decrease of the elongation of concrete caused by the initiation of a crack |
| Δu | relative displacement between the reinforcement and concrete |
| ω | percentage of reinforcement |
| ϕ | creep factor |
| $d\phi/dx$ | rotation |

Subscripts

| | |
|------------|---|
| l,2,c | lower face, upper face and core respectively |
| ref | reference line |
| ex,in | external and internal, respectively |
| co,r,fc | concrete, reinforcement and foamed concrete, respectively |
| bc,ac | before cracking and after cracking, respectively |
| sec | secant |
| j,i | index of the segment and fibre respectively |
| I | layer |
| ϵ | normal and/or bending strain |
| γ | shear strain |

Superscripts

| | |
|----|-----------------|
| cr | creep |
| sh | shrinkage |
| d | dummy restraint |

1. INTRODUCTION

1.1 Subject

A structural sandwich is a particular type of composed structure. The cross-section consists of two strong and stiff sheets (faces) connected by a relatively weak core of low density. At the expense of higher manufacture costs, compared with homogeneous structures, this arrangement combines a high stiffness to weight ratio with good thermal insulation. In the structural sense, the bending moment is carried by the stiff faces and the shear load by the core. The shear deformation of sandwich elements must emphatically be taken into account, since the transverse shear rigidity is provided by the relatively weak core. Bernoulli's law, of plane cross-sections is, therefore, no longer valid. The shear deformation of the weak core influences both the deflection and the stress distribution.

The favourable stiffness to weight ratio has promoted the use of sandwich structures in airplanes. Although lagged behind the aircraft industry, sandwich elements are now generally accepted in building structures (Shendy-El-Barbary, 1981). The continually increasing costs of energy turned the balance. For instance, sandwich beams composed of thin profiled steel facing and a polyurethane core are manufactured industrially with economic benefits (Jungbluth, 1986 and Delsing, 1988). Almost all structural sandwich elements are provided with a foamed plastic core, in view of proper thermal insulation. On the other hand, the application of foamed plastic cores is mainly restricted to wall and roof panels, due to the poor fire resistance and the poor long-term behaviour caused by creep of the core under permanent load.

In this study, the advantages of sandwich elements are to be combined with the typical advantages of concrete by the developing of a fully cement-based sandwich. Particularly in concrete structures both the stiffness to weight ratio and the thermal insulation can be improved considerably. Besides, the loss of weight has an additional advantage of the size of columns and will make it possible to realize higher buildings on the same foundation.

Little attention has been paid in research projects to the use of concrete sandwich elements.

The reason for this may be attributed to the difficulties of producing a lightweight concrete, both technologically and economically, which can satisfy the desired conditions of the core (Shendy-El-Barbary, 1981). Research on lightweight concrete was focussed on lowering the density with maintenance of the structural properties, by applying lightweight aggregates (a.o. Weigler et al. 1981, Karl 1979 and Jaegermann et al. 1976). However, in order to achieve thermal insulation comparable to foamed plastics, the density must be lowered to less than 800 kg/m^3 . Only a few research projects were performed, using very lightweight aggregates like expanded perlite (Zerjeski, 1981), expanded polystyrene (Shendy-El-Barbary) or a foaming agent (see chapter 7). The application of these products were restricted because of at least one of the following reasons:

- (I) Non-uniform properties through the depth caused by the poor distribution of the lightweight aggregate or foam.
- (II) Large statistical variance among different casts.
- (III) Lack of industrial availability.

In recent years, these problems were solved, thanks to substantial progress in the manufacture of foamed concrete. Foamed concrete is a cement based lightweight concrete which contrary to aerated autoclaved concrete, hardens under normal conditions. It consists of cement, water, fine sand and a foaming agent. The density can be decreased to about 400 kg/m^3 , depending on the amount of foaming agent. The recent applications of foamed concrete are based on a combination of good workability, low density, thermal insulation and durability. Besides foamed concrete can be cast in situ.

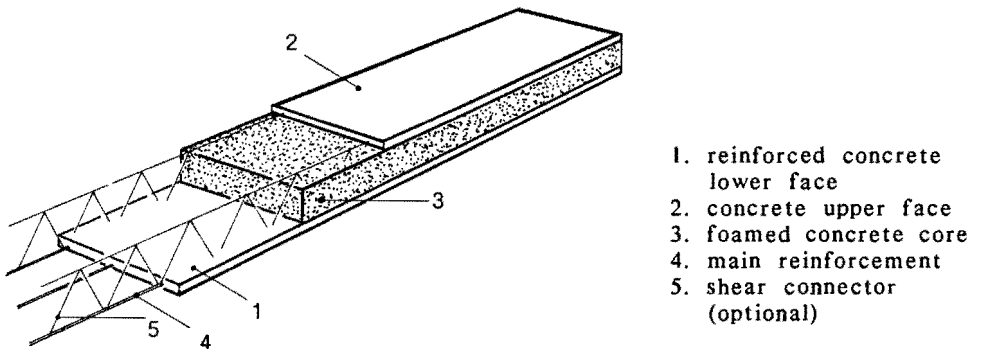


Fig. 1.1 Reinforced concrete sandwich beam with a foamed concrete core.

This study will contribute to the research into the application of sandwich elements in building structures, particularly composed of a foamed concrete core and reinforced concrete faces. Shear connectors between upper and lower faces can be taken into account (see fig. 1.1). However, the general formulation of the problem is such that, with minor modifications, it can be extended to other kinds of core and face materials and geometries.

1.2 Aim of the study

The aim of this study is to analyse the structural behaviour of sandwich beams, particular composed at reinforced concrete faces and a foamed concrete core. Both short-term loading and sustained loading are taken into account. The deflections and the load-bearing capacity of simply supported sandwich beams will be studied under static and symmetric transverse types of load. Normal load and instability phenomena are left out of account.

1.3. Research strategy

The structural behaviour of the multi-layered elements composed of reinforced concrete faces and a foamed concrete core is on the one hand characterized by the shear deformation of the core (sandwich theory) and on the other hand by the typical properties of reinforced concrete and foamed concrete.

A numerical approach is adopted in order to describe its structural behaviour. Distinction is made between a global model, describing the behaviour of a general sandwich beam and three specific material related numerical models. The global model is based on the finite difference analysis in which the structural sandwich behaviour is analytically described and numerically solved.

The three specific models are concerned with

- (i) inhomogeneity and physical nonlinearity
- (ii) creep and shrinkage of concrete and foamed concrete
- (iii) failure criteria

The numerical model is verified by means of experimental research on a restrictive number of sandwich beams. Both short-term and long-term tests are performed in which foamed concrete with a density of 600 kg/m^3 is used.

A parameter study is performed with the numerical model (SANDI = SANDwich DISplacements).

A schematic view of the adopted approach is given in fig. 1.2.

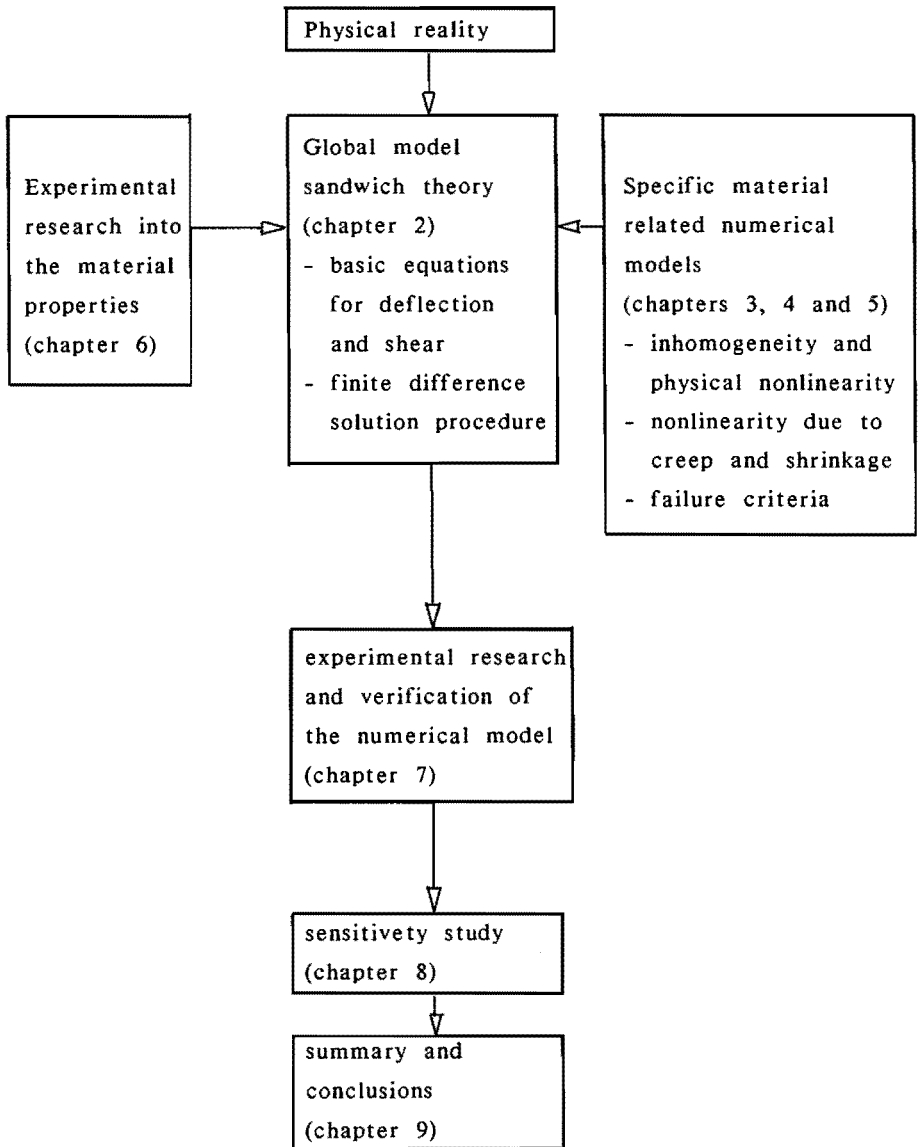


Fig. 1.2 Schematic view of the research strategy with reference to the chapters.

2. FINITE DIFFERENCE ANALYSIS

2.1 Introduction

The theoretical work in the direction of developing analytical methods for predicting the structural behaviour of sandwich beams received a great deal of attention in the past. Extensive reviews and bibliographies of these efforts have been given by the research workers mentioned in the references of this chapter. Basically two strategies have been used;

- (I) Extension of the ordinary theory of bending (a.o. Allen 1969, Hartsock 1969)
- (II) Differential equations using basic equations of elasticity or energy theorems (a.o. Stamm et al 1974, Drysdale et al 1979, Sharma et al 1982 and Wiedeman 1986)

The classical methods of analysis have led to analytical solutions of the governing equations only for a number of simple cases. However, these analytical solutions are rather cumbersome and hardly suitable for simple calculations (Davies, 1986). Although the problem has been solved for sandwich beams with linear elastic material properties by manageable approximations (a.o. Wölfel 1987, Aicher et al 1987 and Aicher 1987), it is evident that if general solutions for sandwich beams with more complicated material properties are to be obtained, recourse must be made to numerical methods of analysis such as the finite element method and the finite difference method.

The literature devoted to the finite element analysis of sandwich beams is extensive. The most direct way to model a sandwich beam for finite element analysis, is to represent the faces by beam elements and to connect these at all nodes to suitable plane stress elements to represent the material properties of the core. Although such a representation allows accurate results, even in complex situations, it is inefficient because of the large number of elements involved (Davies, 1986). Therefore, typical sandwich beam elements have been established by several authors.

An extensive literature study was performed by Sharifi (1970). More recently, stiffness matrices for sandwich beams with thick faces, were described by Kraus [1974], Monforton [1979], Davies [1986] and Al-Quarra [1989].

In order to gain insight into the overall structural behaviour of sandwich beams a finite difference method was preferred in this study.

2.2 Basic differential equations for deflection and shear

2.2.1 General

In most of the analytical studies, the bending stiffness of the (foamed plastic) sandwich core is considered to be of minor importance and therefore neglected, except by Allen (1969), Plantema (1966) and Wiedeman (1986). For cases of identical skins, Allen (1969) showed that simple modifications permit the evaluation of stresses and deflection in sandwich beams with cores which make a substantial contribution to the flexural rigidity of the beam. Likewise, considerations by Plantema (1966) are restricted to sandwich beams with thin faces. Wiedeman (1986) only considers the core stiffness perpendicular to the faces.

In order to obtain a proper description of the structural behaviour of reinforced concrete sandwich beams with foamed concrete cores it is necessary, besides the shear stiffness, also to take the bending stiffness of the core into account for three reasons:

- (i) It is not known if the bending stiffness of foamed concrete can be neglected;
- (ii) Failure due to the biaxial state of stress in the core (see chapter 5, failure mode C) cannot be calculated if the core is loaded in shear only.
- (iii) The influence of creep and shrinkage of the core can only be studied with the model described in chapter 4, if both the normal and bending stiffnesses of the core are taken into account.

In this chapter generalized differential equations for sandwich beams with faces of unequal thickness will be derived.

2.2.2 Basic assumptions

The following assumptions are adopted:

1. the materials behave homogeneously and isotropically;
2. prismatic beams;
3. the deflections are small with respect to the height of the beam; the first order theory is applicable;
4. the deformation in the direction of the layer thickness is left out of account;
5. there is no inter-layer slip between the faces and the core;
6. the shear deformations of the faces are neglected; only the shear deformation of the core is taken into account;
7. warping of the core is neglected.

2.2.3 Displacement-strain relations

The deformed shape of an infinite small part of a loaded sandwich beam is given in Fig. 2.1. The following kinematic equations can be derived from Fig. 2.1.

The shear deformation of the core γ_c can be expressed by

$$\gamma_c = \Phi + w' \quad [2.1]$$

The displacements of the facing and core are given in the equations [2.2]. The first term of the equations describes the position of the centre-line of the overall beam, the second term the centre-line of each separated layer and the third term refers to the thickness of facing and core.

$$u_1 = u + \left\{ (z_{p_{ref}} - h_1) \Phi - (h_1 - z_{p_1}) w' \right\} - z_1 w' \quad [2.2a]$$

$$u_2 = u - \left\{ (h_1 + h_c - z_{ref}) \Phi + (z_{p_2} - h_1 - h_c) w' \right\} - z_2 w' \quad [2.2b]$$

$$u_c = u - (z_{p_c} - z_{ref}) \Phi + (z_c) \Phi \quad [2.2c]$$

The normal strains in the deformed structure are by definition the first derivative of the displacements u .

$$\epsilon_1 = u' + (a_1) \Phi' + (z_{p_1} - h_1) (\Phi' + w'') - z_1 w'' \quad [2.3a]$$

$$\epsilon_2 = u' - (a_2) \Phi' - (h_1 + h_c - z_{ref} - a_2) (\Phi' + w'') - z_2 w'' \quad [2.3b]$$

$$\epsilon_c = u' - (a_c) \Phi' + (z_c) (\Phi' + w'') - z_c w'' \quad [2.3c]$$

With: $a_1 = z_{ref} - z_{p_1}$, $a_2 = z_{p_2} - z_{ref}$, $a_c = z_{p_c} - z_{ref}$

The typical order of the terms in the equations [2.3] is chosen in order to facilitate comparison with the equations described by Stamm et al. (1974).

2.2.4 Stress-strain relations

Linear stress-strain relations are adopted.

$$\sigma_\ell = E_\ell \epsilon_\ell \quad (\ell=1,2 \text{ or } c) \quad [2.4]$$

$$\tau_c = G_c \gamma_c \quad [2.5]$$

2.2.5 Equations of equilibrium

The differential equations of equilibrium of a small part of the sandwich beam are:

$$N = 0 \quad (\text{normal load is left out of account}) \quad [2.6a]$$

$$M' - T = 0 \quad [2.6b]$$

$$T' + q = 0 \quad [2.6c]$$

The cross-section forces are defined by

$$N = \int_A \sigma \, dA = \sum_{\ell=1,2,c} \int_{A_\ell} \sigma_\ell \, dA \quad [2.7]$$

$$M = \int_A \sigma z \, dA = \sum_{\ell=1,2,c} \int_{A_\ell} \sigma_\ell z \, dA \quad [2.8]$$

$$T = \int_A \tau \, dA = \sum_{\ell=1,2,c} \int_{A_\ell} \tau_\ell \, dA = M'_1 + M'_2 + b(a_1 + a_2) \tau_c \quad [2.9]$$

Note that since warping of the core is neglected, there is no contribution M'_c of the core.

2.2.6 The coupled differential equations

The kinematic equations [2.3a, 2.3b, 2.3c] are substituted in the stress-strain relations [2.4] and [2.5] respectively. Substitution of the results in the equations of equilibrium of N [2.7] and M [2.8] and integration gives the equations:

$$N = (E_1 A_1 a_1 + E_2 A_2 a_2 + E_c A_c a_c) u' + (E_1 A_1 a_1 - E_2 A_2 a_2 - E_c A_c a_c) \Phi' + (E_1 A_1 (z_{p_1} - h_1) - E_2 A_2 (h_1 + h_c - z_{ref} - a_2)) (\Phi' + w'') \quad [2.10]$$

$$\text{with } \int_{A_\ell} z_\ell dA = 0 \quad (\ell=1,2 \text{ or } c)$$

$$M = (E_1 A_1 a_1 - E_2 A_2 a_2 - E_c A_c a_c) u' + (E_1 a_1^2 A_1) \Phi' + E_1 A_1 a_1 (z_{p_1} - h_1) (\Phi' + w'') - (E_1 I_1) w'' + (E_2 a_2^2 A_2) \Phi' + E_2 A_2 a_2 (h_1 + h_c - z_{ref} - a_2) (\Phi' + w'') - (E_2 I_2) w'' + (E_c a_c^2 A_c) \Phi' + E_c I_c (\Phi' + w'') - (E_c I_c) w'' \quad [2.11]$$

$$\text{with } \int_{A_\ell} z_\ell^2 dA = I_\ell \quad (\ell=1,2 \text{ or } c)$$

Substitution of the stress-strain relation [2.5] together with relation [2.1] in the definition of T (equation [2.9]) with $M'_1 = -(E_1 I_1) w'''$ and $M'_2 = -(E_2 I_2) w'''$ results in:

$$T = -E_1 I_1 w''' - E_2 I_2 w''' + (G_c b (a_1 + a_2)) (\Phi + w') \quad [2.12]$$

Notice that since warping is neglected, the flexural stiffness of the core does not affect the distribution of the shear stresses. Besides, the equations of N [2.10] and M [2.11] can be simplified by taking the centre-line of the sandwich beam as the reference line $(z_{ref} = z_{p_s})$ with $(E_1 A_1 a_1 - E_2 A_2 a_2 - E_c A_c a_c) = 0$

This means that the second term of equation [2.10] and the third term of equation [2.11] can be left out of account.

Substitution of equations [2.11 and 2.12] in the equations of equilibrium [2.6b] and [2.6c], gives the following differential equations (see appendix A2-1):

$$\left(B_s + B_c\right) \left(\Phi''\right) + R \left(\Phi'' + w'''\right) - K \left(\Phi + w'\right) = 0 \quad [2.13a]$$

$$K \left(\Phi' + w''\right) - \left(B_1 + B_2\right) \left(w'''\right) + q = 0 \quad [2.14a]$$

Using equation [2.1], the equations [2.13a] and [2.14b] can be written as

$$\left(B_s + B_c\right) \left(\gamma_c'' - w'''\right) + (R) \gamma_c'' - (K) \gamma_c = 0 \quad [2.13b]$$

$$(K) \gamma_c' - \left(B_1 + B_2\right) w'''' + q = 0 \quad [2.14b]$$

with

$$K = G_c b \left(a_1 + a_2\right)$$

$$B_\ell = E_\ell I_\ell \quad (\ell=1,2 \text{ or } c)$$

$$B_s = \sum_{\ell=1,2,c} E_\ell A_\ell a_\ell^2$$

$$R = E_1 A_1 a_1 \left(z p_1 - h_1\right) + E_2 A_2 a_2 \left(h_1 + h_c - z p_s - a_2\right)$$

2.2.7 The uncoupled differential equations

Equation [2.14b], the first order derivative of equation [2.13b] and the second order derivative of equation [2.14b], yields after two times integration (see appendix A2-2)

$$-\left(\frac{B_1 + B_2}{K}\right) w'''' + \left(\frac{B_1 + B_2 + B_c + B_s}{B_s + B_c + R}\right) w'' = -\frac{M}{\left(B_s + B_c + R\right)} - \frac{q}{(K)} \quad [2.15a]$$

From equation [2.14b] and the first order derivation of the equation [2.13b] it yields after integration

$$-\left(\frac{B_1 + B_2}{K}\right) \gamma_c'' + \left(\frac{B_1 + B_2 + B_c + B_s}{B_s + B_c + R}\right) \gamma_c' = \frac{T}{K} \left(\frac{B_s + B_c}{B_s + B_c + R}\right) \quad [2.15b]$$

2.3 Finite difference solution procedure

2.3.1 General

The finite difference method is a numerical integration technique for reducing a continuum to a system with a finite number of degrees of freedom. The method, extensively described in textbooks on numerical analysis, is based on the principle that the derivatives of a function at a certain point (pivotal point) can be approximated by an algebraic expression consisting of the values of the function at a pivotal point and several nearby points (grid points). With the finite difference method, a differential equation is approximated by a set of linear equations. The method has been used in various engineering problems among which the calculation of sandwich beams and reinforced concrete analysis.

Berner [1978], Linke [1978] and Vogel [1983] used a central finite difference technique, with second order accuracy, in the analysis of sandwich beams. Not the differential equation, describing the deflection w of the beam, but instead a differential equation describing the Steiner part of the bending moment M_s (see figure 2.1), was approximated by a set of linear equations, with reference to Bergfelder [1974]. This approach is more recently described in a review on German research by Jungbluth [1986]. Blaauwendraad and de Groot [1983] solved the governing differential equation for bending (Bernouilli's law), calculating the stiffness matrix of a reinforced concrete beam. They used the advantage of the finite difference equations in which the stiffness can vary along the axis of the beam.

The finite difference method will be used solving the fourth order differential equation 2.15a defining the deformed shape of the sandwich beam.

2.3.2 Deflection

The beam is subdivided into a finite number of segments along the axis of the beam with constant spacing dx . The mesh and a schematic view of a linear elastic segment are given in Fig. 2.2.

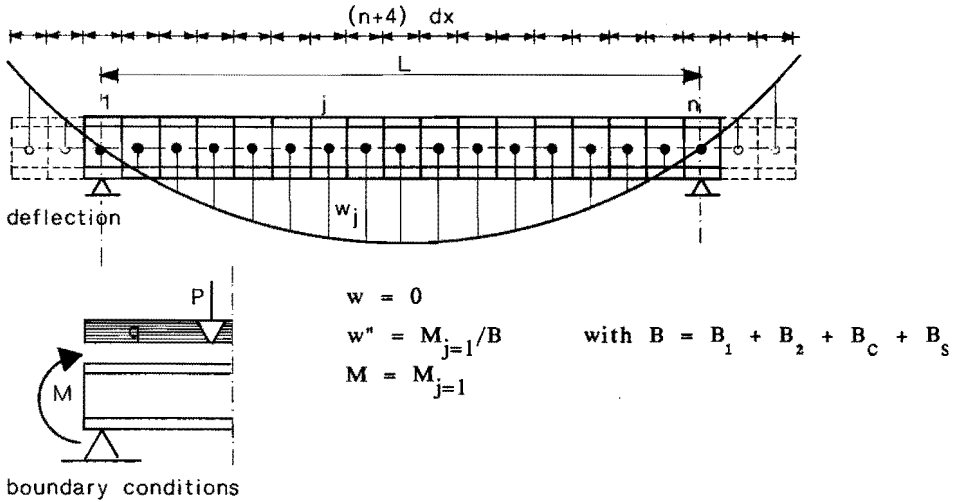


Fig. 2.2 Mesh generation and boundary conditions of a simply supported beam.

The derivatives of the deflection w in differential equation 2.15a (section 2.2.6) at a certain point j , are approximated by the central finite difference expressions with first order accuracy:

$$w' = (w_{j+1} - w_{j-1}) / (2dx) \quad [2.16a]$$

$$w'' = (w_{j+1} - 2w_j + w_{j-1}) / (dx^2) \quad [2.16b]$$

$$w''' = (w_{j+2} - 2w_{j+1} + 2w_{j-1} - w_{j-2}) / (2dx^3) \quad [2.16c]$$

$$w'''' = (w_{j+2} - 4w_{j+1} + 6w_j - 4w_{j-1} + w_{j-2}) / (dx^4) \quad [2.16d]$$

After the finite difference expressions are substituted in equation [2.15a], the corresponding equation to the pivotal point j is

$$\begin{bmatrix} a_1 & a_2 & a_3 & a_2 & a_1 \end{bmatrix} \begin{bmatrix} w_{j-2} \\ w_{j-1} \\ w_j \\ w_{j+1} \\ w_{j+2} \end{bmatrix} = b_j \quad [2.17a]$$

with

$$a_1 = \frac{-(B_1 + B_2)}{K} \quad [2.17b]$$

$$a_2 = \frac{4(B_1 + B_2)}{K} + \frac{dx^2(B_1 + B_2 + B_c + B_s)}{(B_s + B_c + R)} \quad [2.17c]$$

$$a_3 = \frac{-6(B_1 + B_2)}{K} - \frac{2dx^2(B_1 + B_2 + B_c + B_s)}{(B_s + B_c + R)} \quad [2.17d]$$

$$b_j = -dx^4 \left(\frac{M_j}{(B_s + B_c + R)} + \frac{q_j}{K} \right) \quad [2.17e]$$

Applying equation [2.17a] to the pivotal points $j = 1, 2, 3, \dots, n-1, n$ results into a set of n linear equations. Notice that each equation contains five adjacent grid points. At each of the boundary points $j=1$ and $j=n$, the applications of the central finite difference equations will involve two nonexistent values of the deflection w (see figure 2.2). Therefore, two additional equations are needed at each end to obtain a unique solution. These are supplied by the boundary conditions of the supports (see Fig. 2.2). With the boundary conditions of a simply supported sandwich beam the following set of equations is obtained.

$$\overline{A}_w \quad * \quad \overline{w} = \overline{B}_w$$

| | | |
|--|---|--|
| $\begin{bmatrix} 0 & 0 & 1 & 0 & 0 & \cdot & 0 & 0 & 0 & 0 & 0 & \cdot & 0 & 0 & 0 & 0 & 0 \\ 0 & 1 & -2 & 1 & 0 & \cdot & 0 & 0 & 0 & 0 & 0 & \cdot & 0 & 0 & 0 & 0 & 0 \\ a_{1j} & a_{2j} & a_{3j} & a_{2j} & a_{1j} & \cdot & 0 & 0 & 0 & 0 & 0 & \cdot & 0 & 0 & 0 & 0 & 0 \\ \cdot & \cdot & \cdot & \cdot & \cdot & \cdot & \cdot & \cdot & \cdot & \cdot & \cdot & \cdot & \cdot & \cdot & \cdot & \cdot & \cdot \\ \cdot & \cdot & \cdot & \cdot & \cdot & \cdot & \cdot & \cdot & \cdot & \cdot & \cdot & \cdot & \cdot & \cdot & \cdot & \cdot & \cdot \\ 0 & 0 & 0 & 0 & 0 & \cdot & a_{1j} & a_{2j} & a_{3j} & a_{2j} & a_{1j} & \cdot & 0 & 0 & 0 & 0 & 0 \\ \cdot & \cdot & \cdot & \cdot & \cdot & \cdot & \cdot & \cdot & \cdot & \cdot & \cdot & \cdot & \cdot & \cdot & \cdot & \cdot & \cdot \\ \cdot & \cdot & \cdot & \cdot & \cdot & \cdot & \cdot & \cdot & \cdot & \cdot & \cdot & \cdot & \cdot & \cdot & \cdot & \cdot & \cdot \\ 0 & 0 & 0 & 0 & 0 & \cdot & 0 & 0 & 0 & 0 & 0 & \cdot & a_{1j} & a_{2j} & a_{3j} & a_{2j} & a_{1j} \\ 0 & 0 & 0 & 0 & 0 & \cdot & 0 & 0 & 0 & 0 & 0 & \cdot & 0 & 1 & -2 & 1 & 0 \\ 0 & 0 & 0 & 0 & 0 & \cdot & 0 & 0 & 0 & 0 & 0 & \cdot & 0 & 0 & 1 & 0 & 0 \end{bmatrix}$ | $\begin{bmatrix} w_{-1} \\ w_0 \\ w_1 \\ w_2 \\ w_3 \\ \cdot \\ \cdot \\ w_{j-2} \\ w_{j-1} \\ w_j \\ w_{j+1} \\ w_{j+2} \\ \cdot \\ w_{n-2} \\ w_{n-1} \\ w_n \\ w_{n+1} \\ w_{n+2} \end{bmatrix}$ | $= \begin{bmatrix} 0 \\ M/B_{j=1} \\ b_1 \\ b_2 \\ b_3 \\ \cdot \\ \cdot \\ b_{j-2} \\ b_{j-1} \\ b_j \\ b_{j+1} \\ b_{j+2} \\ \cdot \\ b_{n-2} \\ b_{n-1} \\ b_n \\ M/B_{j=1} \\ 0 \end{bmatrix}$ |
|--|---|--|

[2.18]

The stiffness terms a_1 , a_2 and a_3 are provided with a suffix j , in view of physical nonlinearity to be described in chapter 3.

The external moment distribution along the axis of the beam ($M_{ex,j}$) is calculated from the state of equilibrium of the simply supported beam. The centre-lines, the stiffness parameters B_1 , B_2 , B_c , B_s , K and R are calculated from the material properties and the geometry of the faces and core.

Notice that if a concentrated transverse load P is applied in segment j , P has to be distributed along the length L of a segment dx by $q_{ex,j} = P_{ex,j}/dx$.

The deflections are calculated from this set of finite difference equations using Gauss with partial pivoting. [2.19]

2.3.3 Strains

Shear strain

The shear strain $\gamma_{c,j}$ of the core is calculated from the coupled differential equation [2.14b]. After integration of this equation, the shear strain is a function of the third order derivative of the deflection, $\gamma_{c,j} = f(w''')$. The equation is approximated, applying the central finite difference expressions [2.16c] by,

$$\gamma_{c,j} = \frac{(B_1 + B_2)}{K} \frac{(w_{j+1} - 2w_{j+1} + 2w_{j+1} - 20w_{j-2})}{2dx^3} + \frac{T_{ex,j}}{K} \quad [2.20]$$

Normal strain

The normal strains $\epsilon(z)$ in both facing and core are calculated from the displacement-strain relations [2.3] using equation [2.1], hence $\epsilon(z) = f(u', \gamma'_c, w'')$.

In the ordinary theory of bending (Bernouilli's law) there is no normal strain in the centre-line of the beam if only a transverse load is applied. Therefore u' equals zero. However, contrary to Bernouilli's law, the centre-line of a sandwich beam cross-section and the neutral-axis are not the same. From equations [2.10] it follows that with a nonsymmetric cross-section there is a strain unequal to zero in the centre-line of the sandwich beam although no normal load was applied:

$$u'_j = rc * (\Phi'_j + w''_j) \quad [2.21a]$$

$$\text{with } rc = \frac{(E_1 A_1 (z_{p_1} - h_1) - E_2 A_2 (h_1 + h_c - z_{p_s} - a_2))}{(E_1 A_1 + E_2 A_2 + E_c A_c)} \quad [2.21b]$$

Notice that the second term of equation [2.10] is zero with reference to the centre-line (z_{p_s}) of the beam. With symmetric cross-sections rc_j is zero. According to equation [2.21] the normal strain u' is a function of the first derivative of the shear strain and the second derivative of the deflection, $u' = f(\gamma'_c, w'')$, by which the problem is reduced, solving γ'_c and w'' .

The first order derivative of the shear deformation, γ'_c , is written as a function of the fourth order derivative of the deflection, using the coupled differential equation [2.14b].

As a result of this analysis, the normal strains in the lower face, upper face and core are approximated from the deflection curve only, $\epsilon(z) = f(w''''', w'')$;

$$\begin{aligned} \epsilon_{\ell,j}(z_\ell) = c1_\ell * \frac{(B_1 + B_2)}{K} * \frac{(w_{j+2} - 4w_{j+1} + 6w_j - 4w_{j-1} + w_{j-2})}{dx^4} \\ - \frac{q_{ex,j}}{K} + c2_\ell * \frac{(w_{j+1} - 2w_j + w_{j-1})}{dx^2} \end{aligned} \quad [2.22]$$

with $\ell=(1,2, \text{ or } c)$ and

$$\begin{aligned} c1_1 &= z_{p_s} - h_1 + rc & c2_1 &= -z_{p_s} + z_{p_1} - z_1 \\ c1_2 &= z_{p_s} - h_1 - h_c + rc & c2_2 &= -z_{p_s} + z_{p_2} - z_2 \\ \hat{c}1_c &= z_{p_s} - z_{p_c} + z_c + rc & c2_c &= -z_{p_s} + z_{p_c} - z_c \end{aligned}$$

The bending stiffnesses B_1 and B_2 and the shear stiffness K are described in section 2.2.6., while rc is defined in equation [2.21b].

The first order derivative of the shear deformation γ'_c could be approximated by using the concerning finite difference expression [2.16a]. However, the slope of the shear deformation distribution along the axis of the beam shows a strong curvature near the supports if a uniform load is applied, caused by the redistribution of shear load between the core and the faces. A proper approximation demands for many segments in this area, causing an increase of computer time.

2.3.4. Stresses

The shear stress in the core and the normal stress distribution in both facing and core are calculated from the strains using the stress-strain relation [2.4] and [2.5].

2.4. Flow-chart

The flow-chart of the finite difference analysis is given in Fig. 2.3.

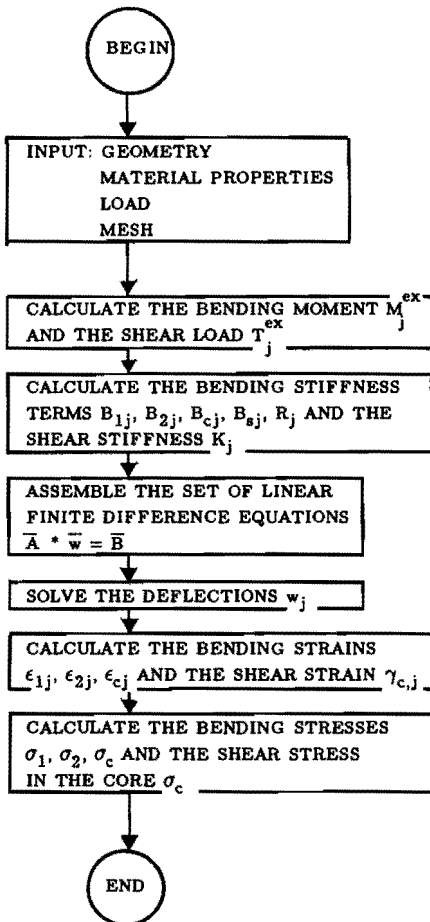


Fig. 2.3. The flow-chart of the finite difference analysis.

2.5 Numerical examples

2.5.1 Comparison between the extended differential equations, the common theory of bending and the common sandwich theory

To compare the results of the equations [2.15a] and [2.15b] presented in section 2.2.7, with the ordinary sandwich theory in which the bending stiffness of the core is left out of account (a.o. Stamm et al, 1974) and the ordinary theory of bending in which the shear deformation is neglected (Bernoulli's law), the sandwich beam having the geometry and material properties shown in Fig. 2.4 is considered. A symmetric cross-section is chosen in order to facilitate comparison with the theory described by Allen (1966). The structure is simply supported and subjected to an uniformly distributed load.

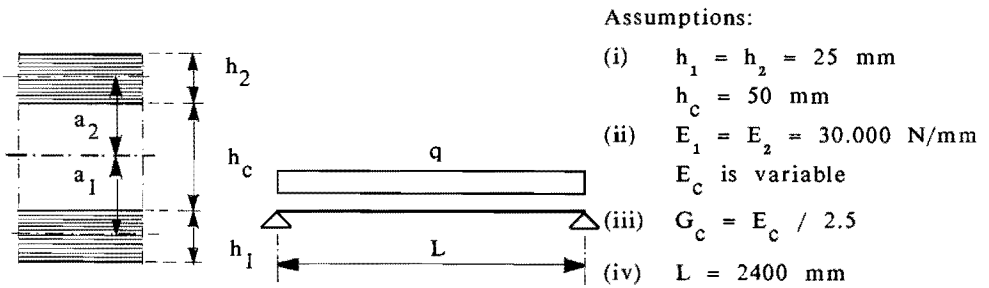


Fig. 2.4 Geometry and type of load of the sandwich beam.

Fig. 2.5. shows the deflections at midspan for various core stiffness to face stiffness ratios $E_c/E_{f=1,2}$, calculated by means of three different methods. The deflections calculated with the ordinary theory of bending (Bernoulli's law) are set up as 100%. The deflections calculated by both the ordinary sandwich theory and the sandwich theory presented in this chapter are compared with the deflections obtained from Bernoulli's law ($G = \infty$) by means of the factor k . The factor k is the ratio between the deflection calculated by one out of the two sandwich theories mentioned and the deflection calculated by the ordinary theory of bending:

$$k = \frac{w \text{ (sandwich theory)}}{w \text{ (ordinary theory of bending)}} * 100\% \quad [2.23]$$

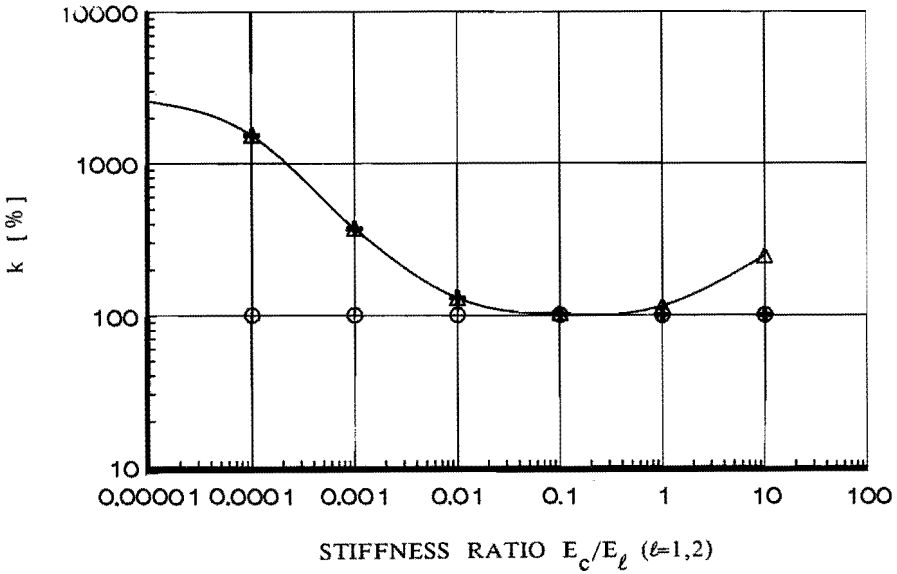


Fig. 2.5 Comparison between the deflections at midspan calculated by the following methods:

- (Δ) ordinary sandwich theory (Stamm et al, 1974)
- (○) ordinary theory of bending (Bernouilli)
- (+) the equations presented in this chapter

It is shown that in case of a weak core ($E_c/E_{l=1,2} < 0,1$) the deflections calculated by means of the ordinary sandwich theories and the extended theory are in close agreement. The deflections calculated by means of the ordinary theory of bending ($G_c = \infty$) are relatively low since the shear deformation of the core is left out of account.

In case of a relatively stiff core ($E_c/E_{l=1,2} > 0,1$), the deflections calculated by means of the equations presented in this chapter are similar to the deflections calculated by the ordinary theory of bending (Bernouilli's law) since the shear deformation is of minor importance. The deflections calculated by means of the ordinary sandwich theory are overestimated in case $E_c/E_{l=1,2} > 0,1$ since the bending stiffness of the core is neglected.

2.5.2 Convergence of the numerical solution procedure

In the following example, the convergence of the numerical solution procedure is considered with respect to the number of segments along the axis of the beam. Linear elastic properties for both faces and core are assumed. The deflection and the ultimate normal strain in the faces at midspan, and the shear stress in the core are numerically calculated and compared with well-known analytical solutions of [Allen, 1969 and Stamm et al, 1974]. The parameters involved are the bending stiffness of the faces, the stiffness of the core and the type of load. The calculations are performed on slender beams with symmetrical cross-sections. Details are given in table 2.1.

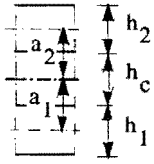
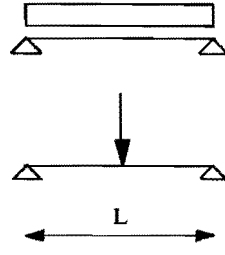
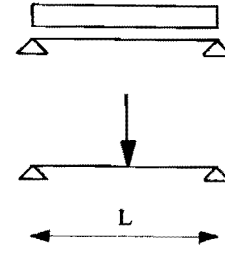
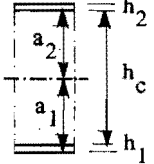
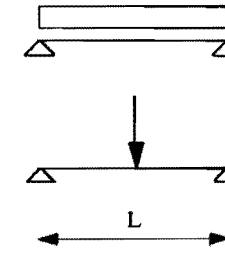
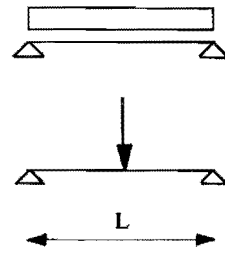
$$L = 30 (a_1 + a_2)$$

The Figs. 2.6 and 2.7 show both the convergence of the deflection and the normal strains at midspan for various types of geometry, stiffnesses of the core and types of loading. The deflections and strains calculated with well-known analytical solutions are set up as 100%.

From this example it follows that:

- (i) the numerical solution converges fast with an increasing number of segments along the length of the beam;
- (ii) the accuracy of the numerical solution already satisfies within engineering accuracy for a small number of about 10 segments;
- (iii) the deflection is overestimated while the normal strains are underestimated.

Table 2.1

| Bending stiffness of the faces | Stiffness of the core ($G_c = \frac{E_c}{2.5}$) | |
|---|---|--|
| | weak core | stiff core |
| | $\frac{E_1}{E_c} = \frac{E_2}{E_c} = 3125$ | $\frac{E_1}{E_c} = \frac{E_2}{E_c} = 1$ |
| <p>Thick faces</p>  <p>$h_1 = h_2 = h_c$</p> | <p>+</p>  | <p>△</p>  |
| <p>Thin faces</p>  <p>$h_1 = h_2 = \frac{1}{60} h_c$</p> | <p>▲</p>  | <p>▽</p>  |

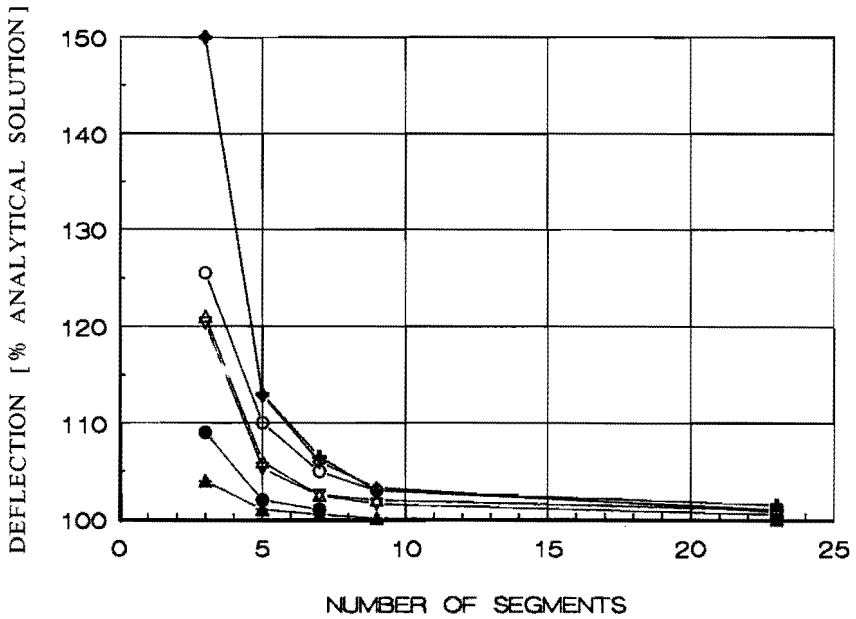


Fig. 2.6 Convergence of the deflection at midspan. The various symbols refer to the different types of geometry, material properties and type of loading given in table 2.1.

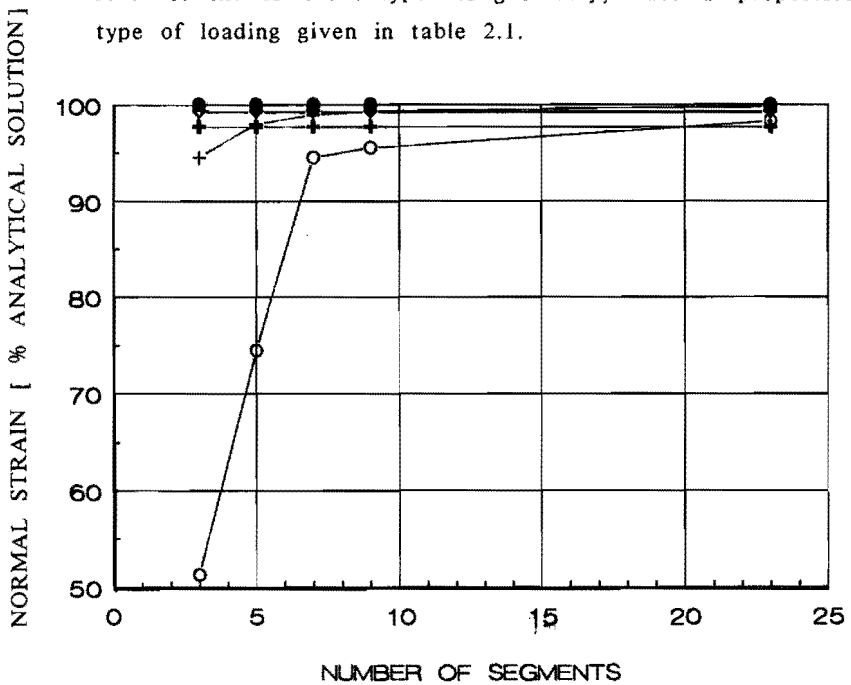


Fig. 2.7 Convergence of the ultimate normal strain at midspan. The various symbols refer to the different types of geometry, material properties and type of loading given in table 2.1.

2.6 Conclusion

The structural behaviour of sandwich beams is described by a fourth order differential equation in the deflection of the beam (w) and a second order differential equation in the shear deformation of the core (γ_c). The shear stiffness as well as the bending stiffness of the core are taken into account. It is demonstrated in an example (section 2.5.1.) that in case of various stiffnesses of the core, the theory of plain cross-sections (Bernouilli's law) fades into the ordinary theory of sandwich beams ($E_c = 0$) with the generalized equations presented in this chapter.

The governing differential equation in the deflection w is approximated by a set of linear equations by means of the finite difference method. The deflections are calculated using Gauss with partial pivoting.

The second example (section 2.5.2.) shows that the finite difference analysis presented:

- is suitable for a large range of both geometrical and physical input data, without numerical problems;
- converges fast.

3. INHOMOGENEITY AND PHYSICAL NONLINEARITY

3.1. Introduction

The deflection and the stress distribution in each cross-section for a given load depend on the flexural stiffness and shear stiffness of the sandwich beam. The stiffnesses are described in the finite difference analysis (chapter 2) based on homogeneous layers and linear elastic material properties. Since these assumptions pass by the typical properties of reinforced concrete and foamed concrete, the finite difference analysis is extended in this chapter with:

- (i) inhomogeneity due to the reinforcement of the faces;
- (ii) material nonlinearity, i.e. nonlinear stress-strain relationships, including a nonlinear τ - γ relationship;
- (iii) structural nonlinearity due to cracking of the reinforced concrete faces loaded in tension.

3.2. Inhomogeneity and material nonlinearity

3.2.1. Inhomogeneity.

The first limitation of the basic differential equations for deflection and shear is the assumed homogeneity of each single layer. However, the presence of reinforcement in the concrete facing is simply taken into account. The strain in the reinforcement is calculated from the assumption of equal strains in the reinforcement and concrete at the same distance from the centre-line. The stresses are calculated from the stress-strain relationships concerned.

3.2.2. Material nonlinearity

The second limitation of the basic differential equations is concerned with the assumed material linearity.

If linear elastic material properties are adopted, the flexural and shear stiffnesses are similar in each segment along the span of the sandwich beam. With nonlinear stress-strain relationships, the moduli of elasticity depend on the state of stress which in turn depends on the moduli of elasticity.

A solution is found by means of an iterative algorithm, based on the secant modulus of elasticity.

The numerical algorithm is initiated with assumed Young's moduli for each layer and a shear modulus for the core. In order to facilitate a computerized calculation, faces and core are subdivided into a number of fibres as shown in Fig. 3.1.

Based on assumed moduli of elasticity, the strains and stresses are calculated in the mid-points of each fibre, as described in section 2.3.3 and 2.3.4. The first assumption of the moduli of elasticity is based on the stiffness at $\sigma = 0$. The stiffnesses are overestimated and therefore the strains are underestimated, just as the stresses calculated from the actual stress-strain relationships.

The criterion set for the solution for deflections and stresses, is a sufficient degree of equilibrium between the internal stresses and the external normal load, flexural moment and shear load in each segment.

The equations of equilibrium for segment j are:

$$\sum_{\ell=1,2} \left[\sum_{i=1}^m (\sigma_{co,\ell,i,j} * A_{co,\ell,i}) + (\sigma_{r,\ell,j} * A_{r,\ell}) \right] + \sum_{i=1}^m (\sigma_{c,i,j} * A_{c,i}) = N_j^{ex} = 0 \quad [3.1a]$$

$$\sum_{\ell=1,2} \left[\sum_{i=1}^m (\sigma_{co,\ell,i,j} * A_{co,\ell,i} * z_j) + (\sigma_{r,\ell,j} * A_{r,\ell} * z_j) \right] + \sum_{i=1}^m (\sigma_{c,i,j} * A_{c,i} * z_j) = M_j^{ex} \quad [3.1b]$$

$$\sum_{\ell=1,2,c} \left[\sum_{i=1}^m (r_{\ell,i,j} * A_{\ell,i}) \right] = T_j^{ex} \quad [3.1c]$$

with m is the total number of fibres in each layer (ℓ).

If there is no satisfying degree of equilibrium, the finite difference analysis is repeated with an improved approximation of the stiffnesses calculated from the quotient between the stress and strain (secant moduli of elasticity) in each fibre,

$$E_{\text{sec},j,i} = \sigma_{j,i} / \epsilon_{j,i} \quad [3.2a]$$

$$G_{\text{sec},j} = \tau_{c,j} / \gamma_{c,j} \quad [3.2b]$$

The stiffness definitions given in section 2.2.6. are substituted by the following nonlinear and inhomogeneous stiffnesses,

$$B_{\ell,j} = \sum_{i=1}^m \left[(E_{\text{sec_co},\ell,j,i} * I_{\text{co},\ell,i}) + (E_{\text{sec_r},\ell,j} * I_{r,\ell}) \right] \quad (\ell = 1 \text{ or } 2) \quad [3.3a]$$

$$B_{c,j} = \sum_{i=1}^m (E_{\text{sec},c,j,i} * I_{c,\ell,i}) \quad [3.3b]$$

$$B_{s,j} = \sum_{\ell=1,2} \left[\sum_{i=1}^m (E_{\text{sec_co},\ell,j,i} * A_{\text{co},\ell,i} * a_{\ell,j}^2) + (E_{\text{sec_r},\ell,j} * A_{r,\ell} * a_{\ell,j}^2) \right] + \sum_{i=1}^m (E_{\text{sec},c,j,i} * A_{c,i} * a_{c,j}^2) \quad [3.3c]$$

$$R_j = \sum_{i=1}^m \left[(E_{\text{sec_co},1,j,i} * A_{\text{co},1,i} * a_{1,j}) * (z_{p_{1,j}} - h_1) + (E_{\text{sec_co},2,j,i} * A_{\text{co},2,i} * a_{2,j}) * (h_1 + h_c - z_{p_{s,j}} - a_{2,j}) \right] + (E_{\text{sec_r},1,j} * A_{r,1} * a_{1,j}) * z_{p_{1,j}} - h_1 + (E_{\text{sec_r},2,j} * A_{r,2} * a_{2,j}) * (h_1 + h_c - z_{p_{s,j}} - a_{2,j}) \quad [3.3d]$$

$$K_j = (G_{\text{sec_fc},c,j}) * b * (a_{1,j} + a_{2,j}) \quad [3.3e]$$

A schematic view of the physical nonlinear iterative algorithm is given in Fig. 3.1.

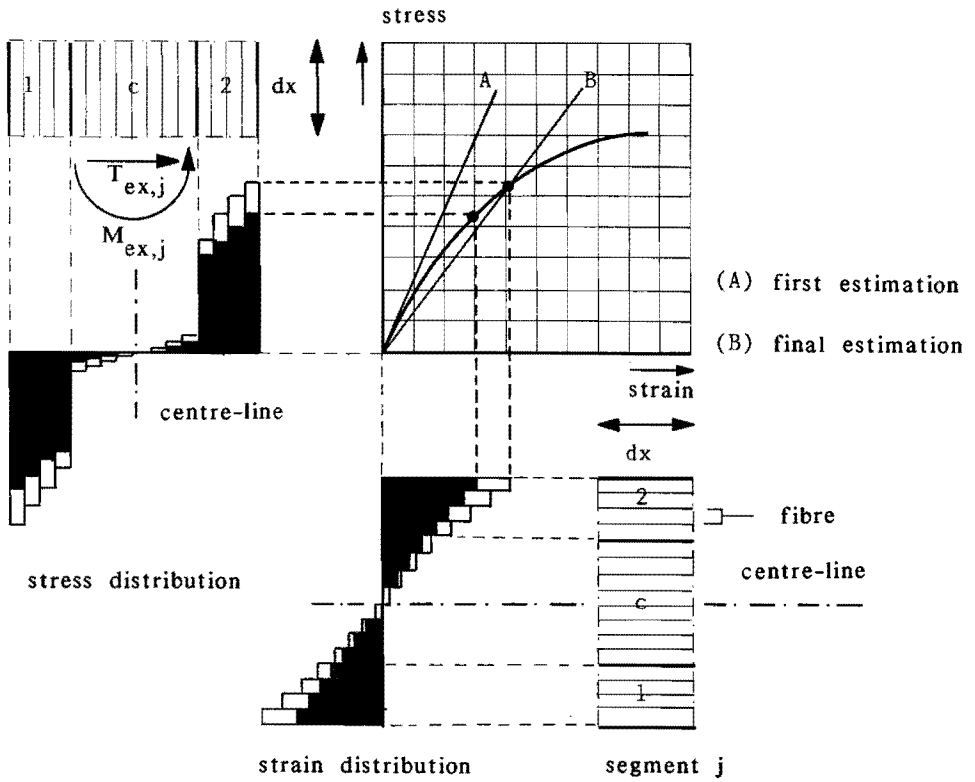
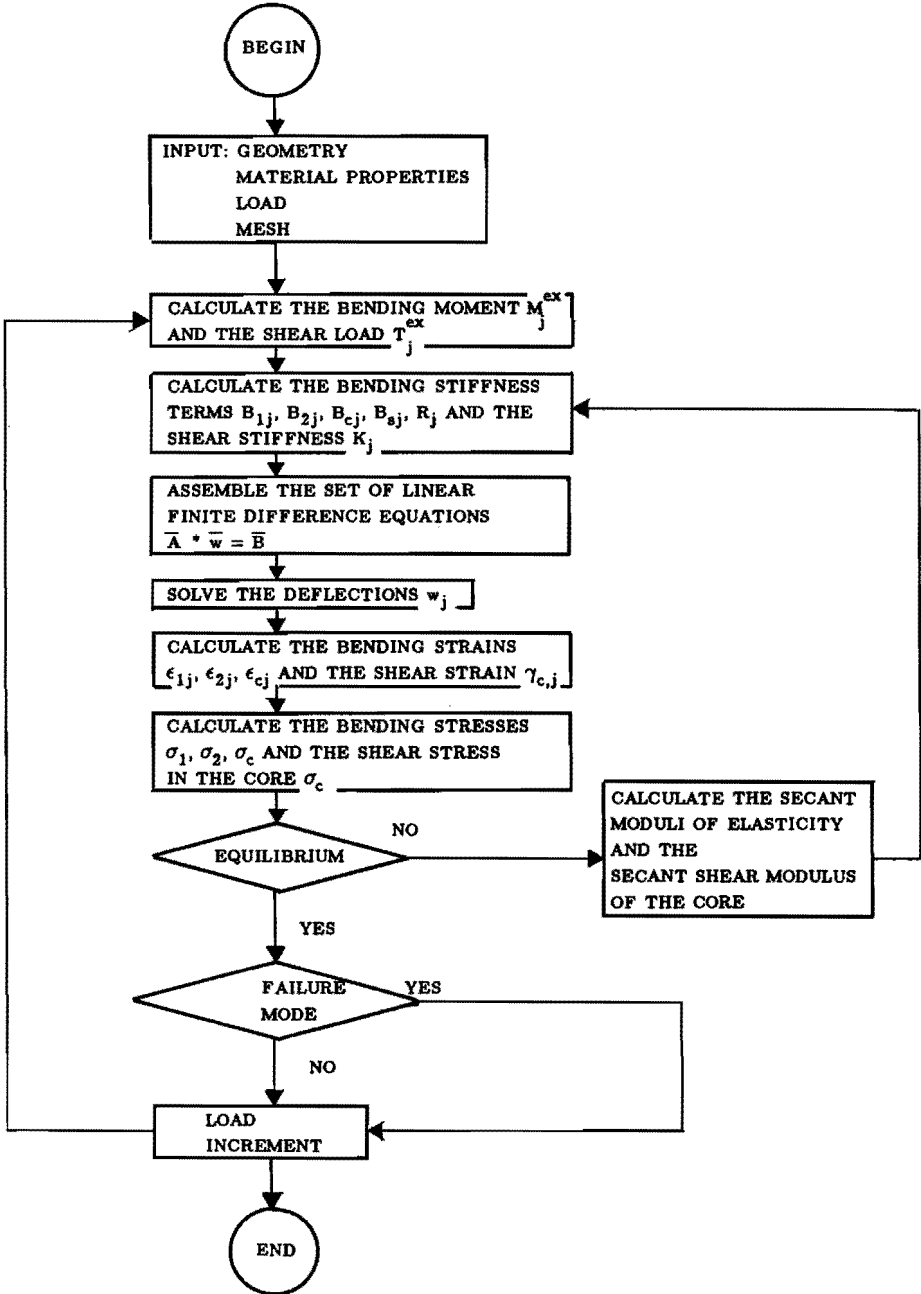


Fig. 3.1. Schematic view of the physical nonlinear iterative algorithm and the subdivision of each layer into a number of fibres.

3.2.3. General flow-chart of the numerical calculation of the short-term behaviour



The failure modes are described in chapter 5.

3.3. Structural nonlinearity due to cracking of the reinforced concrete face loaded in tension

3.3.1. General

Cracking of reinforced concrete is a local phenomenon. If reinforced concrete is loaded in tension, the total load in the cross-section of the crack is resisted by the reinforcement only.

The bar undergoes an additional elongation due to the increase of tensile strain along the transfer lengths on both sides of the crack. The transfer length is defined as that part of the reinforced beam at which the state of stress is affected by the initiation of the crack.

Since the adopted finite difference analysis of sandwich beams is not suitable to take discrete cracks into account, resource is made to an approximation by means of a smeared-out model. In the smeared-out model, the crack is smeared out along the segmentary length dx between two pivotal points, with or without taking an average contribution of the concrete between the cracks into account.

In this section the results and the accuracy of the smeared-out model are investigated in view of:

- (i) the number of segments along the length of the beam;
- (ii) the constant segmentary length dx along the length of the beam;
- (iii) the necessity to take the stiffness contribution of the concrete between the cracks into account.

3.3.2. Smeared-out crack analysis

In the smeared-out model, the reinforced concrete bar (sandwich face) is subdivided into an arbitrary number of segments with a constant segmentary size dx along the length of the bar. The principle of the smeared-out crack analysis is shown in Fig. 3.2. in case of a parabolically distributed tensile load along the length. The average stiffness contribution of the concrete in the vicinity of the cracks is left out of account.

The elongation of the bar is calculated from,

$$\Delta L_{\text{smeared-out}} = \sum_{j=1}^n \frac{N_j \cdot dx}{E_{co,j} A_{co} + E_{r,j} A_r} \quad [3.4]$$

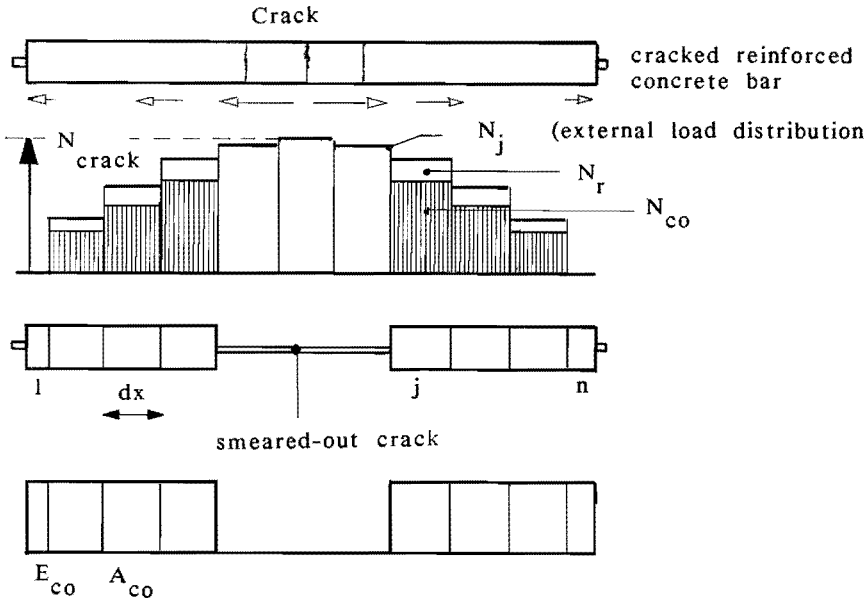


Fig. 3.2. Principle of the smeared-out crack analysis

In case a sandwich beam is loaded in pure bending, the reinforced concrete face is loaded with a constant tensile force along the length of the beam. If the stochastic variations of the tensile strength are left out of account, all cracks arise at the same tensile load. The results obtained from a smeared-out analysis are therefore not affected by either the number of segments nor the assumption of a constant segmentary size. The stiffness of the cracked face and therefore the deflection is better approximated if the tension stiffening, i.e. the stiffness contribution of the concrete between the cracks, is taken into account. The tension stiffening is commonly taken into account by means of a fictitious stress-strain relationship of concrete. This relationship is calculated from either an experimental load-elongation relationship or from a numerically calculated load-elongation relationship in which discrete cracks are taken into account. A numerical calculation is performed in the first example at section 3.4.1.

Generally, a beam is loaded with a uniformly distributed load or with a central point load. The tensile force in the reinforced face of the sandwich beam is nonuniformly distributed along the length. Roughly, the tensile force follows the moment distribution. The numerical result depends on the number of segments. Generally *, the calculated elongation oscillates around an average value dependent on the number of segments. The amplitude decreases if a larger number of segments along the length is used. Therefore, a sufficiently large number of segments (pivotal points) is recommended. It is wondered if in this case the tension stiffening is a parameter of minor importance. An example confirming this statement is given in section 3.4.2.

In order to gain insight into the numerical accuracy with respect to the assumption of a constant segmentary size and the influence of the stiffness contribution of concrete between the cracks, the results are to be compared with the results of a discrete crack model. Therefore, a generalized discrete crack model is presented in the next section. In section 3.4 the results of the smeared-out and discrete crack models are compared by means of a numerical example.

3.3.3. Discrete crack analysis

Although cracking of concrete is a complex and random phenomenon, extensive research performed by various research workers has led to a better understanding of the mechanism behind crack spacing, crack width and the stiffness of a cracked bar loaded in tension. Besides empirical equations described by Beeby [1979], Schiessl [1980], Hartl [1983], Riskalla [1984] and Schiessl [1986] theoretical approaches are available and the correctness has been proved experimentally within engineering accuracy. There is a common consensus that the bond between reinforcement and concrete has a pronounced influence on cracking induced by direct tension. As a result, the available theoretical works are based on the so-called bond theory. Two distinguished approaches are adopted.

*) In case the crack load is reached in just a single cross-section the calculated elongation constantly decreases with an increasing number of segments.

The works of Tassios [1981], Fehling [1983], Noakowski [1985], Bruggeling [1987] and Lee et al [1987] are based on a bond versus slip relationship while Somayaji et al [1979] and Shungsheng Yang et al [1988] assumed a bond stress distribution in the interface between concrete and reinforcement.

However, in all the studies the reinforced bar is subjected to a constant load. In the next sections, a generalized discrete crack model is described in which the reinforced bar is subjected to a nonuniformly distributed tensile load.

The following assumptions are adopted:

- (i) the reinforced concrete bar is loaded in tension. Bending is not considered;
- (ii) statistical variance of the material properties is left out of account;
- (iii) uniform cross-sections along the length of the bar;
- (iv) linear elastic material properties; this means that the analysis is only valid for stresses in the steel below the $\sigma_{0,2}$ and/or the yield stress.

If an uncracked reinforced concrete bar is loaded with a nonuniformly distributed tensile force, the tensile force in each cross-section is resisted by both concrete and reinforcement (see figure 3.3).

From the basic equation of equilibrium,

$$N(x) = N_{co}(x) + N_r(x) \quad [3.5]$$

and the assumption of plane cross-sections before cracking, the normal load distribution between the reinforcement and concrete is given by,

$$N_{r,bc} = \frac{N(x)}{1 + (1/n\omega)} \quad [3.6a]$$

$$N_{co,bc} = \frac{N(x)}{1 + n\omega} \quad (bc = \text{before cracking}) \quad [3.6b]$$

$$\text{with } \omega = \frac{A_r}{A_{co}} \quad \text{and} \quad n = \frac{E_r}{E_{co}}$$

The tensile load at which the ultimate concrete tensile strain capacity in a cross-section is exceeded is given by

$$N_{\text{crack}} = f_{\text{co,tm}} * A_{\text{co}}(1+n\omega) \quad [3.7]$$

Load-elongation relationship at the first crack

If, for matters of simplicity, a symmetric parabolic tensile force distribution is considered, the first crack will arise at midspan. Within the crack the total tensile load N_{crack} is resisted by the reinforcement only as shown in Fig. 3.3. The local tensile force in the reinforcement is transferred to the concrete on both sides of the crack along the transfer length (L_t) by means of the bond. The elongation increment of the reinforced bar is caused by the load increment of the reinforcement given by the area contained between the markers A, B and C (see Fig. 3.3).

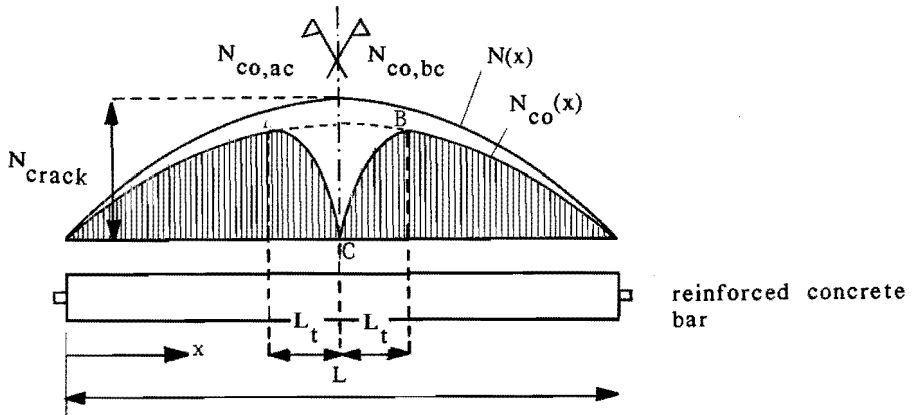


Fig. 3.3. Distribution of the tensile force between concrete and reinforcement just before and after the first crack.

The tensile force distribution along the transfer length is calculated from a bond versus slip relationship. In order to facilitate a numerical calculation, the transfer length is divided into a number (m) of segments with a sufficiently small length Δx , as shown in Fig. 3.4.

Consider a single segment from the transfer zone in detail. The normal load in the reinforcement increases from cross-section i to $i+1$ because of the shear transfer due to bond between concrete and reinforcement.

$$\Delta\Delta N_{r,ac,i+1,\tau_i} = 2\pi r * \Delta x * \Delta\tau_i \quad [3.8a]$$

$$\Delta\Delta N_{co,ac,i+1,\tau_i} = -\Delta\Delta N_{r,ac,i+1,\tau_i} \quad (ac = \text{after cracking}) \quad [3.8b]$$

and the increases of external load between the two cross-sections

$$\Delta\Delta N_{r,ac,i+1,\alpha} = \frac{\Delta\Delta N_{i+1}}{1+(\alpha/n\omega)} \quad [3.8c]$$

$$\Delta\Delta N_{co,ac,i+1,\alpha} = \Delta\Delta N_{i+1} - \Delta\Delta N_{r,ac,i+1,\alpha} \quad [3.8d]$$

$$\text{with } \alpha = \frac{\epsilon_{co,i}}{\epsilon_{r,i}} \quad [3.8e]$$

In a crack ($\alpha=0$), the increase of tensile load is taken by the reinforcement only, while at the end of the transfer length the tensile load increment is again distributed according to the equations [3.6a] and [3.6b].

The total tensile load in the reinforcement and the concrete of cross-section $i+1$ are respectively given by

$$N_{r,ac,i+1} = N_{r,bc,i=0} + \sum_1^{i+1} (\Delta\Delta N_{r,ac,i+1,\tau_i} + \Delta\Delta N_{r,ac,i+1,\alpha}) \quad [3.9a]$$

$$N_{co,ac,i+1} = N_{i+1} - N_{r,ac,i+1} \quad [3.9b]$$

The computerized algorithm begins at the end of an assumed transfer length at which the relative displacement between the reinforcement and concrete $\Delta u_{i=0} = 0$. The bond stress between $i=0$ and $i=1$ is initiated by a typical choice of the bond versus slip relationship (Rehm, [1961] and Martin [1973]),

$$\Delta\tau_i = \left[a + b\sqrt{\Delta u_i} \right] * f'_{co,cm} \quad [3.10]$$

This relationship is intentionally chosen in view of the initiation of the algorithm although physically meaningless at $i=0$ ($\Delta\tau_i = af'_{co,cm}$!). The equation given in [3.10] is the best-fitting equation of the actual bond versus slip relationship in which the slip is small up to a stress level $\Delta\tau$; the increase of tensile force between two succeeding cross-sections and the total tensile forces in both concrete and reinforcement are calculated from the equations 3.8 and 3.9, respectively.

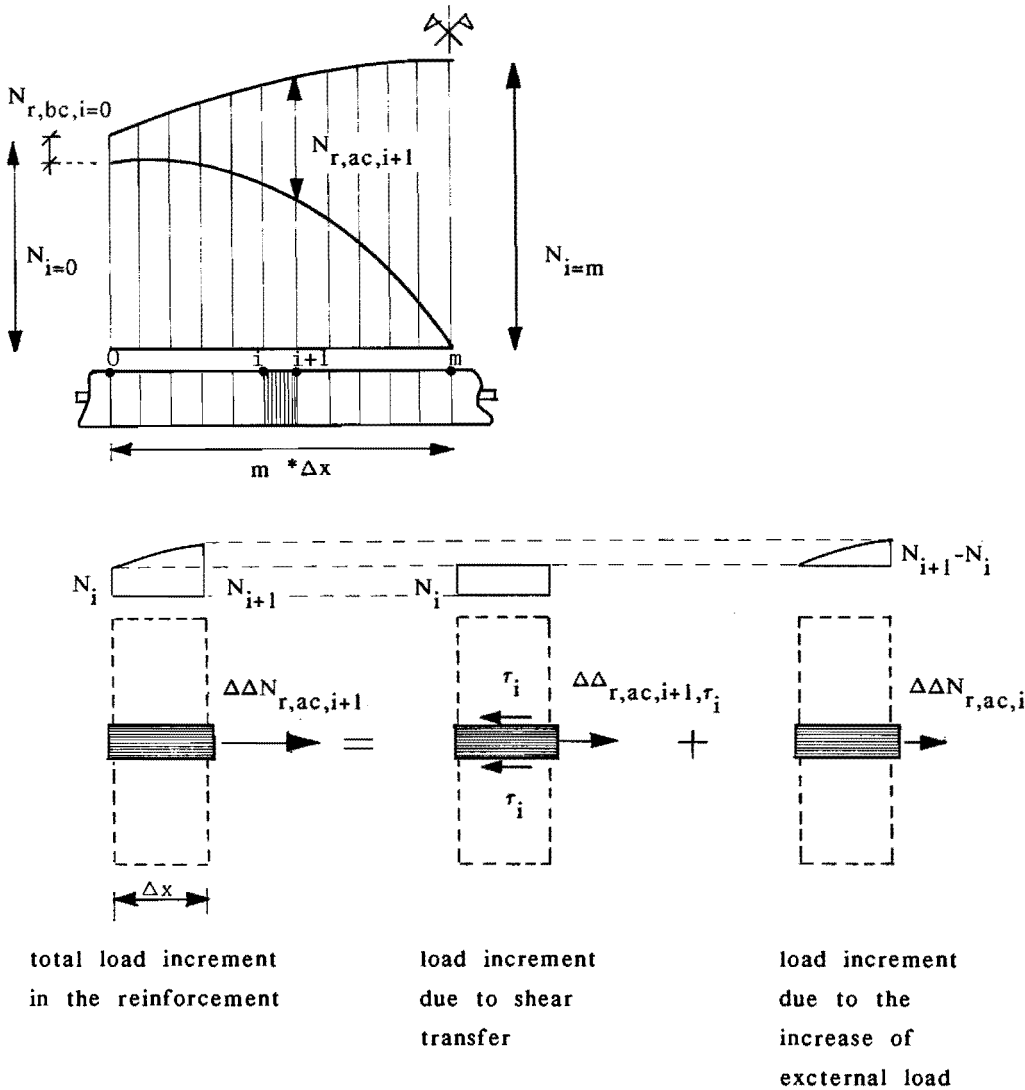


Fig. 3.4. Transfer of tensile load

At the end of a segment Δx the relative displacement increment from i to $i+1$ between reinforcement and concrete is given by,

$$\Delta \Delta u_{i+1} = \Delta \Delta u_{r, i+1} - \Delta \Delta u_{co, i+1} \quad [3.11a]$$

with

$$\Delta\Delta u_{r,i+1} = \frac{N_{r,ac,i} \cdot \Delta x}{E_r A_r} + \frac{0,5 \cdot \Delta\Delta N_{r,ac,i+1} \cdot \Delta x}{E_r A_r} \quad [3.11b]$$

$$\Delta\Delta u_{co,i+1} = \frac{N_{co,ac,i} \cdot \Delta x}{E_{co} A_{co}} + \frac{0,5 \cdot \Delta\Delta N_{co,ac,i+1} \cdot \Delta x}{E_{co} A_{co}} \quad [3.11c]$$

as shown in Fig. 3.5. The total relative displacement between concrete and reinforcement in cross-section $i+1$ is thereby

$$\Delta u_{i+1} = \Delta u_i + \Delta\Delta u_{i+1} \quad [3.11d]$$

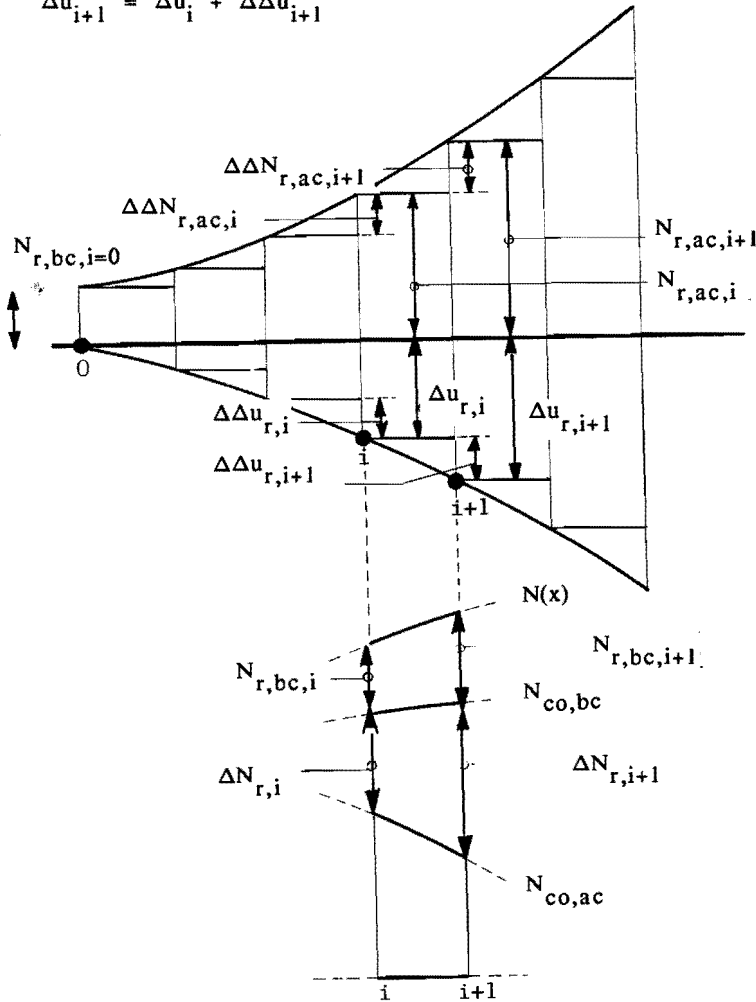


Fig. 3.5. Definitions of the load increments

The calculation is repeated until the concrete tensile load equals zero and all the tensile load is thereby transferred to the reinforcement. The transfer length is given as

$$L_t = m * \Delta x \quad [3.12]$$

However, the assumed and calculated transfer length will generally not coincide. Therefore an iterative algorithm is performed until the concrete tensile load equals zero at the position of the crack. If this condition has been met, the elongation of the bar at the given load is calculated from the normal load in the reinforcement, by

$$\Delta L_{\text{discrete}} = \int_0^L \frac{N}{E_r A_r + E_{co} A_{co}} dx + \sum_{i+1}^{2m} \left(\left(\frac{\Delta N_{r,i} * dx}{E_r A_r} \right) + \left(\frac{(\Delta N_{r,i+1} - \Delta N_{r,i}) dx}{2 * E_r A_r} \right) \right) \quad [3.13a]$$

with

$$\Delta N_{r,i} = N_{r,ac,i} - N_{r,bc,i} \quad (\text{see equation 3.6 and equation 3.9}) \quad [3.13b]$$

The first term of equation [3.13a] gives the elongation just before the crack and the second term the increment caused by the initiation of the crack.

Load-elongation relationship with forthcoming cracks

If a reinforced concrete bar is loaded with a constant direct tensile force, the distance between two succeeding cracks is somewhere between one and two times the transfer length. The crack spacing is determined by the stochastic properties of concrete only. Generally, a crack spacing of $1,5 * L_t$ is assumed. However, if the tensile load is nonuniformly distributed, the position of the cracks is also affected by the external load distribution. Forthcoming cracks are located at the end of the transfer zone L_t of the former cracks, since the ultimate concrete tensile strain is first reached at this point (see Fig. 3.3). Since the external load is not critical at the end of the transfer length of the former crack, the next crack only arises with an increase of external load $\Delta N(x)$. The transfer length of the former cracks, and thereby the location of the next crack, changes with an increase of external tensile force.

The tensile force is increased until the tensile load at the end of the transfer zone reaches the crack load N_{crack} (equation 3.7).

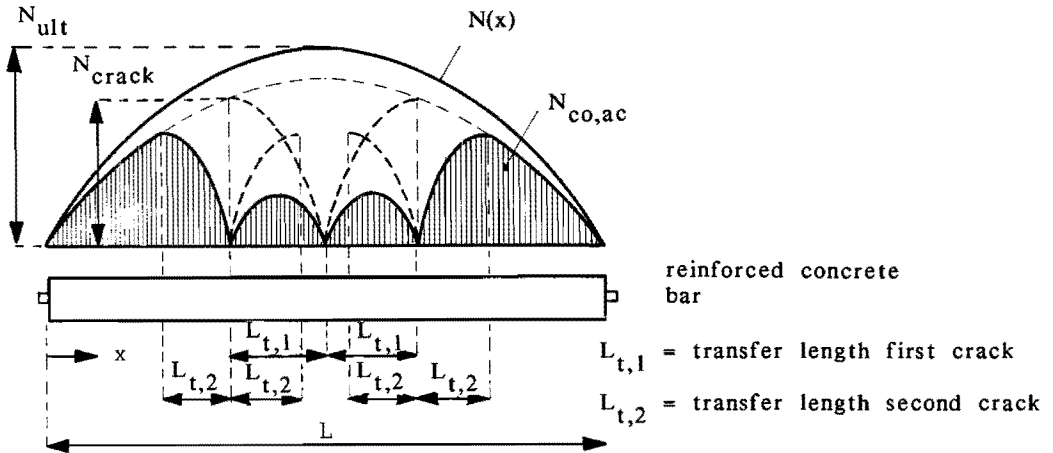
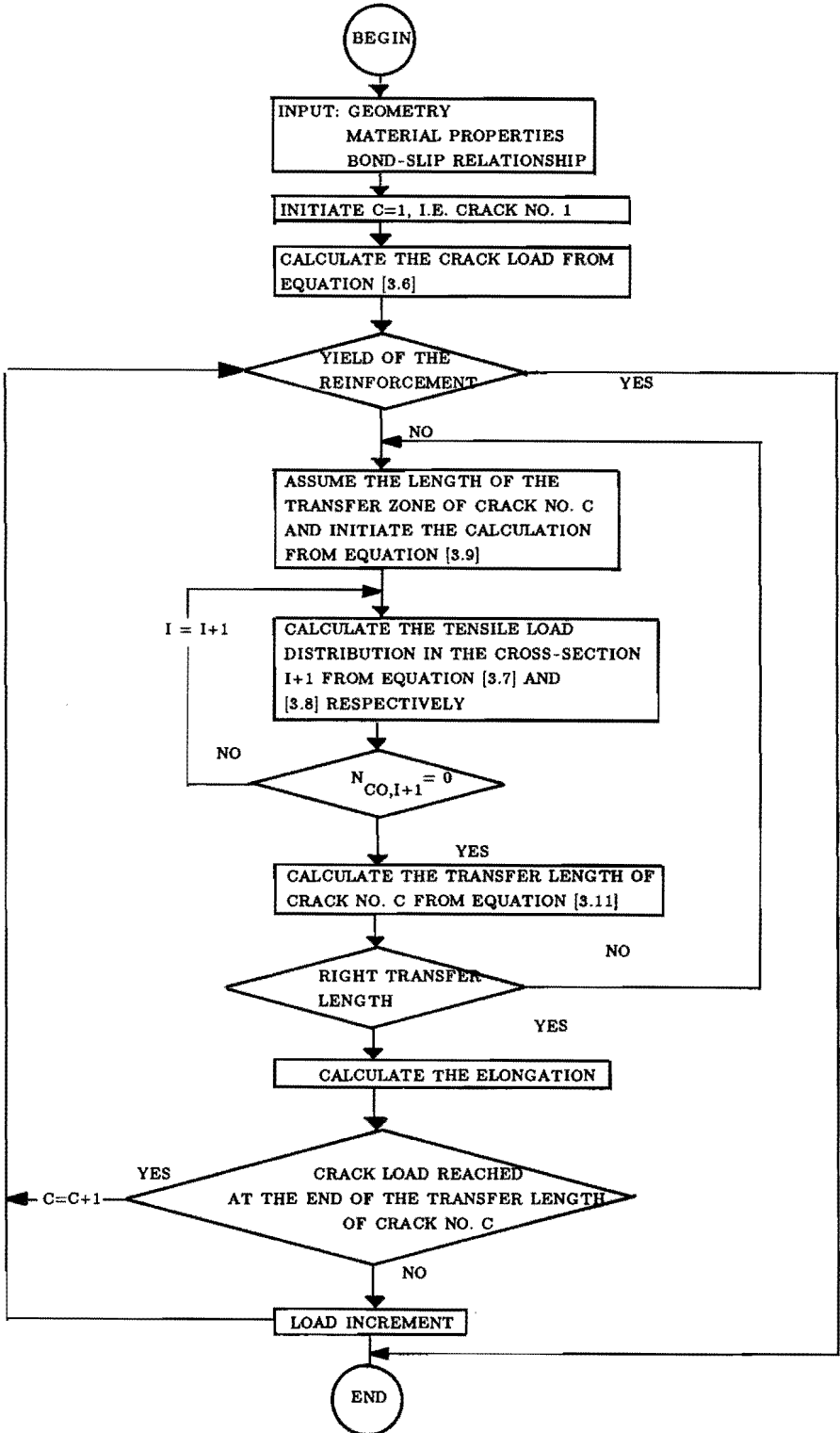


Fig. 3.6. Forthcoming cracks

The transfer of load from the concrete to the reinforcement in a transferzone, is reflected at both sides of a crack. The transfer lengths of two succeeding cracks overlap, as shown in Fig. 3.6. It is generally assumed that the transfer zones will not influence each other. The tensile load distribution and the elongation in encountered transfer zones is therefore calculated from the principle of superposition. Discrete crack analysis based on the assumption of a constant tensile load, has already shown that the tension stiffening is only of (slight) importance in the engineering practice in case a low percentage of reinforcement is adopted (large crack spacing). In case of, for instance, a parabolically distributed tensile force, the crack spacing is substantially smaller (L_t instead of $1.5 L_t$) since the position of the cracks is also affected by the tensile force distribution and therefore not only by the stochastic variance in the tensile strength of concrete. Therefore, it is likely that the stiffness of the cracked concrete may be neglected. This is illustrated in the second example of section 3.4.

The flow charts of the discrete crack analyses is given in section 3.3.4.

3.3.4. Flow chart of the discrete crack analysis

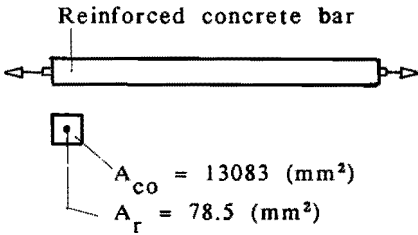


3.4. Numerical examples

3.4.1. The stiffness of a reinforced concrete bar subjected to a constant tensile load.

A reinforced concrete bar is subjected to a constant tensile load along the length. The bond versus slip relationship is taken as

$\Delta\tau = (0.07 + 0.32 \sqrt{\Delta u}) * f'_{co,cm}$ which is the best-fit mean value of commonly used equations in case of centre bars described by Schiessl [1976] and Martin [1973] (see also Noakowski [1978]), respectively.



The material properties are:

- (i) $E_{co} = 32500 \text{ (N/mm}^2\text{)}$
- (ii) $E_r = 210\ 000 \text{ (N/mm}^2\text{)}$
- (iii) $f_{co,tm} = 1.5 \text{ (N/mm}^2\text{)}$
- (iv) $f'_{co,cm} = 25 \text{ (N/mm}^2\text{)}$
- (v) $f_{r,tm} = 800 \text{ (N/mm}^2\text{)}$

Fig. 3.7 Reinforced concrete bar subjected to a constant tensile load along the length.

The load-elongation relationship is shown in Fig. 3.8.

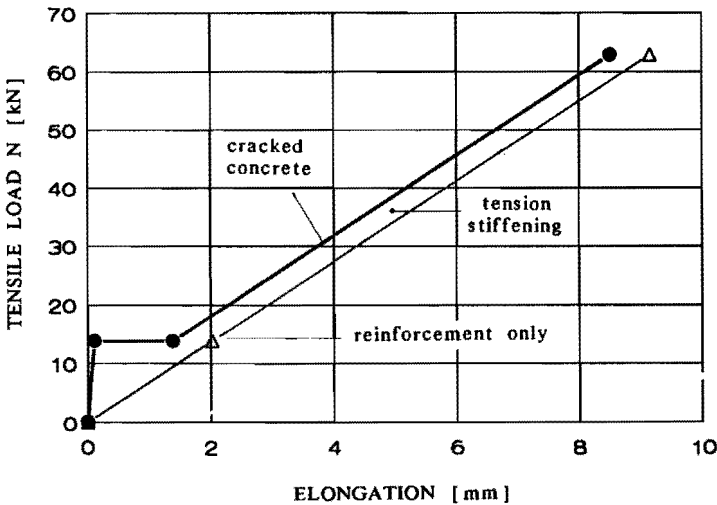


Fig. 3.8 Load elongation relationship calculated by means of a discrete crack model in case of a constant tensile load distribution.

The fictitious stress-strain relationship for concrete calculated from the load-elongation relationship, is shown in Fig. 3.9. With this σ - ϵ relationship an average concrete stiffness is taken into account by a smeared-out model for cracked concrete.

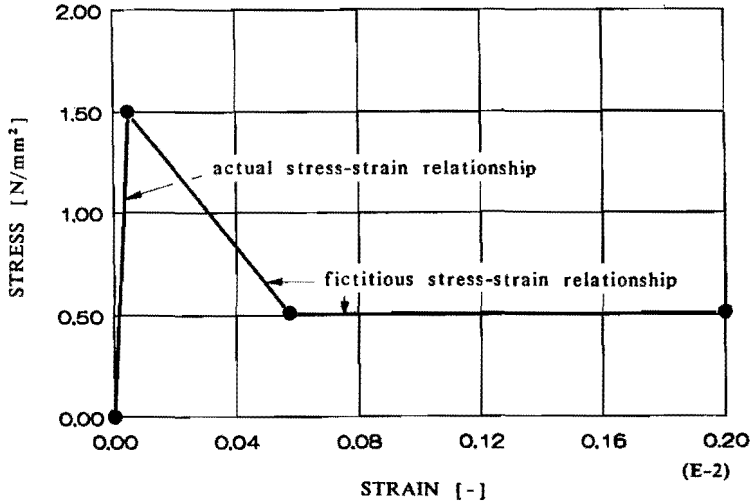


Fig. 3.9. Fictitious stress-strain relationship for concrete in case of a constant tensile load.

3.4.2. The stiffness of a reinforced concrete bar subjected to a sinusoidally distributed tensile load.

The same bar as described in the previous example (section 3.4.1.) is subjected to a sinusoidally distributed tensile load along the length.

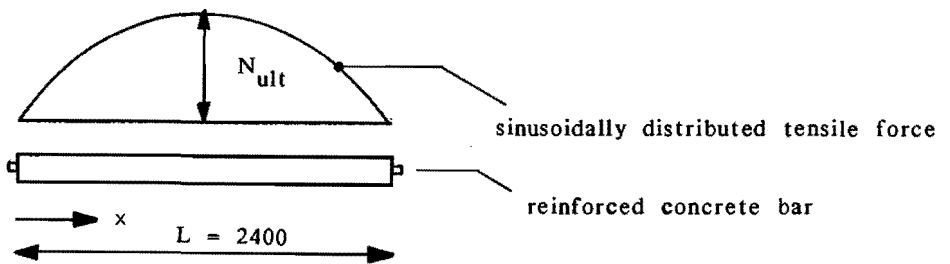


Fig. 3.10 Reinforced concrete bar subjected to a sinusoidal tensile load.

The load-elongation relationship calculated by the discrete crack model (section 3.3.3.) is shown in Fig. 3.11.

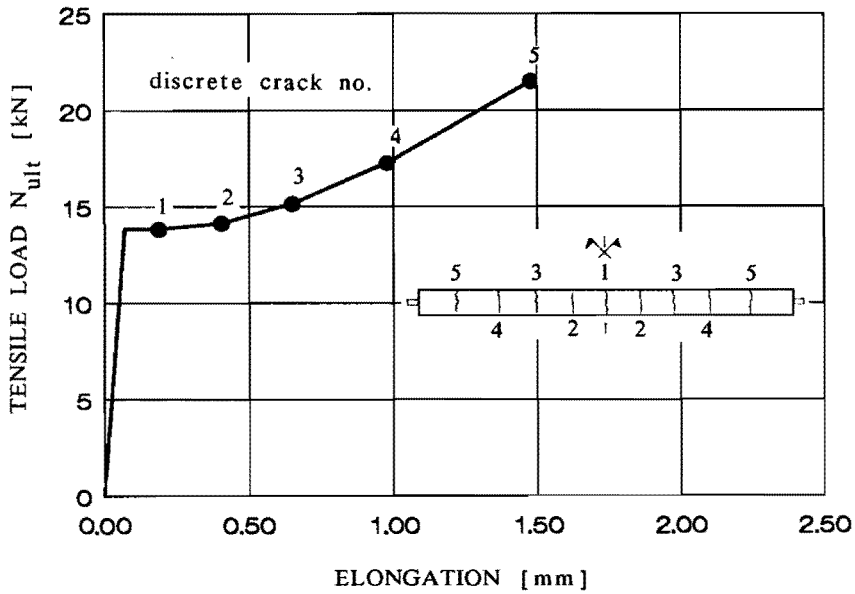
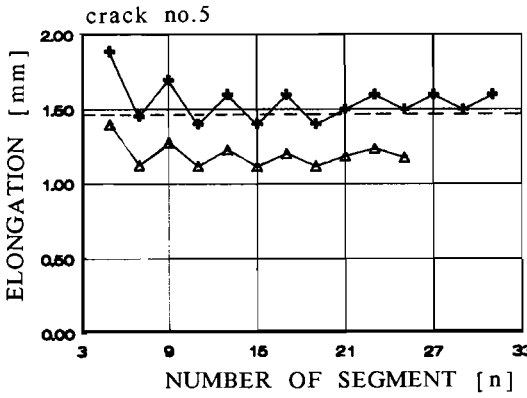
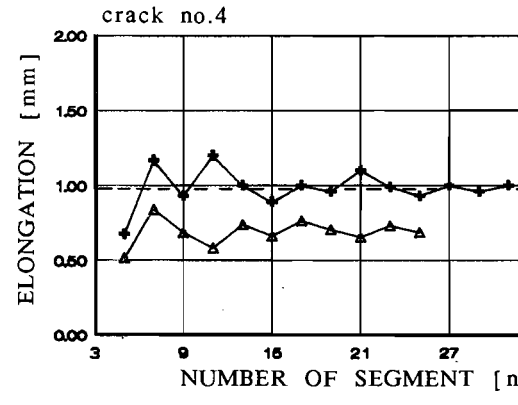
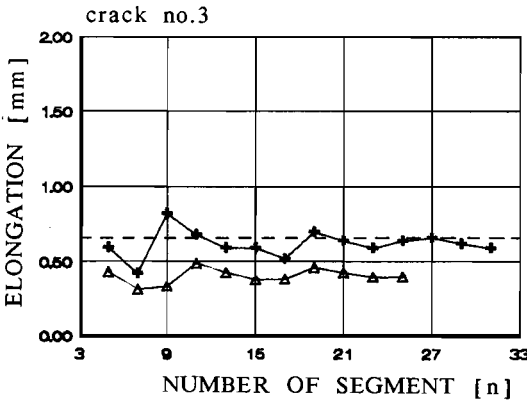
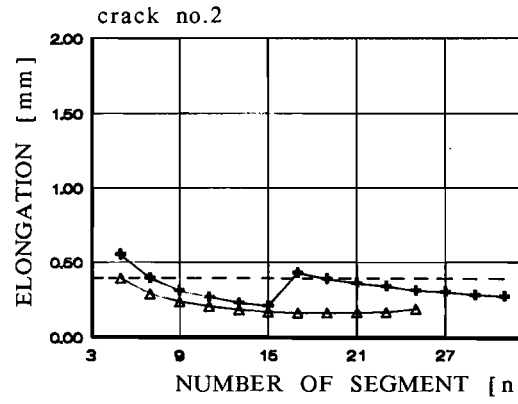
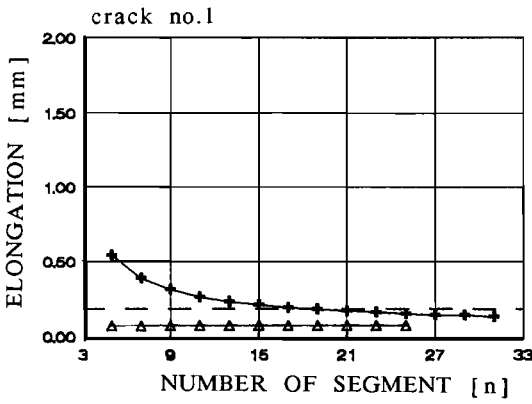


Fig. 3.11. Load-elongation relationship calculated by the discrete crack model. The elongations are calculated immediately after the initiation of a crack.

The elongations, calculated after the initiation of each crack, are compared with the numerical result from the smeared-out model for various numbers of segments. (= number of pivotal points n in Fig. 2.2) In view of the smeared-out model two different calculations are performed. In the first calculation, denoted by the symbol (+) the stiffness contribution between the cracks is neglected. In the second calculation, denoted by the symbol (Δ), the tension stiffening is taken into account by means of the fictitious stress-strain relationships calculated from the bars with a constant tensile force, as shown in the previous example.



- + smeared-out analysis (without tension stiffening)
- Δ smeared-out analysis (with tension stiffening calculated from the model based on a constant tensile load, by means of a fictitious stress-strain relationship)
- discrete analysis

Fig. 3.12. Elongations calculated by the smeared-out analysis of various tensile forces with respect to various numbers of segments. Comparison with the results from the discrete analysis.

3.5. Conclusions

The finite difference analysis of sandwich beams is supported by a physical nonlinear algorithm, taking into account the inhomogeneity of the layers due to the reinforcement.

The material nonlinearity of the faces and the core is calculated by means of an iteration by successive substitution, based on the secant moduli of elasticity. An nonlinear τ - γ relationship is included.

Cracking of the reinforced concrete face loaded in tension is a major source of physical nonlinearity. Since the finite difference analysis, described in chapter 2, is not suitable to take discrete cracks into account, a smeared-out concept has been used. The numerical results of a smeared-out analysis depend on the number of pivotal points (segments) in case of a uniformly distributed load or a central point load acting on the beam. Generally, the numerical solution converges oscillating to a mean value with an increasing number of segments. In order to avoid substantial casual failures, a sufficient large number of pivotal points (in the order of magnitude $n = L/h$) is recommended.

The application of the smeared-out concept is supported by a separated discrete crack analysis considering a reinforced concrete bar (the faces of the sandwich beam).

Since the existing models are concerned with a constant tensile load along the length, a generalized discrete crack model is described in this chapter to take a nonuniformly distributed tensile force into account.

The tension stiffening is usually calculated from the assumption of a constant tensile load distribution along the length, i.e. pure bending or approximately a four point bending load acting on a beam. The stiffness contribution of the cracked concrete is only of any importance in case of a low percentage of reinforcement.

In case of a parabolically distributed tensile load, i.e. approximately a uniformly distributed type of load acting on a beam, the tension stiffening is even in case of a low percentage of reinforcement of minor importance.

The reason for this is that the crack spacing is smaller since the position of the cracks is also affected by the distribution of the tensile force. Application of the fictitious stress-strain relationships, calculated from models based on a constant tensile load along the length, therefore results in a substantial overestimation of the stiffness of the cracked concrete face.

In case of stiffness analysis based on the smeared-out model with a constant segmentary size, the stiffness of the cracked concrete is of minor importance for the engineering practice and therefore can be neglected.

CHAPTER 4. NONLINEARITY DUE TO CREEP AND SHRINKAGE

4.1. Introduction

When concrete is subjected to load, its response is both instantaneous and time-dependent. The deformation of a specimen gradually increases with time due to creep under sustained load and by shrinkage. The time-dependent strains of concrete cause increase of deflection and redistribution of stresses at service load in simply supported sandwich beams composed of reinforced concrete facing and a foamed concrete core. In addition, the redistribution of stresses may cause cracks which in turn could lead to a loss of serviceability or durability failures. In order to predict these effects two basic prerequisites are necessary [Gilbert, 1988]:

- (i) Reliable data for the creep and shrinkage characteristics
- (ii) Theoretical procedures for the inclusion of the time effects in structural elements.

The volume of literature devoted to the magnitude of creep and shrinkage strains is so vast that it is not possible to present an overview in this thesis. A detailed description of the time-dependent behaviour of concrete and the factors which affect them is given in the books by Neville [1970] and Neville et al. [1983]. In this chapter, references are only made to recent textbooks by Gilbert [1988], Smërda et al. [1988] and Rüsçh et al. [1983]. Contrary to concrete, very little is known about the long-term properties of foamed concrete.

In view of the effects of creep and shrinkage a distinction is made between reinforced concrete structures and sandwich elements.

A number of techniques are available for the time-dependent analysis of concrete structures, among which analytical and numerical methods. Each has its own simplifying assumptions, advantages and disadvantages. An overview of some well-known methods is given in table 4.1. The suitability of the models depends on the problem considered. The factors which most complicate any time-dependent analysis are the interdependences of moisture conditions, creep strain, stress history and aging properties of concrete. The magnitude of creep strain at a given time in a reinforced concrete structure depends on the previous stress history, the age of the concrete and the moisture content.

However, the stress history in turn depends on the development of creep and shrinkage strains.

By far the most general method is the step-by-step method, particularly suitable for computerization. In this method, the time is divided into a number of intervals Δt . Since the analytical integral is substituted by a finite sum, the method is suitable to predict behaviour due to even very complicated stress histories using any creep and shrinkage curves.

Table 4.1. Characteristics of various creep and shrinkage models

| Method | Type of analysis | | | Stress History | Aging of concrete | Fysical properties | | Estimation with increasing stress history |
|--------|------------------|---|---|----------------|-------------------|--------------------|-----|---|
| | A | T | N | | | LE | NLE | |
| EMM | • | | | | | • | | + |
| AAEMM | | • | | • | • | • | | (o) |
| RCM | • | | | • | o | • | | - |
| IDM | • | | | • | • | • | | -/+ |
| SSM | | | • | • | • | | o | (o) |

EMM = Effective Modulus Method

AAEMM = Age-Adjusted Effective Modulus Method (Troost-Bazant)

RCM = Rate of Creep Method (Dischinger)

IDM = Improved Dischinger Method

SSM = Step-by-Step Method

LE = Linear Elastic NLE = Non Linear Elastic

A = Analytical T = Tabela N = Numerical

(o) = exactly (o) approximately

Contrary to concrete structures only a few theoretical studies have been found in the literature predicting the long-term behaviour of sandwich beams. By far the most simple approximation is described by Hartsock [1969]. The creep of the core loaded in shear is described by means of an effective shear modulus, analogous to Faber [1927] with respect to Young's modulus. However, this analysis is only valid in case of thin facing in which the stress in the core does not change due to creep since the cross-section is statically determined.

A solution for this problem was found by Wolfel [1987]. In case of thin faces the same effective shear modulus was adopted. In case of bending stiff faces the method is extended similar to the age-adjusted-effective modulus method (see table 4.1.). Stamm et al. [1974] describes the creep of the core loaded in shear by means of a differential equation.

Ackermann [1983] and Branti [1980] extended the equations of Stamm et al with creep of the facing due to normal load. Their application is restricted to sandwich beams with thin facing.

The objective of this chapter is to describe a general method in which all of the following time-dependent strains are taken into account with allowance for both stress-history and aging properties:

- (i) Shrinkage of faces and core
- (ii) Creep of faces and core due to bending stresses
- (iii) Creep of the core due to shear stresses

In view of the complexity and in order to link the approach with the finite difference method, the numerical step-by-step analysis has been adopted.

The following assumptions have been adopted,

- (i) The short-term stress-strain relationships are constant with time
- (ii) Creep and shrinkage in cracked concrete and cracked foamed concrete are left out of account
- (iii) Shrinkage is constant over the depth of faces and core
- (iv) Nonlinear elastic material behaviour ($\sigma < 0,5f'_{co}$)

4.2. Principle of the relaxation model (RM)

The principle and the relevant equations of the relaxation model [Smërda, 1988] are shown by means of a simple arrangement of a symmetrically reinforced column section under a constant sustained axial compressive load. The deformation of the reinforced column and the redistribution of internal stresses due to the gradual development of creep and shrinkage strains are examined.

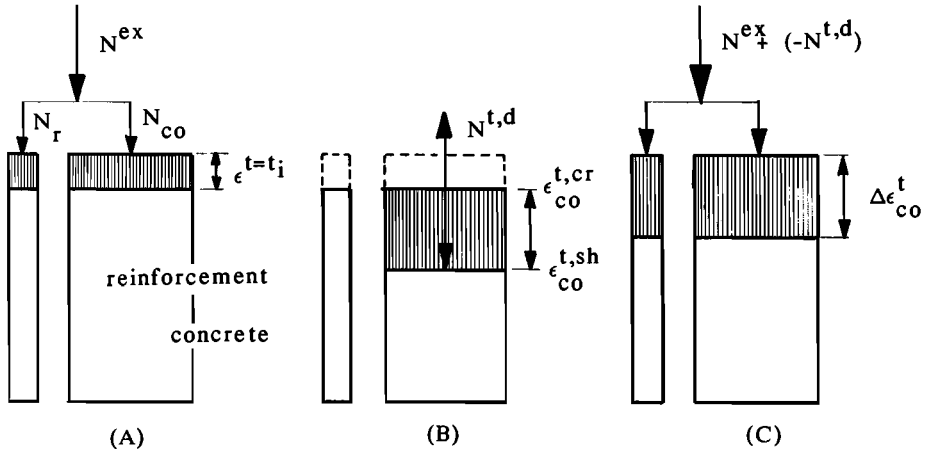


Fig. 4.1. Schematic view of an axially loaded column section

The external compressive load N^{ex} , fitted at $t=t_1$, is resisted by both concrete (N_{co}) and reinforcement (N_r) as shown in Fig. 4.1-A. The instantaneous strain in both concrete and reinforcement is calculated from

$$\epsilon = \frac{N}{E_{sec,co} A_{co} + E_{sec,r} A_r} \quad [4.1]$$

with $N = N^{ex}$ and $\epsilon_{co}^{t=t_1} = \epsilon_r^{t=t_1} = \epsilon$

The development of the creep and shrinkage strains with time is shown in Fig. 4.2. Creep due to normal load is described in terms of the creep coefficients ϕ_ϵ , with

$$\phi_\epsilon = \frac{\epsilon_{co}^{t,cr} + \epsilon_{co}^{t,sh}}{\epsilon} \quad [4.2a]$$

For an estimation of creep under variable load the principle of superposition is used, which means that the strains produced in concrete at any time t by a stress increment (positive or negative) applied at any time t_1 are independent of the effects of any stress applied either earlier or later than t_1 [McHenry, 1943].

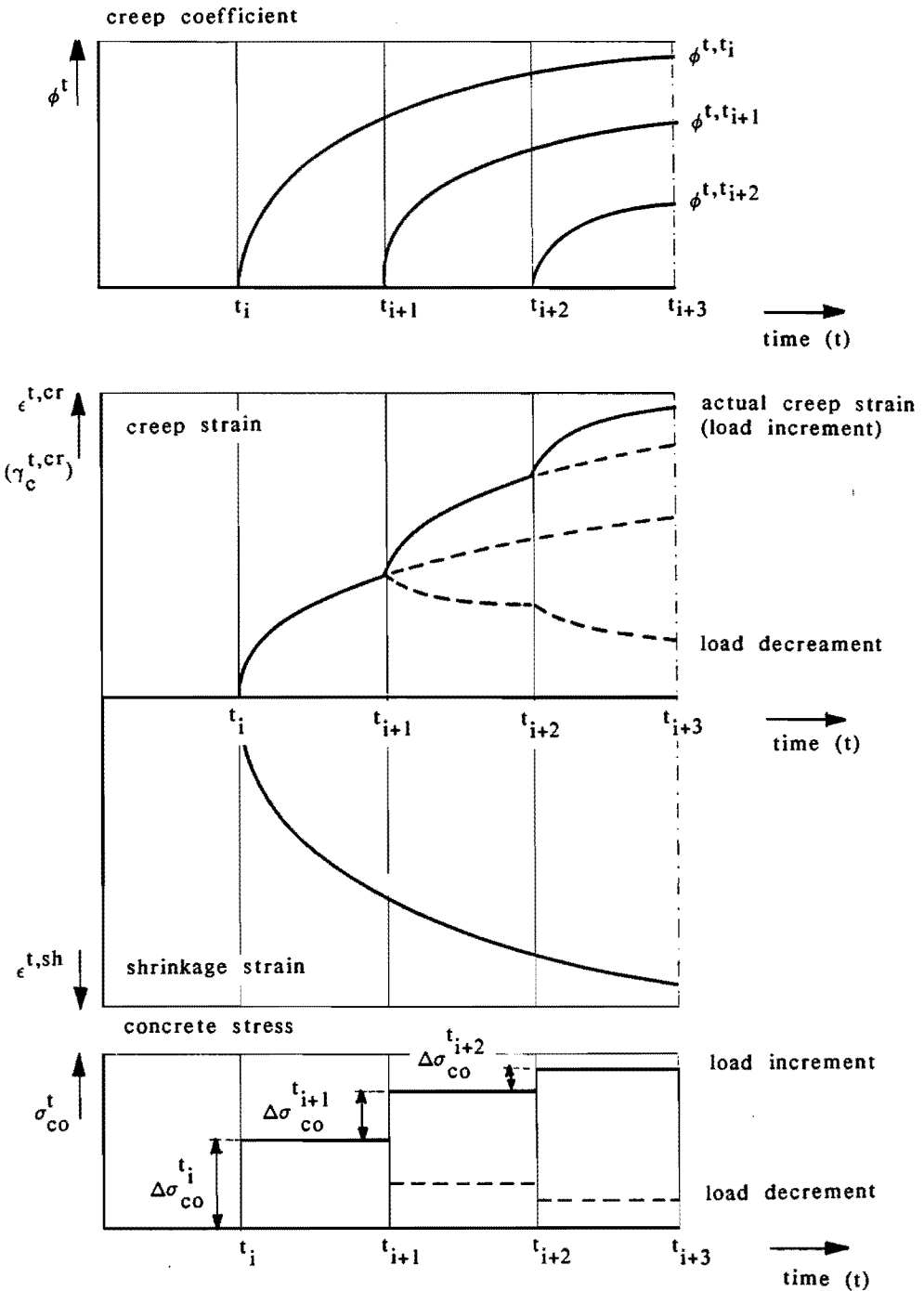


Fig. 4.2. The principle of superposition; the development of creep and shrinkage strains with time. For matters of simplicity equal time intervals are taken into account in this figure.

The time investigated is divided into a finite number of relatively short partial time intervals. For matters of simplicity Fig. 4.2 and the equation given below refer to constant time-intervals Δt . However, the computer program also allows variable time steps in such a way that a situation is approximated in which $\Delta \epsilon^t$ is at the same order of magnitude for each time-step. This leads to the best results for any given number of time-steps. The stresses and strains are assumed to be constant in the course of an interval in this study (rectangular rule).

The time-dependent behaviour of the reinforced column, described by means of the relaxation method, consists of two steps in each time interval. In the first step the time-dependent strains within a time interval are calculated. The shrinkage strain $\epsilon_{co}^{t,sh}$ follows directly from the shrinkage-time relationship, whilst the creep strain is generally given by means of the principle of superposition as shown in figure 4.2,

$$\epsilon_{co}^{t,cr} = \sum_i \frac{\Delta \sigma_{co}^{t_i}}{E_{sec,co}^{t_i}} * \phi^{t,t_i} \quad [4.3]$$

In the numerical calculations performed in this study, a simplification is made in view of the adopted creep functions (aging of concrete) by assuming the rate of creep law (i.e. Whitney and Dischinger). This means that the increment of the creep coefficient in each time interval Δt is equal for each of the creep functions as shown in Fig. 4.3, so

$$\Delta \phi^{t,t_i} = \Delta \phi^{t,t_{i+1}} = \Delta \phi^{t,t_{i+2}}$$

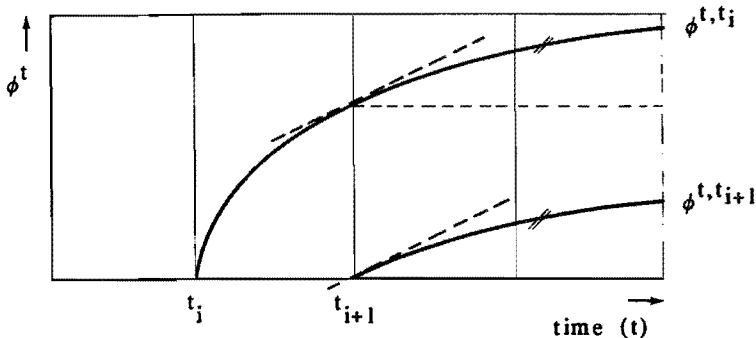


Fig. 4.3 The principle of Whitney and Dishinger.

With this simplification the creep strain at a time t is preferably described by means of the sum of the time-dependent strain increments within succeeding time intervals:

$$\epsilon_{co}^{t,cr} = \sum_t \Delta \epsilon_{co}^{t,cr} \quad [4.4a]$$

$$\Delta \epsilon_{co}^{t,cr} = \sum_i \frac{\Delta \sigma_{co}^{t_i}}{E_{sec,co}^{t_i}} * (\phi^t - \phi^{t-\Delta t}) \quad [4.4b]$$

and therefore,

$$\Delta \epsilon_{co}^{t,cr} = \frac{\sigma_{co}^{t-\Delta t}}{E_{sec,co}^{t-\Delta t}} * (\phi^t - \phi^{t-\Delta t}) \quad [4.4c]$$

Notice that the creep strain within a time interval is calculated from the state of stress and strain at the end of the previous time interval (step-by-step analysis).

The time-dependent strains are prevented by a dummy restraint acting on the concrete. Simultaneously, the relaxation of stresses takes place in the concrete. The force taken by the dummy restraint is the sum of the relaxation stresses, i.e. the force is

$$N^{t,d} = - \sum_t (\epsilon_{co}^{t,cr} + \epsilon_{co}^{t,sh}) * E_{sec,co}^t * A_{co} \quad [4.5]$$

In order to restore the state of equilibrium, the reinforced column section is loaded by the dummy restraint with a negative sign ($-N^{t,d}$) as shown in figure 4.2-B.

In the second stage of the analysis, the actual strains in the reinforcement ϵ_r^t and concrete ϵ_{co}^t are equal. The strains are calculated from equation [4.1] by means of the external force and the dummy restraint (see figure 4.2-C), i.e. by the force

$$N = N^{ex} + (-N^{t,d}) \quad [4.6]$$

The normal stress in the reinforcement is calculated from the stress-strain relationship. However, the normal stress in the concrete matrix is calculated from the sum of the strain calculated in the second step of the analysis and the time-dependent relaxation strain, i.e.

$$\epsilon_{co}^t = \epsilon_r^t - (\epsilon_{co}^{t,cr} + \epsilon_{co}^{t,sh}) \quad [4.7]$$

The time-dependent calculation is repeated using the improved secant moduli of elasticity if there is not a sufficient state of equilibrium between the external forces and the sum of the internal stresses.

Notice that the accuracy of this analysis depends on:

- (i) the number of time-intervals;
- (ii) the accuracy of the adopted creep model;

In view of the inherent inaccuracies of the adopted creep model, there is no sense in taking many time intervals.

4.3. Elaboration of the relaxation model for sandwich beams

The time-dependent model described in the previous section is elaborated in order to predict the long-term behaviour of sandwich beams composed of reinforced concrete facing and a foamed concrete core.

Fig. 4.4. shows a small part (segment) of the sandwich beam with segmentary length dx as known from the finite difference analysis (see also chapter 3). Each layer is subdivided into a number of fibres corresponding to the physical nonlinear analysis described in chapter 3. The time-dependent strain in each layer due to shrinkage $\epsilon_{\ell,i,j}^{t,sh}$ is given by means of the shrinkage-time relationship. The time-dependent strains due to creep are analogous to the example of the reinforced bar (section 4.2) given by

$$\epsilon_{\ell,i,j}^{t,cr} = \sum_i \frac{\Delta \sigma_{\ell,i,j}^{t,i}}{E_{sec,\ell,i,j}^{t,i}} * \phi_{\epsilon}^{t,t_i} \quad (\ell = 1,2 \text{ or } c) \quad [4.8a]$$

The time-dependent strain due to shear creep of the core is analogous given by

$$\gamma_c^{t,cr} = \sum_i \frac{\Delta r_{c,j}^{t_i}}{G_{sec,c,j}^{t_i}} * \phi_{\gamma}^{t,t_i} \quad [4.8b]$$

With the assumption of the rate of creep theory (Dishinger) the general equations [4.8a] and [4.8b] are written as,

$$\epsilon_{\ell,i,j}^{t,cr} = \sum_t \Delta \epsilon_{\ell,i,j}^{t,cr} \text{ with} \quad [4.9a]$$

$$\Delta \epsilon_{\ell,i,j}^{t,cr} = \frac{\sigma_{\ell,i,j}^{t-\Delta t}}{E_{sec,\ell,i,j}^{t-\Delta t}} * (\phi_{\epsilon}^t - \phi_{\epsilon}^{t-\Delta t}) \quad [4.9b]$$

$$\gamma_{c,j}^{t,cr} = \sum_t \Delta \gamma_{c,j}^{t,cr} \text{ with} \quad [4.9c]$$

$$\Delta \gamma_{c,j}^{t,cr} = \frac{r_{c,j}^{t-\Delta t}}{G_{sec,c,j}^{t-\Delta t}} * (\phi_{\gamma}^t - \phi_{\gamma}^{t-\Delta t}) \quad [4.9d]$$

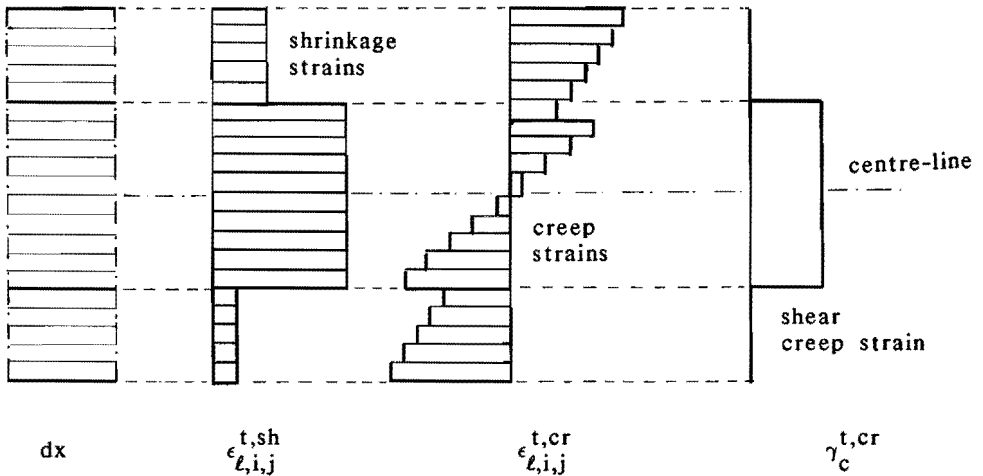


Fig. 4.4. Time-dependent strains in a cross-section of the sandwich beam.

In order to provide a link to the finite difference analysis, the local dummy restraints of each single fibre are gathered into a global dummy restraint acting in the reference line (centre-line) of the sandwich beam. The global dummy restraints of a sandwich cross-section are:

$$N_j^{t,d} = - \sum_{\ell=1,2,c} \sum_{i=1}^m (\epsilon_{\ell,i,j}^{t,cr} + \epsilon_{\ell,i,j}^{t,sh}) * E_{sec_co,i,j}^t * A_{\ell,i} \quad [4.10a]$$

$$M_j^{t,d} = - \sum_{\ell=1,2,c} \sum_{i=1}^m (\epsilon_{\ell,i,j}^{t,cr} + \epsilon_{\ell,i,j}^{t,sh}) * E_{sec_co,i,j}^t * A_{\ell,i} * z \quad [4.10b]$$

$$T_j^{t,d} = - \gamma_{c,j}^{t,cr} * G_{sec,c,j} * b * (z_{p2} - z_{p1}) \quad [4.10c]$$

$$q_j^{t,p} = - \frac{dT_j^{t,d}}{dx} \quad [4.10d]$$

The elaboration of equation [4.10c] is given in appendix A4-1.

The deflection and redistribution of internal stresses of the sandwich beam are calculated by means of the finite difference analysis, in which the external load is replaced by the sum of external load and the global dummy restraints with a negative sign.

$$M_j = M_j^{ex} + (-M_j^{t,d}) \quad [4.11a]$$

$$T_j = T_j^{ex} + (-T_j^{t,d}) \quad (\text{see also appendix A4-1}) \quad [4.11b]$$

$$q_j = q_j^{ex} + (-dT_j^{t,d}/dx) \quad [4.11c]$$

The bending stress in each fibre of faces and core and the shear stress in the core are calculated from the sum of the strain in the first step of the analysis and the relaxation strain, by means of the stress-strain relationships. If there is no equilibrium between the external cross-sectional forces and the sum of the internal stresses, the time-dependent calculation is repeated by again calculating the global dummy restraints from the secant moduli of elasticity, as shown in the flow chart in section 4.5.

4.4. Numerical examples

4.4.1. Reinforced concrete bar loaded in permanent compression

The relaxation method presented in this chapter is illustrated by means of a symmetrically reinforced column section under a sustained compressive load. The concrete and steel strains are calculated at selected times for the cross-section shown in Fig. 4.5. The numerical results are compared with results from the analyses mentioned in table 4.1, performed by Gilbert (1988).

The external load $P = 1000$ kN. Shrinkage is assumed to commence at $t_1 = 10$ days. Cross-sectional and material properties are as follows:

$$A_{co} = 90\,000 \text{ mm}^2; A_r = 1\,800 \text{ mm}^2; E_{co} = 25\,000 \text{ N/mm}^2;$$

$$E_s = 200\,000 \text{ N/mm}^2$$

Table 4.2. Creep and shrinkage data.

| | | | |
|----------------------------|---|---------------------|---------------------|
| $t-t_1$ in days | 0 | 25 | 100 |
| $\phi_\epsilon^{t-t_1}$ | 0 | 1 | 2 |
| $\epsilon_{co}^{t,t_1,sh}$ | 0 | $200 \cdot 10^{-6}$ | $400 \cdot 10^{-6}$ |

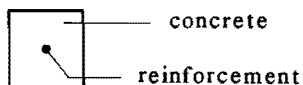


Figure 4.5 Geometry of the bar.

The results are given in table 4.3. Since the creep strain is calculated in the relaxation method based on the rate of creep approach, the comparison between RCM and the relaxation method (RM) is of special interest. Table 4.3. shows a close agreement among the results calculated by these methods.

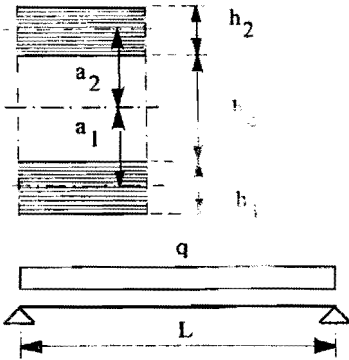
Table 4.3. Comparison of the test results of the relaxation method (RM) by using various methods as given in table 4.1.

| Method * of Analysis | Duration of load (t) (days) | Stress (N/mm ²) | | Total strain (-) |
|------------------------------|--------------------------------------|-----------------------------|-------------------------------|----------------------------|
| | | concrete σ_{co}^t | reinforcement σ_r^t | |
| All methods | 0 | 9,58 | 76,6 | 383.10^{-6} |
| EMM | 25 | 7,81 | 165 | 825.10^{-6} |
| | 100 | 6,43 | 234 | 1171.10^{-6} |
| AEMH | 25 | 7,78 | 167 | 833.10^{-6} |
| | 100 | 6,28 | 241 | 1207.10^{-6} |
| RCM | 25 | 7,70 | 170 | 852.10^{-6} |
| | 100 | 6,07 | 252 | 1261.10^{-6} |
| IDM | 25 | 8,42 | 135 | 673.10^{-6} |
| | 100 | 6,69 | 221 | 1106.10^{-6} |
| RM (relaxation method) | 25 | 7,63 | 174 | 868.10^{-6} |
| | 100 | 6,01 | 255 | 1275.10^{-6} |

*) The notations of the various methods are given in table 4.1.

4.4.2. The influence of the shear stiffness of the core on the effects of time-dependent strains induced by the faces

In the following example, the influence of an arbitrarily chosen creep and shrinkage of the upper face is shown for various stiffness ratios between the faces and the core. Distinction is made between a sandwich beam with thick (bending stiff) faces and thin faces. In order to show the influence of the shear stiffness of the core, control calculations are performed in which, independent of the stiffness ratio, the shear modulus of the core is taken as infinite ($G_c = \infty$). The geometry and material properties are shown in Fig. 4.5. The deflections caused by shrinkage are calculated from an unloaded sandwich beam ($q = 0$), whereas the deflections due to creep are calculated from a loaded sandwich beam ($q = 1 \text{ N/mm}^2$). The numerically calculated increase of deflection ($\Delta w^{t=100} = w^{t=100} - w^{t=0}$) at midspan is shown in table 4.2. and table 4.3.



Material properties and assumptions

1. $E_1 = E_2 = 30.000$
2. $\Delta t = 2 \text{ days}$
3. 25 segments, 15 fibres
4. $\epsilon_2^{t,sh} = 2,0 \cdot 10^{-5} + 6,0 \cdot 10^{-5} \ln(t)$
 $\Phi_{\epsilon,2}^t = 0,5 + 1,5 \ln(t)$
5. $b = 280 \text{ mm}$

Fig. 4.5. Geometry, material properties and assumptions.

Table 4.2. Increase of deflections $\Delta w^{t=100} = w^{t=100} - w^{t=0}$ (mm) at midspan due to creep and shrinkage in case of thin faces ($t = 100$ days).

| Type of strain | Shear stiffness | Stiffness ratio E_c/E_f ($f=1,2$) | | | | | |
|----------------|-----------------|---------------------------------------|-------------------|-------------------|-------------------|-------------------|------|
| | | $1 \cdot 10^{-5}$ | $1 \cdot 10^{-4}$ | $1 \cdot 10^{-3}$ | $1 \cdot 10^{-2}$ | $1 \cdot 10^{-1}$ | 1 |
| Shrinkage | $G = E/3$ | 2.11 | 2.11 | 2.11 | 1.90 | 0.96 | 0.16 |
| | $G = \infty$ | 2.11 | 2.11 | 2.11 | 1.90 | 0.96 | 0.16 |
| Creep | $G = E/3$ | 67.7 | 67.1 | 61.5 | 31.0 | 2.9 | 0.06 |
| | $G = \infty$ | 67.8 | 67.1 | 61.5 | 31.0 | 2.9 | 0.06 |

Table 4.3. Increase of deflections $\Delta w^{t=100} = w^{t=100} - w^{t=0}$ (mm) at midspan due to creep and shrinkage in case of thick faces ($t = 100$ days).

| Type of strain | Shear stiffness | Stiffness ratio E_c/E_ℓ ($\ell = 1,2$) | | | | | |
|----------------|-----------------|---|-------------|-------------|-------------|-------------|------|
| | | 1.10^{-5} | 1.10^{-4} | 1.10^{-3} | 1.10^{-2} | 1.10^{-1} | 1 |
| Shrinkage | $G = E/3$ | 2.0 | 2.0 | 2.0 | 2.0 | 2.0 | 1.8 |
| | $G = \infty$ | 2.0 | 2.0 | 2.0 | 2.0 | 2.0 | 1.8 |
| Creep | $G = E/3$ | 0.13 | 0.92 | 2.17 | 2.43 | 2.09 | 0.82 |
| | $G = \infty$ | 2.52 | 2.52 | 2.52 | 2.47 | 2.09 | 0.82 |

The tables 4.2 and 4.3 show that the increase of deflection $\Delta w^{t=100}$:

- due to shrinkage of the upper face is not affected by the shear stiffness of the core;
- due to creep of the upper face is only affected by the shear stiffness of the core in case of bending stiff (thick) faces.

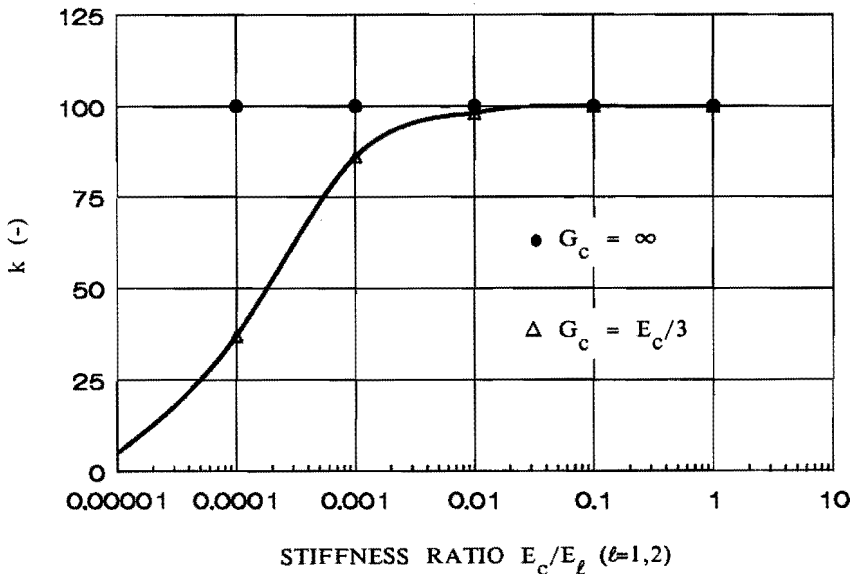


Fig. 4.7. Decrease of the time-dependent deflection caused by creep of the core dependent on the shear stiffness of the core, in case of sandwich beams with thick faces.

The deflection caused by creep of the upper face in case of bending stiff faces is graphically presented in Fig. 4.7 for various stiffness ratios. The increase of deflection $\Delta w^{t=100}$ in case $G_c = \infty$ is set up as 100% in Fig. 4.7, so

$$k = \frac{\Delta w^{t=100} (G_c = E/3)}{\Delta w^{t=100} (G_c = \infty)} * 100$$

4.4.3. Creep of the core under sustained shear load

The third example of this chapter shows the influence of the creep of the core under sustained shear load on the deflection of sandwich beams with both thick (bending stiff) and thin faces. Various stiffness ratios between the faces and core (E_c/E_f) are considered. The numerical results obtained from the Relaxation Method (RM) presented in this chapter, are compared with calculations based on the Effective Modulus Method (EMM) in case of sandwich beams with thin faces. The geometry, type of load and assumptions are given in Fig. 4.8. The numerically calculated deflections are given in table 4.4 and table 4.5.

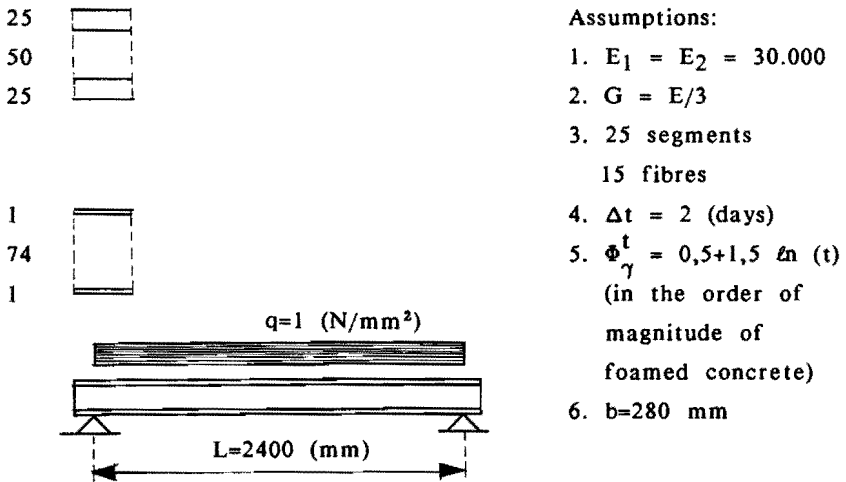


Fig. 4.8 Geometry, load and assumptions

Table 4.4. Deflections due to shear creep of the core in case of thin faces (mm)

| Duration of load t (days) | Type of method | Stiffness ratio E_c/E_ℓ ($\ell=1,2$) | | | | |
|---------------------------|----------------|---|-------------|-------------|-------------|-----|
| | | 1.10^{-4} | 1.10^{-3} | 1.10^{-2} | 1.10^{-1} | 1 |
| 0 | | 52.1 | 21.5 | 16.7 | 8.4 | 1.4 |
| 8 | EMM | 174.5 | 33.7 | 17.9 | 8.5 | 1.4 |
| | RM | 163.7 | 32.6 | 17.8 | 8.5 | 1.4 |
| 20 | EMM | 220.7 | 38.4 | 18.4 | 8.5 | 1.4 |
| | RM | 205.9 | 36.9 | 18.2 | 8.5 | 1.4 |
| 100 | EMM | 302.3 | 46.5 | 19.2 | 8.6 | 1.4 |
| | RM | 280.0 | 44.3 | 19.0 | 8.6 | 1.4 |

Table 4.5. Deflections due to shear creep at the core in case of thick faces (mm)

| Duration of load t (days) | Type of method | Stiffness ratio E_c/E_ℓ ($\ell=1,2$) | | | | |
|---------------------------|----------------|---|-------------|-------------|-------------|------|
| | | 1.10^{-4} | 1.10^{-3} | 1.10^{-2} | 1.10^{-1} | 1 |
| 0 | RM | 10.8 | 2.6 | 0.9 | 0.72 | 0.62 |
| 8 | | 18.8 | 7.6 | 1.6 | 0.79 | 0.63 |
| 20 | | 19.1 | 8.9 | 1.8 | 0.81 | 0.63 |
| 100 | | 19.3 | 10.8 | 2.2 | 0.86 | 0.64 |

In table 4.4. (thin faces) it is shown that the results of the relaxation method, presented in this chapter, are in close agreement with the results obtained by the effective modulus method.

The deflections of sandwich beams with thick faces caused by creep of the core under a sustained shear load (see table 4.5) are graphically presented in Fig. 4.9 by means of

$$k = (w^{t=100}/w^{t=0}) * 100$$

In this example, it is shown that in case of a large stiffness of the core ($E_c/E_\ell > 0.1$), the creep of the core under a sustained shear load is of minor importance.

The influence of the shear deformation caused by creep of the core under a sustained shear load increases from $E_c/E_\ell = 0.1$ to $E_c/E_\ell = 0.001$. With further lowering of the stiffness ratio, the deflection increment is reduced since the beam more and more acts like two separated faces ($\tau_c^{t=100} \rightarrow 0$). The loss of cooperation between the faces is shown in Fig. 4.10 by means of the shear stress near the supports (cross-section I-I) for $t=0$ and $t=100$.

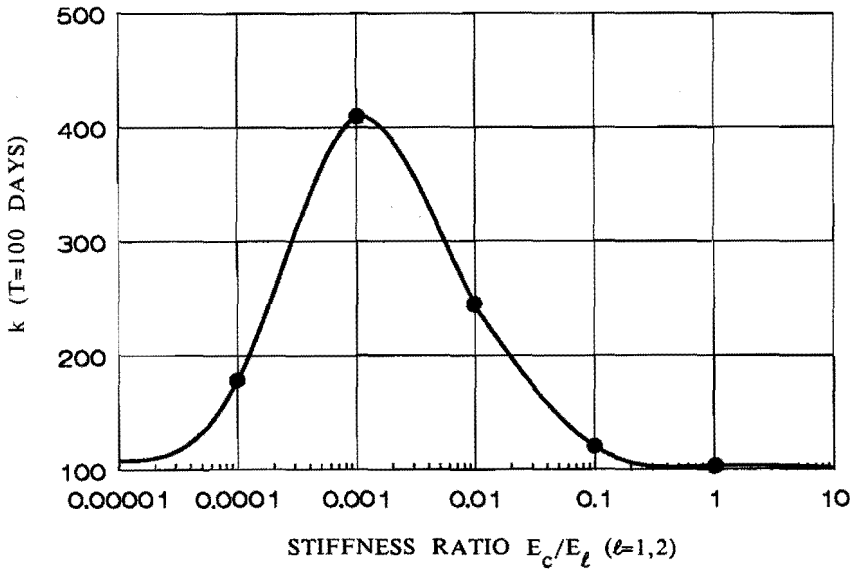


Fig. 4.9. Increase of deflection at midspan due to creep of the core under sustained shear load in case of sandwich beams with thick facing; $k = (w_{t=100} / w_{t=0}) * 100$.

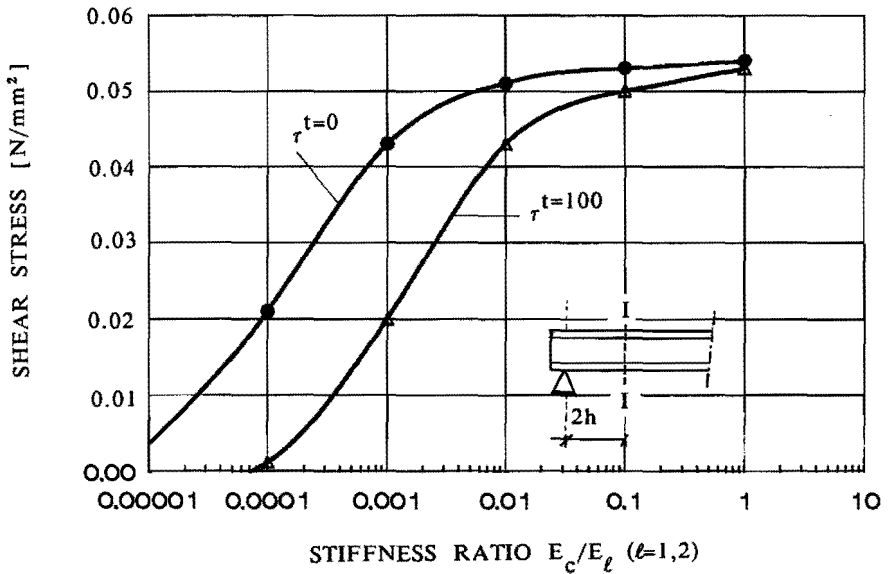
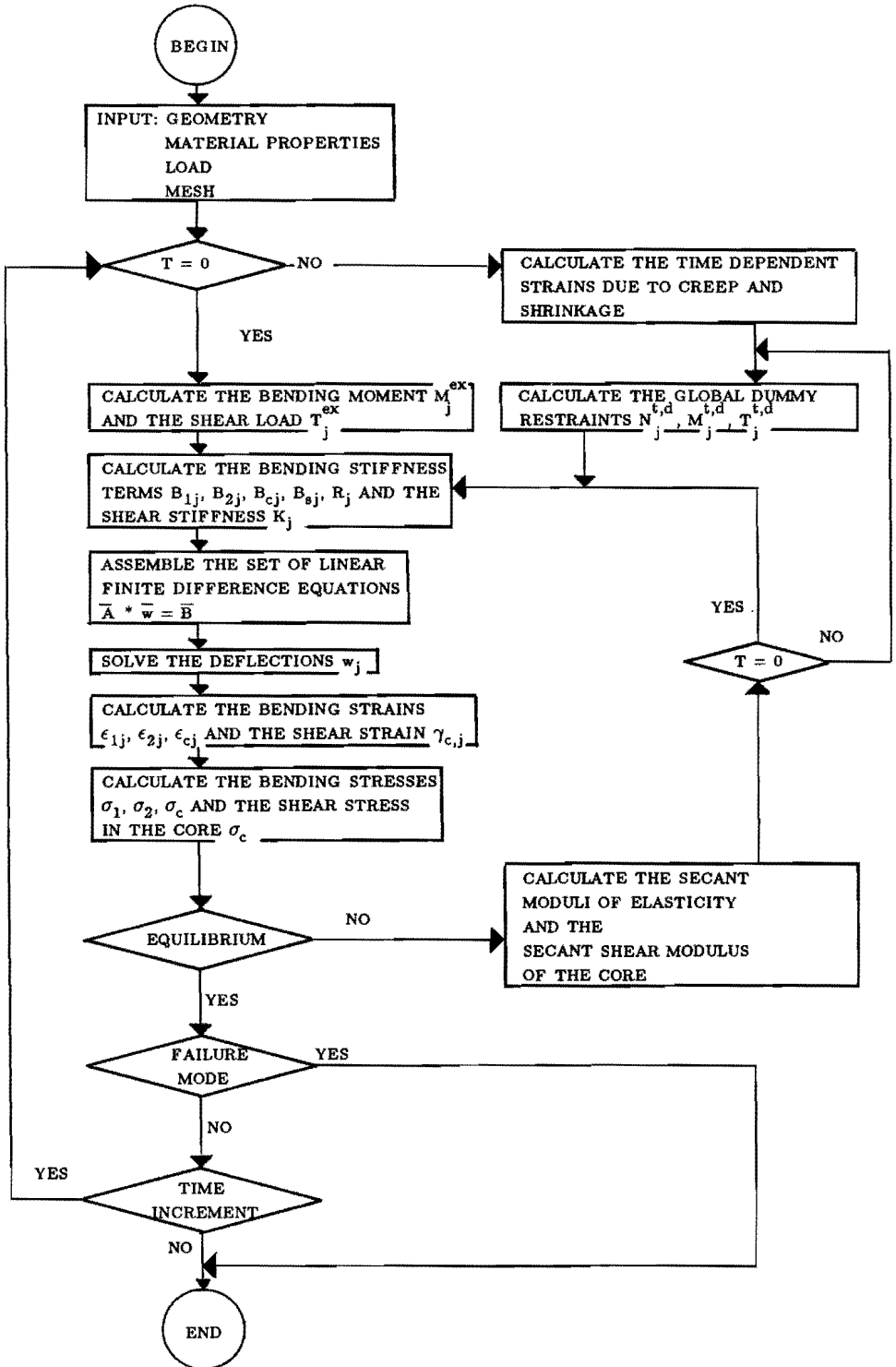


Fig. 4.10. Loss of sandwich action due to creep of the core shown by the decrease of shear stresses in cross-section I-I.

4.5. Flow chart



4.6. Discussion and conclusions

The numerical model is extended in the fourth chapter by the time-dependent behaviour caused by creep and shrinkage. Creep and shrinkage are taken into account by means of a generalized relaxation method. The initial strains due to creep and shrinkage are counterbalanced by means of dummy restraints. The so-called step-by-step analysis is based on the superposition principle of McHenry, and takes the stress-history into account. Although the theory is generally described, a simplification is made in the computer model (see the manual SANDI90, Vianen and Salet 1990) with respect to the time-dependent creep functions (aging) by assuming the rate of creep law.

This simplification is justified by the combination of the following facts.

- (i) Aging demands a tremendous amount of input data, especially with sandwich beams;
- (ii) The aging properties of foamed concrete are not yet known;
- (iii) The accuracy of the numerical prediction is basically affected by a large statistical variance in the creep and shrinkage properties and the type of creep and shrinkage tests;
- (iv) The rate of creep method underestimates the creep strains while the principle of superposition overestimates the creep strains.

The method has the additional advantage that it provides insight into the problem under consideration. It is demonstrated that:

- in case other solutions are available, the results are in close agreement;
- the deflections and stress-redistribution due to shrinkage of the faces are not affected by the shear stiffness of the core;
- the deflections and stress-redistribution due to creep of the faces are only affected by the shear stiffness of the core in case of sandwich beams with bending stiff faces;
- the outcome of the creep of the core under sustained shear load depends on the stiffness of the core; both in case of stiff and weak cores the increase of deflection and redistribution of stresses are small.

5. FAILURE CRITERIA

5.1. Introduction

The structural behaviour of the sandwich beams is characterized by the deflection and the load-bearing capacity. In view of the latter, not only the ultimate load is of interest, but also the failure mode which determines the structural safety of the element. In order to judge the numerical calculations, suitable criteria are to be established. The following criteria are discussed in this chapter with reference to Fig. 5.1.:

- (i) ultimate bending moment (A-A)
- (ii) ultimate shear load (B-B)
- (iii) horizontal slip (C-C)

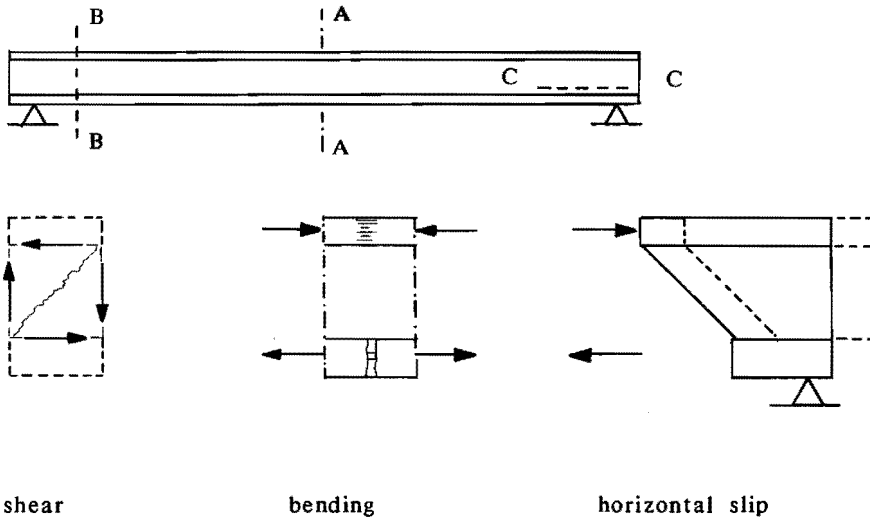


Fig. 5.1. Possible failure modes.

5.2. Ultimate bending moment

The ultimate bending moment capacity of a cross-section is determined by the strain capacity of either the concrete face loaded in compression or the reinforcement loaded in tension.

In view of the safety of a reinforced concrete structure the following conditions are commonly made:

- (i) the reinforcement is capable to carry the total tensile load of the lower reinforced concrete face after cracking;
- (ii) yield of the reinforcement before the ultimate strain capacity in the concrete face loaded in compression is exceeded.

5.3. Ultimate shear load

Although rarely critical in traditional slabs, in this case shear failure must be taken into account in view of the relatively low shear (tensile) strength of the foamed concrete core. The ultimate shear load is determined by the tensile strain capacity of the core. The external load in a cross-section is carried by the faces and the core as shown in Fig. 2.1. The mutual distribution of the shear load between the faces and the core depends on the ratio between the shear stiffness of the core and the bending stiffness of the faces, i.e. $(E_1 I_1 + E_2 I_2) / GA$. *

5.4. Horizontal slip of the reinforced concrete face loaded in tension

A typical failure mode with respect to multi-layered elements is concerned with the horizontal slip in the interface between two layers. This type of failure has also been identified by Zerjeski [1982], Annamalai et al [1977], Shendy-El-Berbary [1981] and Parton and Shendy-El-Barbary [1982] as a possible failure mode for sandwich beams composed of concrete components. As shown in Fig. 7.1. (see chapter 7) none of these sandwich beams, tested by the research workers mentioned, were provided with either a steel bar reinforcement or with a foamed concrete core.

In order to gain insight into the sensitivity of the sandwich beams for failure induced by horizontal slip, the following (simplified) model is used.

In case of a uniformly distributed load, the load-bearing capacity with respect to shear is also affected by the boundary conditions set for a simply support. The conditions $w=0$ and $M=0$ (see section 2.3.2.) can be written using equation [2.11] and equation [2.1] respectively, to $\gamma'_c=0$. This results in a reduction of the shear load in the core near a support at the expense of an increment of shear load in the faces.

In the following description, a uniformly distributed load is taken in mind.

Before cracking of the foamed concrete core, the shear load between the faces is transferred by means of shear stresses, as assumed in the sandwich theory (Fig. 5.2-I). With larger loads, inevitable cracks arise in the foamed concrete core. The first cracks arise near midspan and their direction is perpendicular to the span of the beam (tensile cracks). With further load increments the cracked section of the core extends and the direction of the cracks is more and more affected by the shear stresses. It is assumed that the transfer of shear load is still possible in the cracked section of the core since the beam in reality behaves somewhere between an open-beam girder and a tied arch, as shown in Fig. 5.2-II.

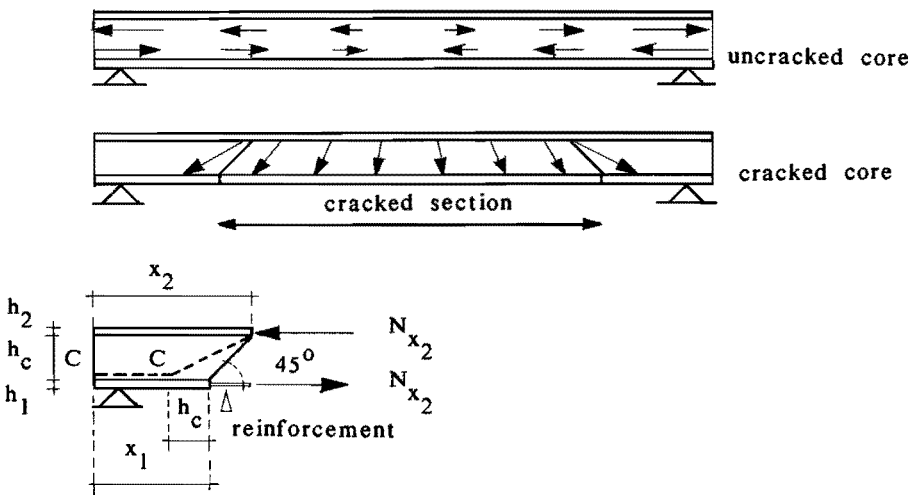


Fig. 5.2. The method of shear transference in the sandwich beam and the numerical modelling of the horizontal slip.

The state of stress within the cracked core is not calculated by the numerical model. The state of equilibrium of the uncracked section near the supports is considered in order to trace the sensitivity of the sandwich elements for failure induced by horizontal slip (Fig. 5.2-III).

The normal load acting in the upper face N_{x_2} , i.e.

$$N_{x_2} = \sum_{i=1}^m \sigma_2 * b * \frac{h_2}{m} \quad [5.1]$$

must be carried in the foamed concrete core along the length C-C.

N_{x_2} is affected by the length x_2 and by the external load. The length C-C is affected by x_1 and by the actual dispersion of the normal load N_{x_2} in the core, as shown in Fig. 5.2.

Horizontal slip arises along section C-C if N_{x_2} exceeds the load bearing capacity of the foamed concrete along section C-C, so

$$N_{x_2} > f_{fc,tm} * b * |C-C| \quad [5.2]$$

with $|C-C|$ is the length of section C-C. The risk that this will happen increases when a large percentage of reinforcement is chosen together with a low tensile strength $f_{fc,tm}$ of the foamed concrete.

In order to allow a numerical calculation, the length of section C-C and the location of x_2 are calculated from the following relationships,

$$(i) \quad x_2 = x_1 + h_c, \quad \text{based on the direction (45°) of the cracks in the core near a support *;} \quad [5.3a]$$

$$(ii) \quad |C-C| = x_1 - h_c, \quad \text{in view of the dispersion of the normal load in the core.} \quad [5.3b]$$

The remaining unknown parameter x_1 is calculated from the state of principal stresses in the core by means of the following algorithm:

1. Calculate the principal stresses in the fibre $i=m$ of the core (see Fig. 5.3) in each segment j along the span of the beam from the bending stress ($\sigma_{c,j,i=m}$) and the shear stress ($\tau_{c,j}$):

$$\bar{\sigma}_{c,j,i} = \frac{\sigma_{c,j,i=m}}{2} \pm \sqrt{\frac{\sigma_{c,j,i=m}^2}{4} + \tau_{c,j}^2} \quad [5.4]$$

This assumption can be verified afterwards since the direction of the principal stresses in the core are also calculated by the numerical model, from $\tan 2\alpha_{c,j,i} = 2\tau_{c,j} / \sigma_{c,j,i}$.

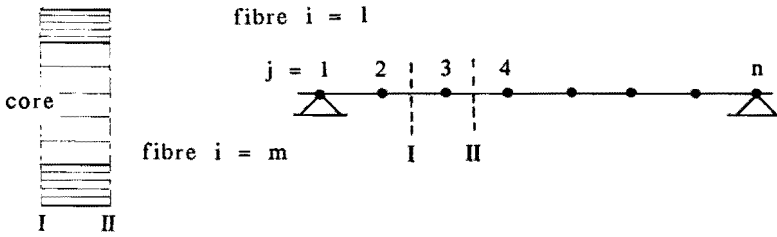


Fig. 5.3 Definition of the fibres in the core

2. Check if the circle of Mohr belonging to the principal stresses $\bar{\sigma}_{c,j,i}$ in the fibres $i=m$ in each segment j along the span of the beam exceeds the ultimate state of stress defined by a (linear) intrinsic curve, as shown in Fig. 5.4.

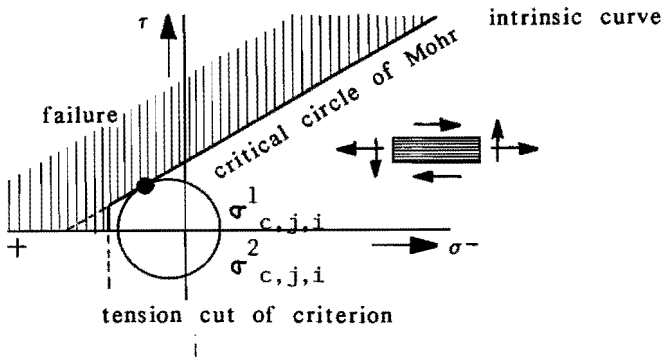


Fig. 5.4 The circle of Mohr belonging to a critical state of the principal stresses.

3. The unknown length x_1 is defined as that part of the beam in which the circles of Mohr belonging to principal stresses $\bar{\sigma}_{c,j,i=m}$ do not exceed the intrinsic curve, as shown in Fig. 5.5.

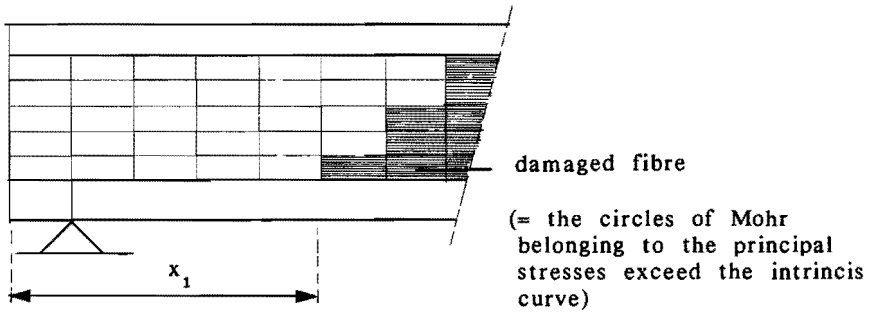


Fig. 5.5. Definition of the length x_1

5.5. Discussion and conclusions

In order to describe the load-bearing capacity of the sandwich beams, criteria are set with respect to the ultimate bending moment and shear load and the horizontal slip.

An imperfection of the numerical analysis of the sandwich beams by means of the finite difference analysis, is concerned with the method of shear transference in the cracked foamed concrete core. With an increase of the cracked section of the foamed concrete core, the beam behaves more and more somewhere between an open-beam girder and a tied arch, instead of a sandwich beam.

In order to trace the sensitivity of the sandwich beams for failure induced by horizontal slip the state of shear stress in the section C-C (see figure 5.1) is adapted to the actual method of shear transference (a combination of open-beam girder and tied arch behaviour) by means of a simplified model.

6. EXPERIMENTAL RESEARCH INTO THE STRUCTURAL PROPERTIES OF THE FOAMED CONCRETE CORE, CONCRETE FACES AND REINFORCEMENT

6.1 Introduction

In order to compare the experimental and numerical test results, the material properties of the actually constructed sandwich elements (see chapter 7) were determined on samples obtained from the same casts.

Since the experimentally tested sandwich beams were manufactured in two different cast series, two series of control specimens were also supplied. A survey of the tests performed is given in table 6.1.

Table 6.1 The type of test performed

| type of test | type of material tested | | | |
|------------------------------|-------------------------|------------|------------|---------------|
| | foamed concrete | concrete | | reinforcement |
| | | lower face | upper face | |
| compression | ● ○ | ● ○ | ● ○ | |
| tension | ● | ● | | ● |
| shear (torsion) | ● ○ | | | |
| creep under compression load | ○ | ○ | ○ | |
| creep under shear load | ○ | | | |
| shrinkage | ○ | ○ | ○ | |

- Tests on samples from cast 1 (short-term tested sandwich beams).
- Tests on samples from cast 2 (long-term tested sandwich beams).

The strength and deformation response of the samples depend to a large extent on the type of load application system. In all tests, a uniform boundary displacement condition was chosen in order to simplify matters concerned to deformation measurements.

In that case a non-uniform stress distribution will emerge and only an average strength can be determined [van Mier, 1984]. In order to obtain the input for the numerical model, the test results are presented as stress-strain, creep and shrinkage functions. The functions are fitted from the actual test results using the method of least squares by Gauss.

6.2 Foamed concrete

6.2.1 Mix proportion and manufacture

In this study foamed concrete with a density of about 600 kg/m³ was chosen. For all the tests the same mix was used. Throughout all the casts made, cement, sand and foaming agent came from the same batch. The contents of cement, sand, water and foam are given in table 6.2.

Table 6.2 Mix quantities of fresh foamed concrete.

| Mix designation | Mass quantities (kg/m ³) | | | | Volume quantities (m ³ /m ³) | | | |
|-----------------|--------------------------------------|-------|------|------|---|-------|-------|-------|
| | Cement | Water | Sand | Foam | Cement | Water | Sand | Foam |
| SB600 | 340 | 136 | 70 | 50 | 0.110 | 0.136 | 0.024 | 0.730 |

The type of cement used was an ordinary blast-furnace cement (type A). Cement, water and glacial sand (0-1 mm) were mixed in a tilting type of concrete mixer. In view of the requirements which had to be set for the workability of the cement paste, a water/cement ratio of 0.40 was chosen. A protein foam with a density of 50 kg/m³ was prepared and added to the cement slurry and mixed for 3 minutes. The foam mainly consists of water. Therefore the overall water/cement ratio became 0.55. As a result the workability of the mix was high.

The fresh foamed concrete was poured immediately after mixing. The moulds were not vibrated, in order to respect the foam structure. The casting-surfaces were finished and covered with pvc-foil to avoid drying out. Two days after casting, the specimens were demoulded and stored in a control room at a constant relative humidity of near 100% at a temperature of 20° ± 1°C.

In case of surface measurements, the specimens were taken to the testing site one day before testing and the measuring facilities were glued to the surfaces. The age of the specimens at the time of testing varied between 25 and 30 days.

6.2.2 Compression tests

A schematic view of a specimen is given in Fig. 6.1. The tests were deformation controlled. The applied deformation rate was 0.5 mm/min. The deformation was controlled by an LVDT (Linear Voltage Displacement Transducer) registering the displacements of the jack. The tests were performed with a compression testing machine, type Schenck M1600. The force was determined by a load cell, located between the vessel and the specimen. The deformations of the samples were measured with two LVDTs with a base of 250 mm, positioned on two opposite casting-surfaces (see Fig. 6.1).

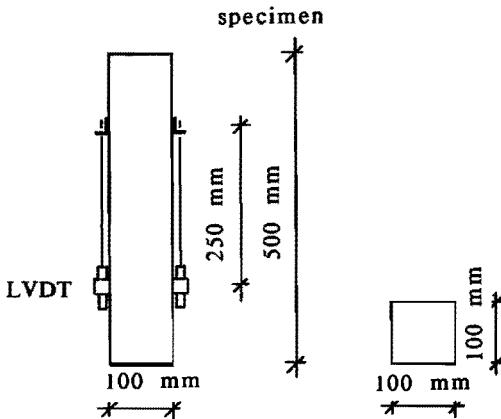


Fig. 6.1 Foamed concrete specimen prepared for testing

The stress-strain relationships for both casts are plotted in Fig. 6.2.

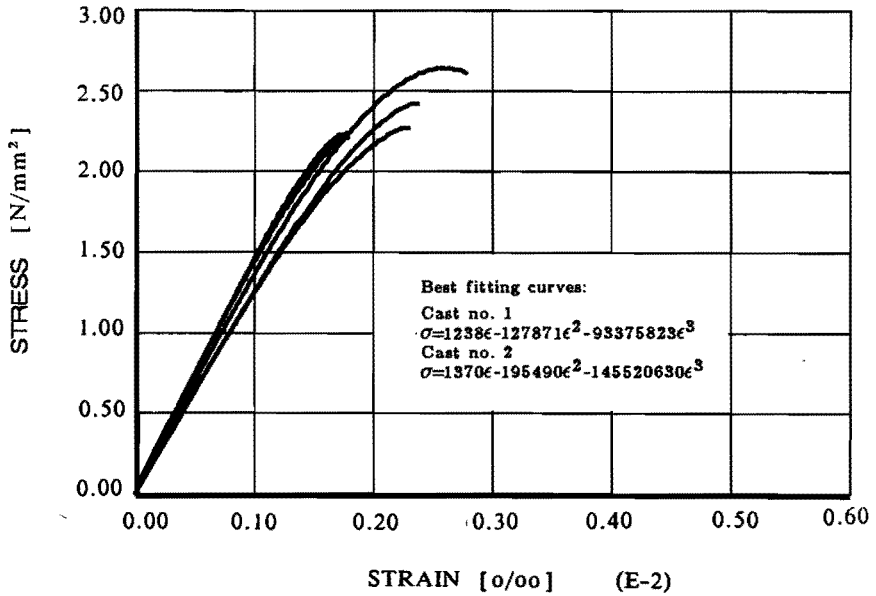


Fig. 6.2 Typical stress-strain relationships of foamed concrete from both casts under compression load and the best fitting equations.

6.2.3 Torsion tests

Torsion shear tests were performed on circular samples. Contrary to Shendy-El-Baraby (1981) who tested solid circular cylinders of polystyrene lightweight concrete, hollow specimens were used in order to avoid initial stresses due to non-uniform shrinkage.

The cylinders were cast in a wooden outer mould, consisting of two halves. The inner mould was made of an inflated cylindrical membrane, in order to prevent initial stresses caused by shrinkage during the first 24 hours of hardening. The mould is shown in Fig. 6.3. The height of the specimens was 270 mm with an inner radius of 120 mm and an outer radius of 160 mm, as shown in Fig. 6.4. The top and bottom surfaces of the samples were rubbed with sand-paper. After removing the dust, stiff steel rings were glued on both ends. The samples have conical ends in order to prevent failure in the plane of the adhesive. This loading application system results in a uniform strain distribution in the major part of the samples between the conical ends.

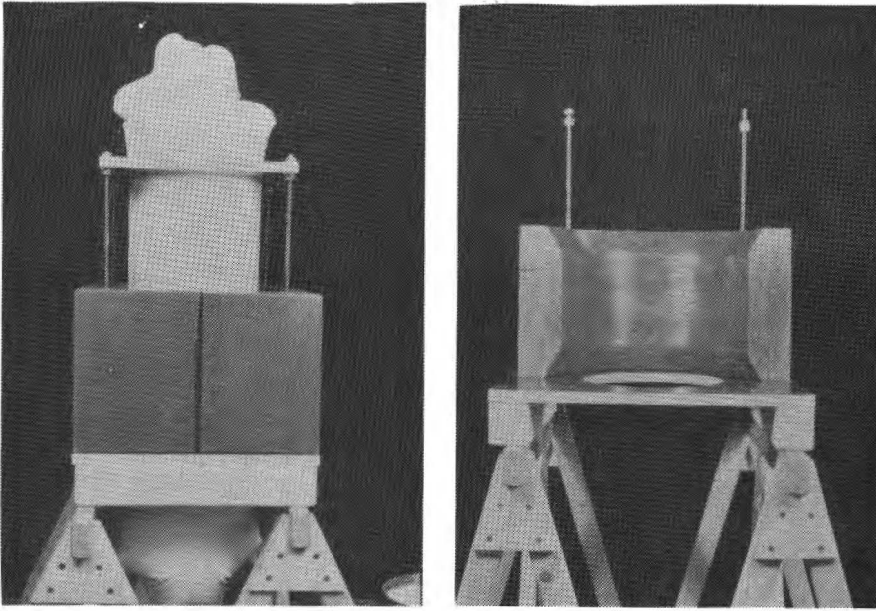
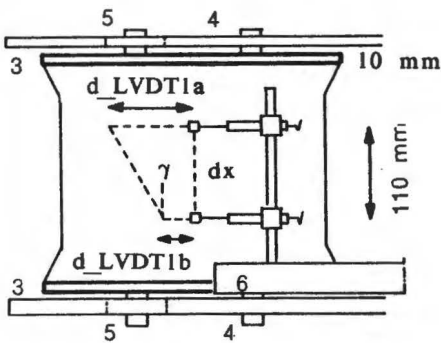
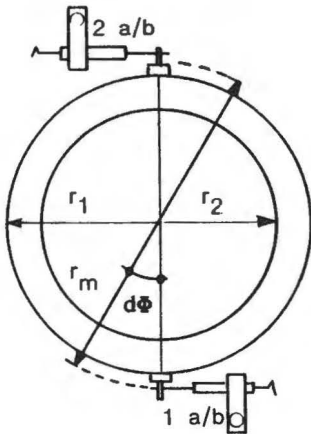


Fig. 6.3 Mould for the hollow circular samples of foamed concrete.



- σ_m = radius at the position of the measuring devices
- σ_1 = outer radius
- σ_2 = inner radius
- $\frac{d\Phi}{dx}$ = specific rotation
- γ = shear strain



- 1a/b = LVDT1a and LVDT1b
- 2a/b = LVDT2a and LVDT2b
- 3 = stiff steel ring
- 4 = round fitting hole
- 5 = rectangular hole
- 6 = separated measuring frame

Fig. 6.4 Specimen and measuring devices of the torsion testing system.

The general assembly of the torsion testing-system and measuring equipment, developed for this torsion test are shown in Figs. 6.5 and 6.6. A vertical load F_v is inverted into two equal and opposite horizontal forces F_h (torsional moment), using a flexible steel cable structure.

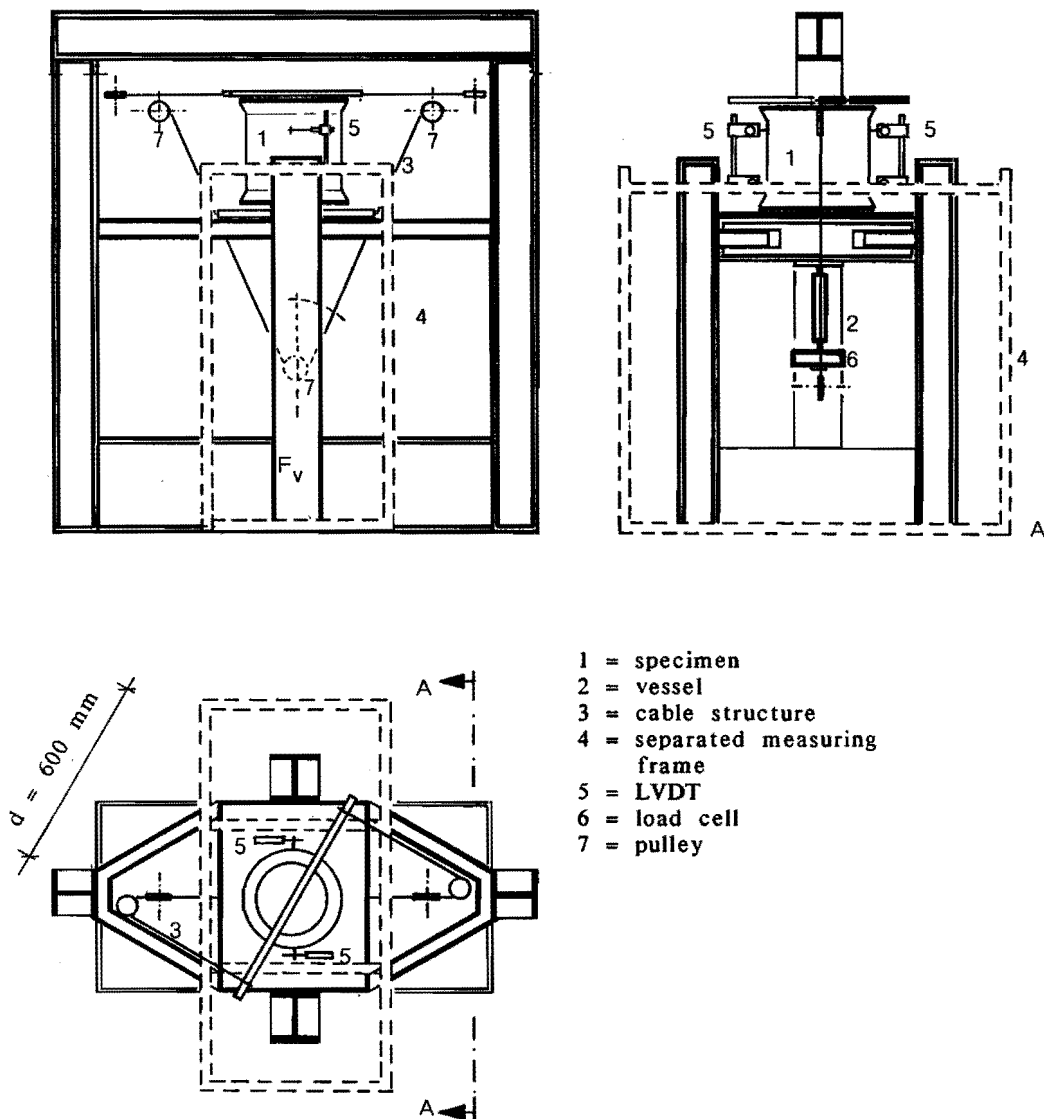


Fig. 6.5 General assembly short-term torsion testing rig.

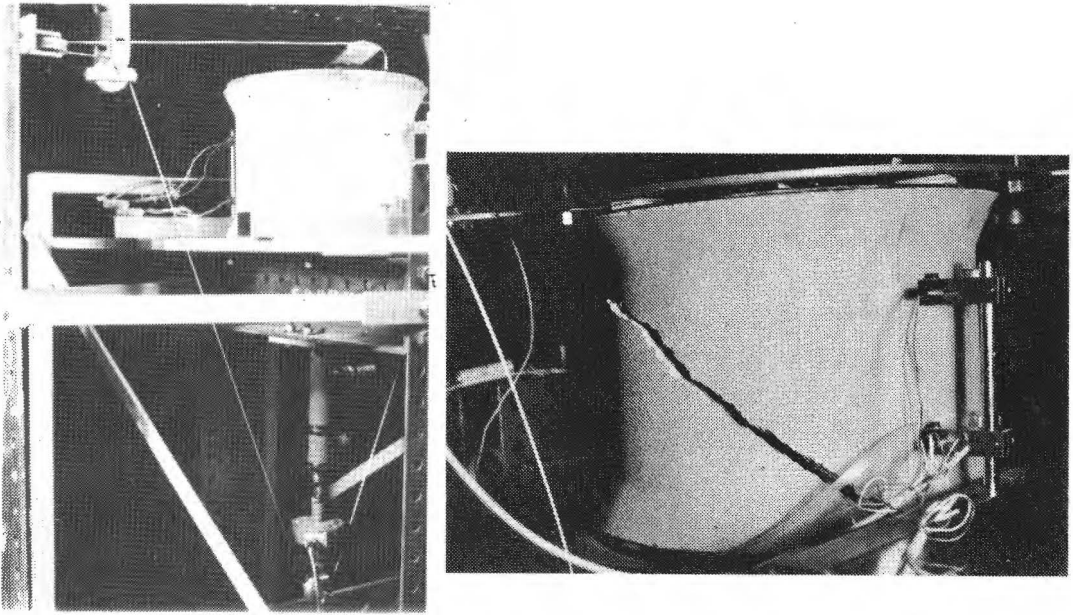


Fig. 6.6. The torsion testing rig and the typical failure mode of a test specimen

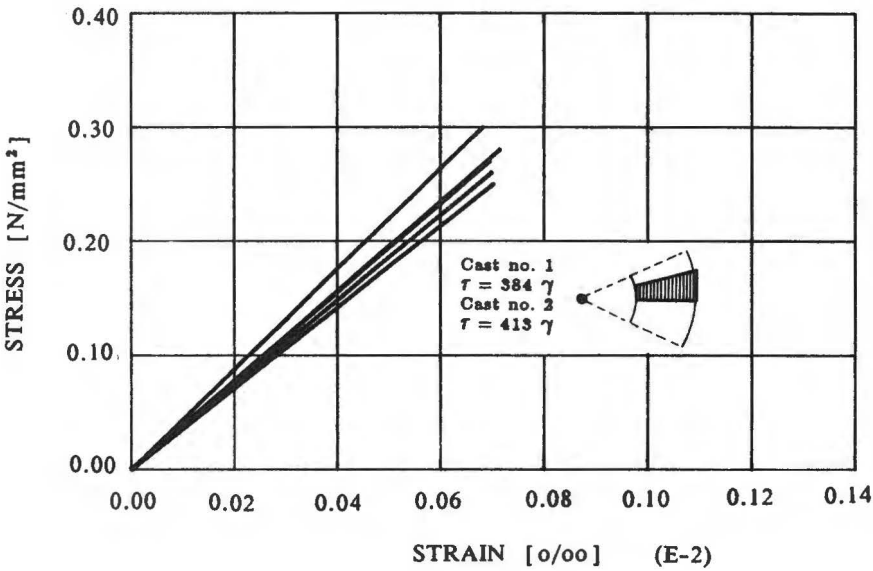


Fig. 6.7 Typical shear stress-strain relationships of foamed concrete from both casts loaded in shear and the best-fitted equations. The stresses at the outer radius are considered in this figure.

The loading arrangement is deformation controlled and the vertical load F_v (see Fig. 6.5) is determined by a load cell located between the jack and the pulley acting on the steel cable structure.

The deformations were measured using four LVDTs, two on opposite sides of the specimen as described in Fig. 6.4. The measuring length between two LVDTs on one side was 110 mm. The diameter between two LVDTs on one side and the other side of the sample 350 mm. The average deformation rate $\frac{d\phi}{dx}$ was about 2.10^{-6} (rad/mm)/min.

The shear stress-strain relationships are plotted in Fig. 6.7 with regard to the stresses at the outer radius. The theory behind this is elaborated in Appendix A6-1 if necessary, taking physical non-linearity into account.

6.2.4 Tensile tests

Although the tensile strength could be calculated from the torsion tests, there were still two reasons to perform tensile tests. The first reason was the verification of the results obtained from the torsion test, and the second to gain insight into the plastic flow (if any) of foamed concrete under tensile load.

The results of deformation controlled direct tensile tests are shown in Fig. 6.8 [Hordijk and Salet 1989].

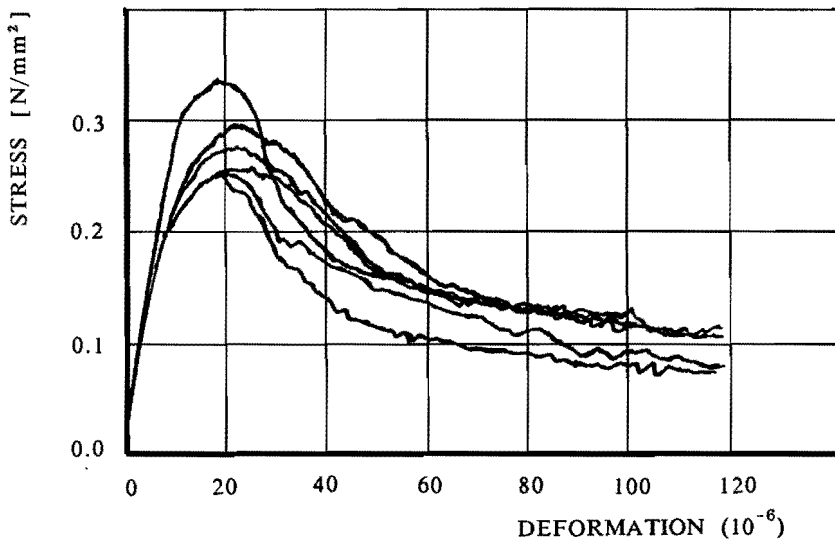


Fig. 6.8 Stress-deformation relation deformation controlled direct tensile tests.

6.2.5 Failure criterion for shear and normal load

Each state of shear stress can be transformed into principal stresses. This is graphically represented by Mohr's circles. In Fig. 6.9 Mohr's circles are shown for the ultimate states of pure tension, torsion and compression. These values are summarized in table 6.4 (section 6.5).

The ultimate state of stress in the core is described by an intrinsic curve. In Fig. 6.9 a linear intrinsic curve is assumed, similar to Sell and Zelger (1970) in research on autoclaved cellular concrete.

$$L: \tau = -1.12\sigma + 0.42$$

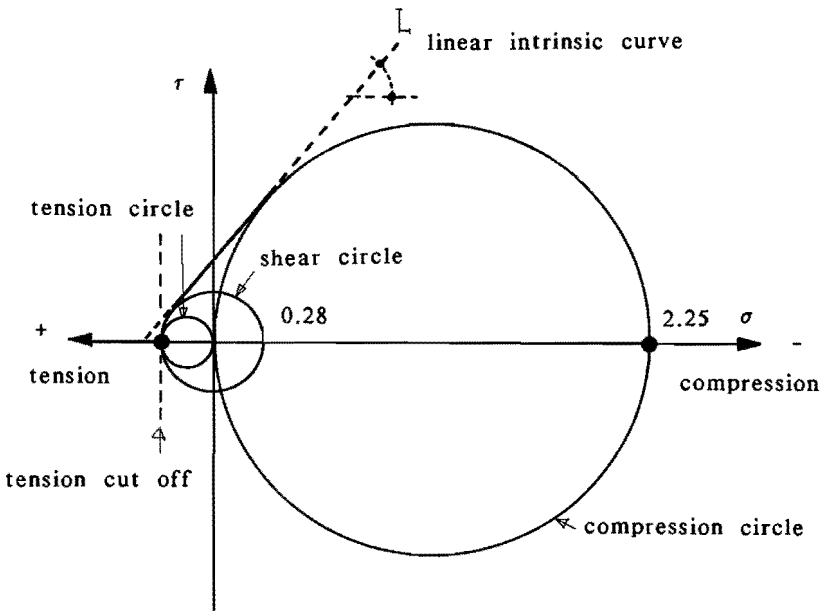


Fig. 6.9 Mohr's circles and the linear intrinsic curve.

6.2.6 Creep and shrinkage tests

Creep and shrinkage tests were performed. Since the core is biaxially loaded, both creep under compression load and shear load were studied. All tests started 28 days after the upper, concrete face of the sandwich was poured (see chapter 7). The specimens were stored in a control room at a relative humidity of 60 % and a temperature of 20°C.

Long-term tests on prisms

The creep and shrinkage tests were performed on prisms with the dimensions 100x100x500 mm³. The prisms for the creep tests were loaded in compression with 7500 [N] each, being approximately 1/3 of the ultimate load. The prisms for the shrinkage tests were not loaded. The deformations were measured with a pfender gauge on two opposite casting surfaces with a measuring length of 300 mm.

A schematic view of the testing rig [see Cornelissen, 1979 and Rusch, 1960] is given in Fig. 6.10. The test results are plotted in Fig. 6.11 and 6.12.

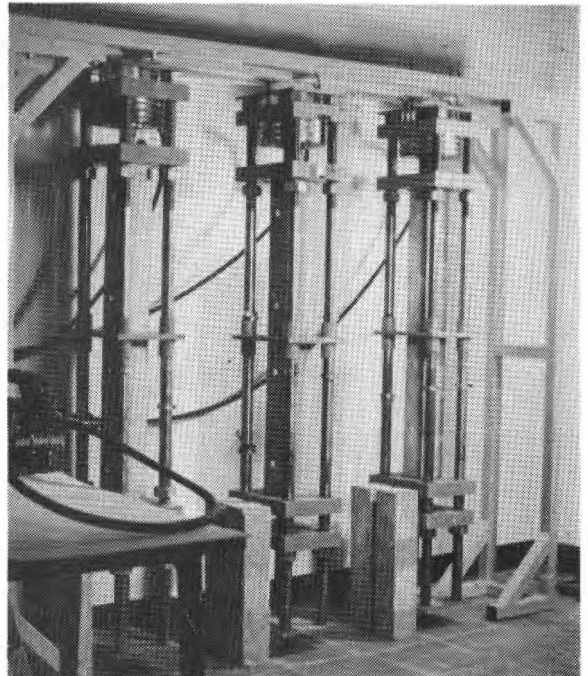
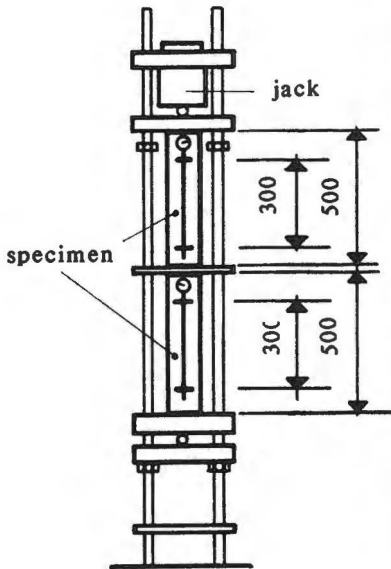


Fig. 6.10 Schematic view of the creep testing rig on prisms.

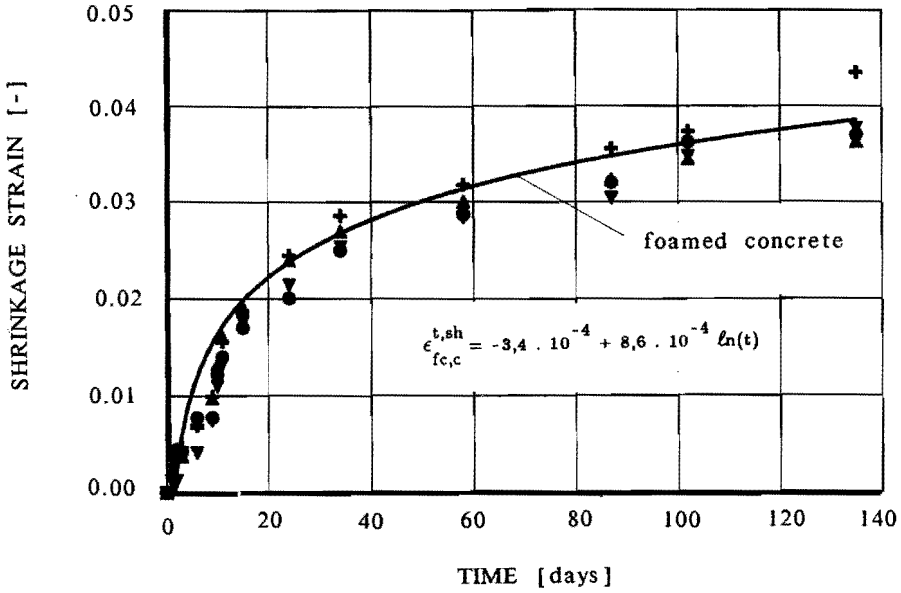


Fig. 6.11 Shrinkage of foamed concrete measured on prisms. The shrinkage measured on the hollow circular cylinders is within the same range.

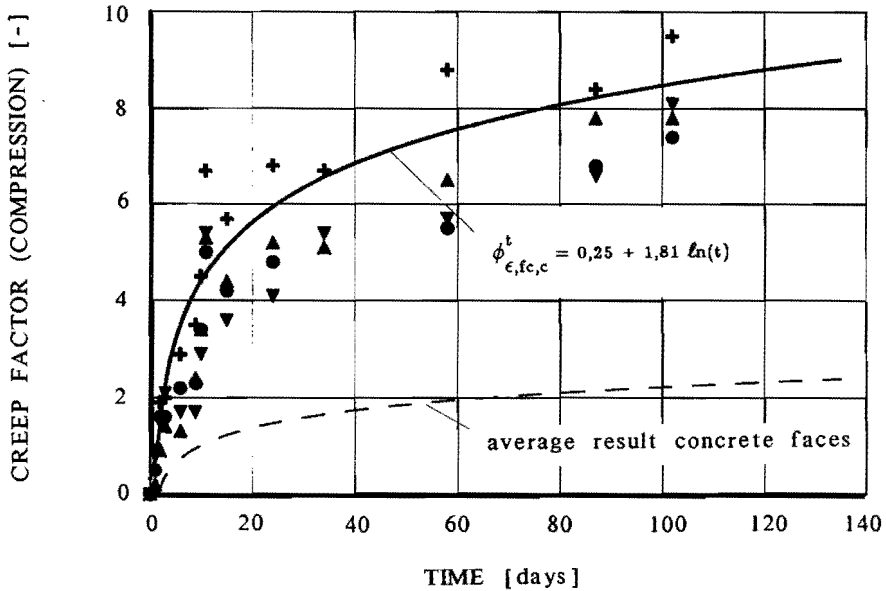


Fig. 6.12 Creep of foamed concrete loaded in compression, i.e. $\phi_{\epsilon,fc} = \epsilon_{fc}^{cr,t} / \epsilon_{fc}^{t=0}$. The creep is calculated as the total time-dependent deformation minus shrinkage.

Long-term tests on hollow circular cylinders

Creep tests, attended with additional shrinkage tests, were performed on hollow circular cylinders, from cast no. 2, described in Fig. 6.4. The short-term torsion testing system, shown in Fig. 6.5, was modified in order to perform long-term torsion tests. The general assembly of the long-term torsion testing system is shown in Figs. 6.13 and 6.14. Contrary to the loading application system used in the short-term torsion tests, no stiff steel rings were used. Stiff rings would definitely cause failure of the specimens due to shrinkage. Instead six small steel plates were glued onto the surfaces of the specimens as shown in Fig. 6.4. The torsional moment of 0.126 kNm, being about 1/10 of the ultimate torsional load, is introduced using six vertical loads of 300 N, acting on both the upper and lower surface with 150 N. The deformations were measured with four LVDTs, as described in Fig. 6.4.



Fig. 6.13 General assembly of the long-term torsion creep testing rig.

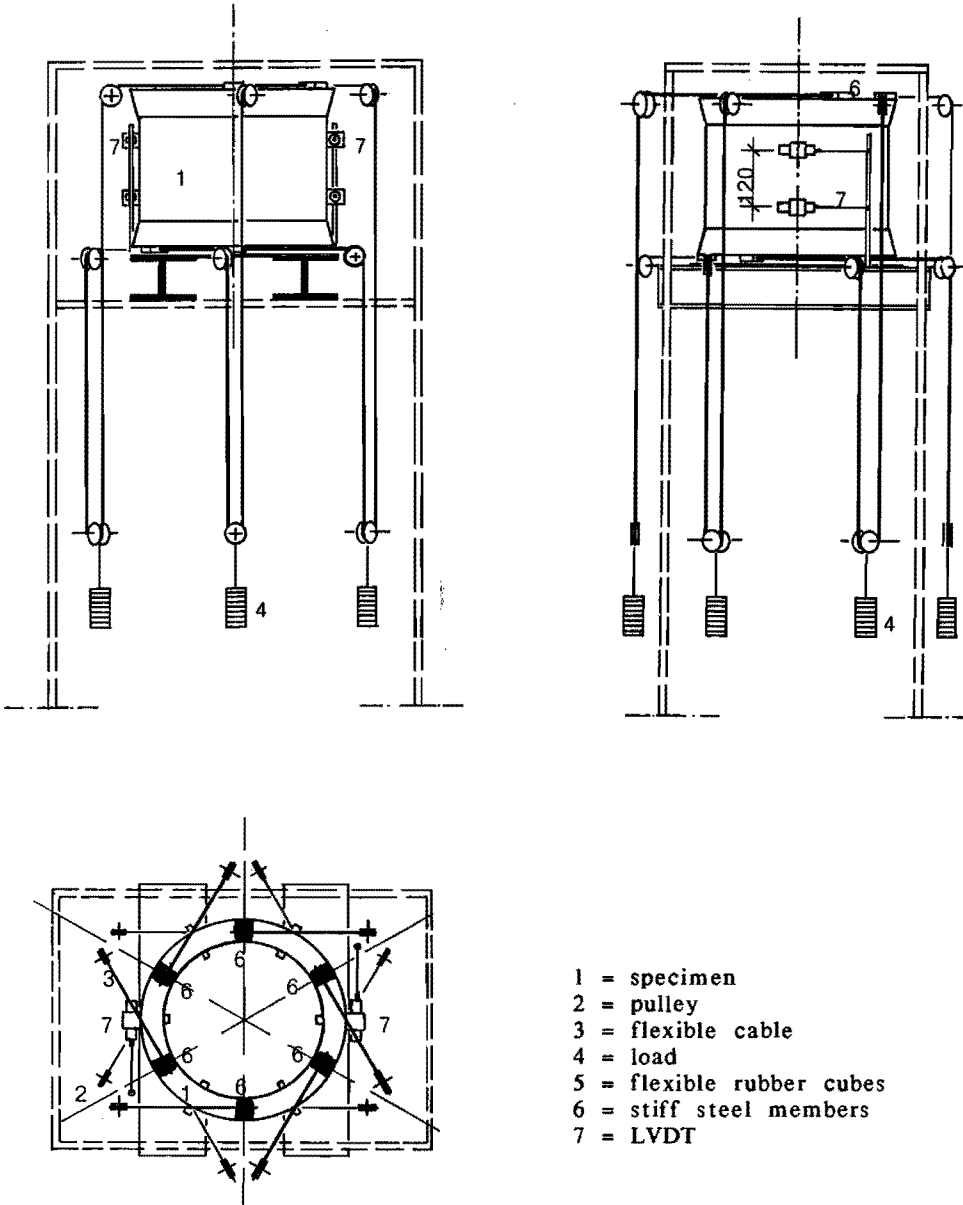


Fig. 6.14 Schematic view of the long-term torsion creep testing rig.

The results of two tests + and δ are given in Fig. 6.15. The results show a large variance. The average result is slightly higher compared with the creep of foamed concrete under sustained compression, as shown in Fig. 6.12.

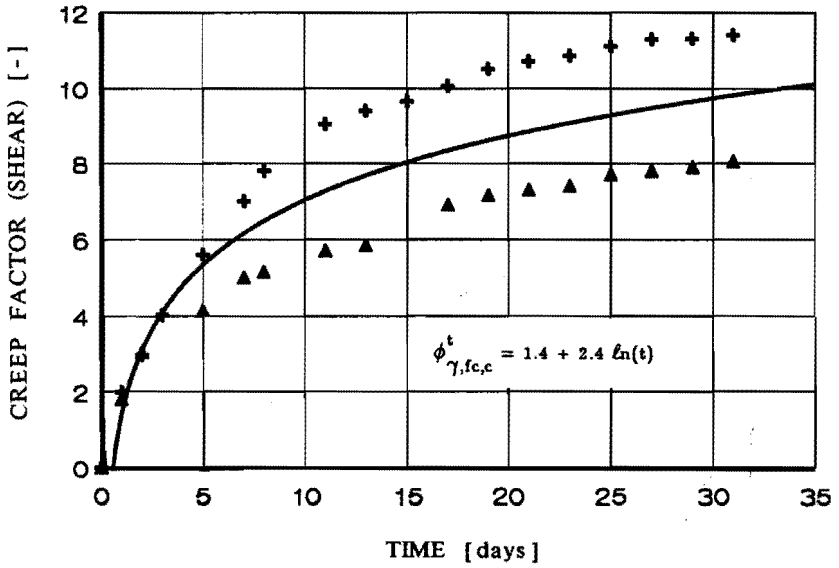


Fig. 6.15 Creep of foamed concrete loaded in shear, i.e. $\phi_{\gamma} = \gamma^{cr,t} / \gamma^{t=0}$.

6.3 Concrete

6.3.1 Mix proportions

In order to construct sandwich beams with an upper and lower face thickness of about 20 mm, the maximum aggregate size chosen was 8 mm. The contents of cement, coarse aggregate, sand and water are given in table 6.3. For all the tests the same mix was used.

Table 6.3 Mix quantities of the fresh concrete.

| Mix designation | Mass quantities (kg/m ³) | | | | Volume quantities (m ³ /m ³) | | | |
|-----------------|--------------------------------------|-------|-------|------|---|-------|-------|-------|
| | Cement | Water | Grain | Sand | Cement | Water | Grain | Sand |
| C2400 | 340 | 187 | 1275 | 590 | 0.110 | 0.187 | 0.500 | 0.203 |

Contrary to foamed concrete, an ordinary portland cement (type A) was used. The storing conditions of the specimens correspond with the storage of foamed concrete, described in chapter 6.2.1.

6.3.2 Compression and tension tests

All tests were performed on small prisms with the dimensions 40x40x160 mm³, as shown in Fig. 6.16. The tests were deformation controlled at a rate of 0.5 mm/min.

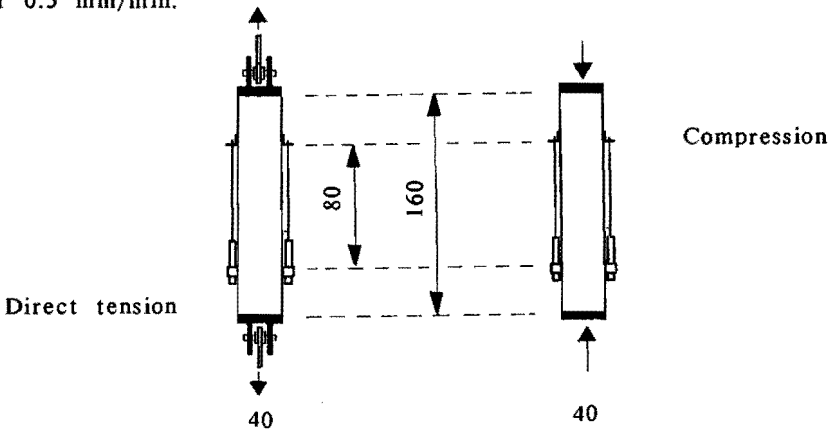


Fig. 6.16 Concrete compression and tension test specimens prepared for testing.

The best fitting test results for the concrete samples under compression are given in Fig. 6.17, the test results for the concrete samples under tension are given in Fig. 6.18.

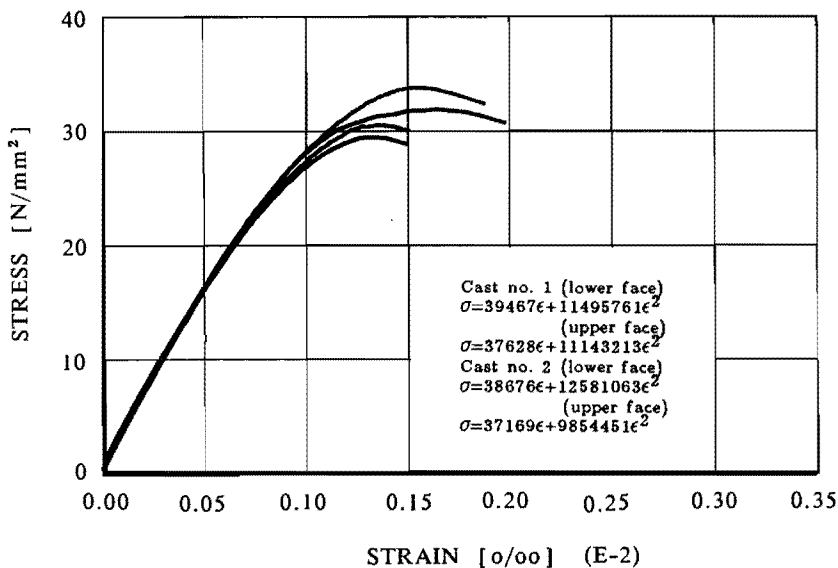


Fig. 6.17 Typical stress-strain relationships for concrete (cast no. 1, upper face) under compression and the best-fitting equations.

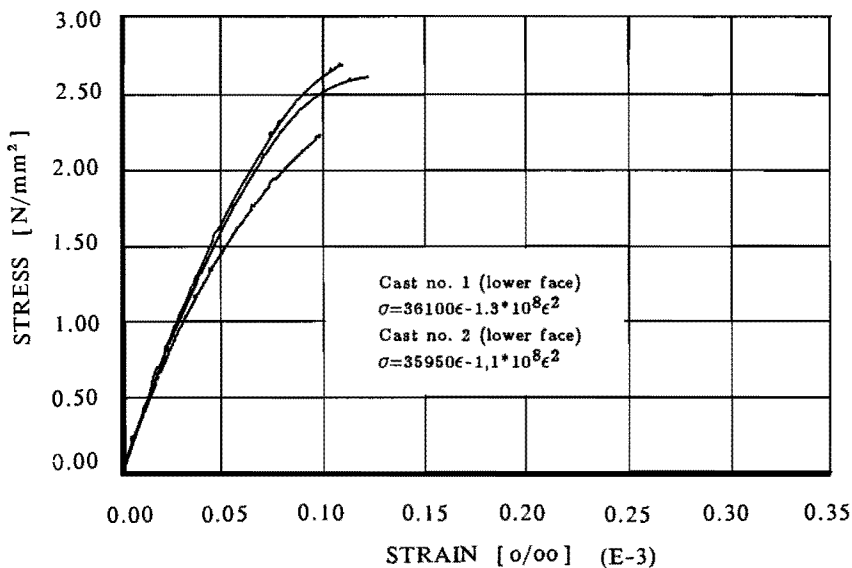


Fig. 6.18 Typical stress strain relationships for concrete (cast no. 1, lower face) under tension and the best-fitting equations.

6.3.3 Creep and shrinkage tests

Creep and shrinkage tests were performed on prisms with the dimensions 100x100x500 mm³. Four prisms for the creep tests were loaded in compression with 100 kN each, being about 1/3 of the ultimate load. The four prisms for the shrinkage tests were not loaded. Deformations were measured with dial gauges with a measuring length of 300 mm. All tests started 28 days after casting. The specimens were stored in a control room at a relative humidity of 60% and a temperature of 20°C. A schematic view of the testing rig is shown in Fig. 6.11.

The creep again is calculated as the total time-dependent deformation minus the shrinkage deformation. The test results are given in Figs. 6.19 and 6.20.

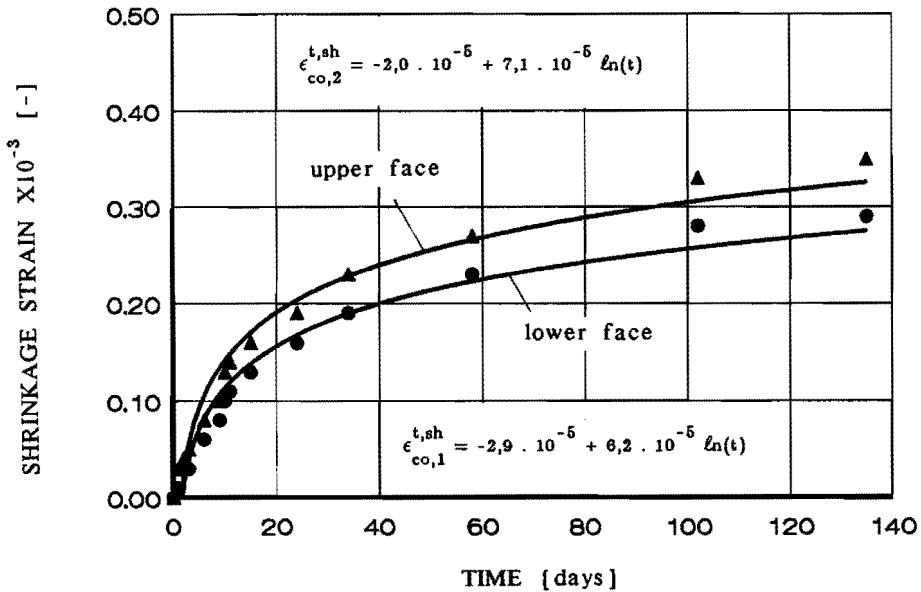


Fig. 6.19 Shrinkage of the concrete faces.

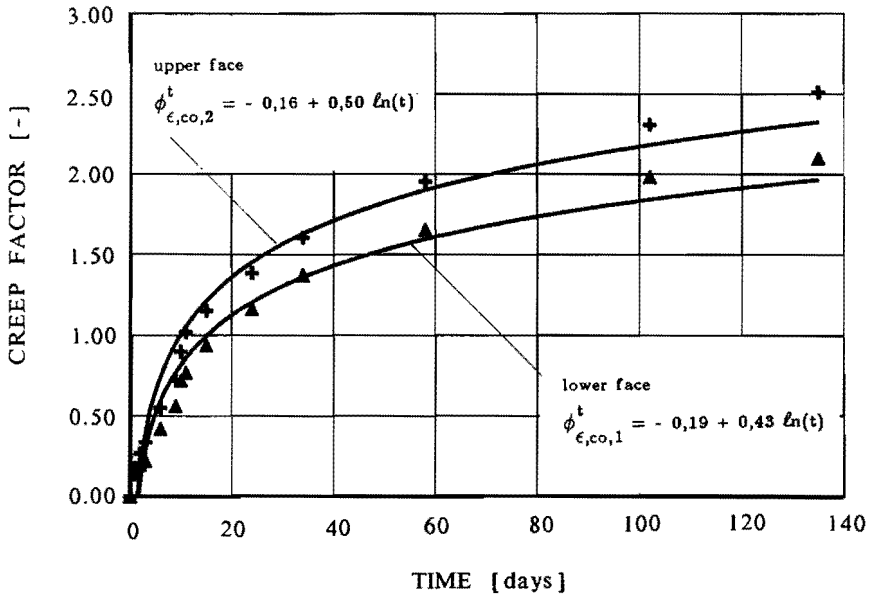


Fig. 6.20 Creep of the concrete faces, i.e., $\phi_{\epsilon,co}^t = \epsilon_{co}^{cr,t} / \epsilon_{co}^{t=0}$.

6.4 Reinforcement

The stress-strain relation for the main reinforcement under tensile load was studied by means of deformation controlled tensile tests on bars with a length of 500 mm. The applied deformation rate was 0.5 mm/min. The deformations were measured with a pfender gauge with data storage equipment, on a measuring length of 100 mm. The stress-strain relation, together with the best fitting equations, are given in Fig. 6.21.

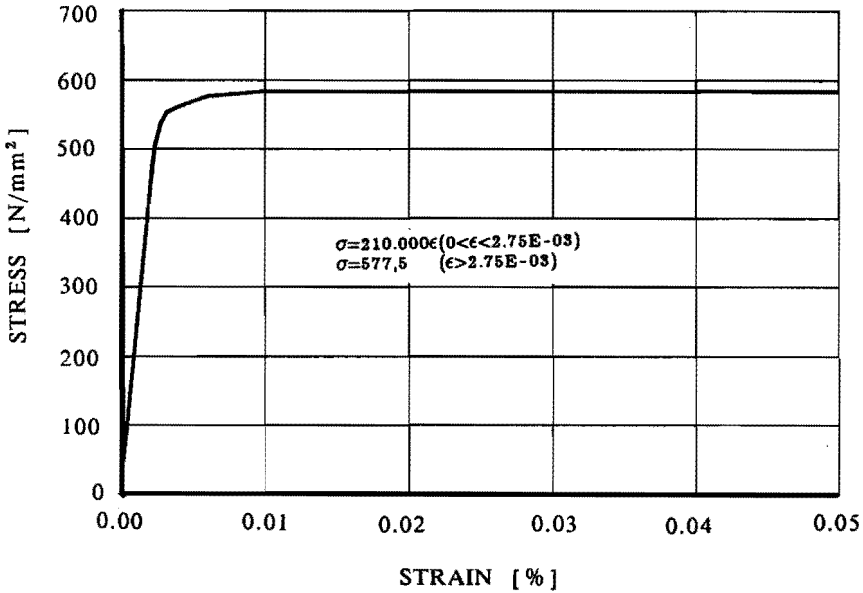


Fig. 6.21 Typical stress-strain relation of the reinforcement and the best fitting equations.

6.5 Summary of the test results

Values for the different parameters for the mechanical behaviour of foamed concrete are listed in table 6.4 and 6.5. The Young's modulus and the shear modulus of foamed concrete are determined by the secant modulus for the data points of a stress of about 1/3 of the average ultimate stress, being 0.075 N/mm² for both the torsion and deformation controlled direct tensile tests and 0.75 N/mm² for the compression tests. The Young's modulus of concrete is determined with linear regression analysis up to a stress of 10 N/mm² for the compression tests and 1 N/mm² for the tension tests.

Table 6.4. Average structural parameters of the concrete faces and the foamed concrete core under short-term load.

| Type of test | Parameter | Foamed concrete | | Concrete | | | |
|--------------|---|---|---|--|-------------|-------------|------------|
| | | Cast no.1 | Cast no.2 | Cast no. 1 | | Cast no. 2 | |
| | | | | lower face | upper face | lower face | upper face |
| Compression | strength f' [N/mm ²] | 2.25 (7.5) | 2.22 (9.9) | 33.2 (6.6) | 31.8 (5.8) | 34.8 (4.0) | 29.6 (6.3) |
| | strain ϵ' [mm/m] | 2.40 (12.0) | 2.16 (14.5) | 1.72 (2.3) | 1.61 (8.0) | 1.74 (9.0) | 2.0 (1.0) |
| | Young's E' [N/mm ²] modulus | 1303 (3.8) | 1489 (0.6) | 34.934(1.4) | 34.910(3.0) | 33492(2.8) | 32629(2.0) |
| Tension | strength f [N/mm ²] | 0.28 ³ (12.1) | - | 2.5 (14.4) | - | 2.7 (15.0) | - |
| | strain ϵ [mm/m] | - | - | 0.12 (35.0) | - | 0.12 (33.7) | - |
| | Young's E [N/mm ²] modulus | 1506 (12.0) | - | 36100(6.4) | - | 35950 (8.3) | - |
| Shear | strength f [N/mm ²] | 0.22 ¹ (14.0) 0.29 ² | 0.20 ¹ (16.1) 0.27 ² | () = statistical variance in % for four samples in each test 1) ultimate strength inner radius of the hollow circular cilinder 2) ultimate strength outer radius of the hollow circular cilinder 3) deformation controlled direct tensile tests, Hordijk and Salet, 1989 | | | |
| | shear G [N/mm ²] modulus | 384 (14.0) | 413 (9.9) | | | | |

Table 6.5 Average structural parameters of the concrete faces and the foamed concrete core under permanent load.

| Type of test | Symbol | Foamed concrete cast no. 2 | Concrete cast no. 2 | |
|----------------------------|-------------------------|-------------------------------|------------------------|---------------------|
| | | | lower face | upper face |
| Shrinkage | $\epsilon_{sh,t=135}$ | $4.10 \cdot 10^{-3}$ | $2.9 \cdot 10^{-4}$ | $3.5 \cdot 10^{-4}$ |
| | $\epsilon_{sh,t=28}$ | $2.5 \cdot 10^{-3}$ | $1.8 \cdot 10^{-4}$ | $2.2 \cdot 10^{-4}$ |
| Creep under compression | $\phi_{\epsilon,t=135}$ | 9 | 2.1 | 2.5 |
| | $\phi_{\epsilon,t=28}$ | 6 | 1.3 | 1.6 |
| Creep under shear | $\phi_{\gamma,t=28}$ | 10 | | |

6.6. Discussion and conclusions

The structural properties of the concrete faces, the foamed concrete core and reinforcement applied in the experimentally tested sandwich beams (chapter 7) are determined. A summary of the test results is given in the tables 6.4 and 6.5.

With respect to the foamed concrete used in the tests, the following conclusions are drawn:

Short-term behaviour

- (i) The shape of the σ - ϵ relationship is best fitted by means of the third order polynomial equation instead of a second order which is preferred for the normal concrete;
- (ii) The hollow circular cylinders loaded in torsion showed failure in the tensile mode. The ultimate tensile strength is found in these tests likewise to the tensile strength obtained from direct tensile test.

Long-term behaviour

- (i) The shrinkage of the foamed concrete after 135 days of exposure in a control room (r.h. = 60%) is about 13 times higher compared with the normal concrete;
- (ii) The creep factor depends on the type of load. In case of compression, the creep factor is 9 after 135 days. In case of a shear load, the creep factor is even about 30% higher;
- (iii) The shrinkage of the prisms and hollow circular cylinders is similar despite the different size of the samples.

7. EXPERIMENTAL RESEARCH AND VERIFICATION OF THE NUMERICAL MODEL.

7.1 Introduction

Rather few sandwich elements with concrete components are described in the literature. All studies described were found to be experimental and restricted to short-term tests. A review of the literature is given in table 7.1. The materials of the components are given, together with the typical cast order and loading conditions. Details with regard to the parameters investigated and the results obtained, are included.

Sandwich beams composed of both concrete facing and a lightweight concrete core have only been studied by Pfeifer et al (1965), Annamalai et al (1977) and Shendy el Barbary (1981). The main reason may be attributed to the difficulty of producing a lightweight concrete which can satisfy the recommended conditions of the core. Pfeifer et al (1965), Pathan (1982) and Lee et al (1986) studied sandwich beams with concrete faces and polystyrene cores. Typical shear connectors were provided in at least one of the test series performed by Pfeifer (1965) and Lee et al. (1986).

Zerjeski (1982) constructed, amongst others, hybrid faces consisting of a thin profiled steel upper sheet and a fibre reinforced concrete lower face. Various lightweight aggregate concrete cores were tested. Vogel (1983) also used different materials for both faces. However, the thin profiled steel and fibre reinforced concrete faces were connected by screws instead of by a lightweight aggregate concrete core. An extended survey of both studies has more recently been given by Jungbluth (1986).

This chapter describes the construction and testing of a new type of sandwich beam comprising a foamed concrete core and bar reinforced concrete facing. The flexural behaviour was studied, with respect to both short-term and long-term performance. The major parameter of the study was the method of shear transfer between the faces. Tests were conducted on sandwich beams with and without traditional full beam shear connectors.

Table 7.1 Experimental research on reinforced concrete sandwich beams

| Author | Specimen and cast order | Type of loading | Parameters ** | Results ** |
|--------------------------|--|-----------------|---------------|------------|
| Pfeifer (1965) | <p>2 — light-weight 1 — aggregate 2 — concrete</p> | | 1,2,5 | a |
| Annamalai (1977) | <p>2 — ferro-cement 1 — gas concrete 2 — ferro-cement 1 — ferro-cement</p> | | 1,2,4 | a,b,c,d |
| Shendy (1981) | <p>3 — ferro-cement 2 — polystyrene concrete 1 — ferro-cement</p> | | 1,5 | a,b,d,e |
| Parton and Shendy (1982) | <p>3 — ferro-cement 2 — polystyrene concrete 1 — ferro-cement</p> | | | |
| Zerjeski (1982) | <p>1 — folded steel plate 2 — glass fibre reinforced concrete 3 — folded steel 1 — folded steel</p> | | 5,1,3,7 | a,b,d |
| Pathan (1982) | <p>3 — glass fibre reinforced high alumina cement 1 — polystyrene 2 — glass fibre reinforced high alumina cement</p> | | | a,b,c,d |
| Vogel (1982) | <p>3 — folded steel plate 2 — light-weight concrete 1 — folded steel plate</p> | | 2,3,4,5 | a,b,d |
| Lee (1986) | <p>3 — bar and wire reinforced mortar 1 — polystyrene 2 — bar and wire reinforced mortar</p> | | 1,2,4,5 | a,c,d |

*) Documentation on the works of Wright (1977) and Saglam (1979) could not be made available.

***) The meaning of the designations is given on the next page.

designations

| parameters | results |
|---|------------------------------------|
| 1. Type and/or amount of face reinforcement | a. Deflection |
| 2. Type and/or amount of shear connectors | b. Strains/stresses |
| 3. Core thickness | c. Crack load and/or crack pattern |
| 4. Face thickness | d. Failure load and failure mode |
| 5. Core material and/or mix proportions | e. Position of the centre-line |
| 6. Face material and/or mix proportions | |
| 7. Span of the beam | |

The experimental test results are compared with the results calculated by the finite difference analysis described in previous chapters.

7.2 Specimens characteristics and manufacture

A total of twelve concrete sandwich beams spread over two different casts were constructed. The eight specimens of the first cast were submitted to a short-term test, while the four specimens of the second cast were studied under permanent load. The overall length of the samples was 2500 mm with a width of 280 mm. Details of the beam cross-section are given in table 7.2.

The main parameter of the test specimens refers to the type of reinforcement provided. Six samples were provided with only a main reinforcement (designated with MR = Main Reinforcement) in the lower face. The main reinforcement consisted of three ribbed steel bars, with a diameter of 6 mm each. The other samples were provided with a reinforcing cage, consisting of the same main reinforcement in the lower face (3 ϕ 6 mm), additional reinforcement in the upper facing (2 ϕ 6 mm) and shear connectors (2 ϕ 4 mm) in between (see Fig. 7.1).

These specimens were designated with SMR (SMR = Shear and Main Reinforcement). The reinforcements were placed in the centre of each face.

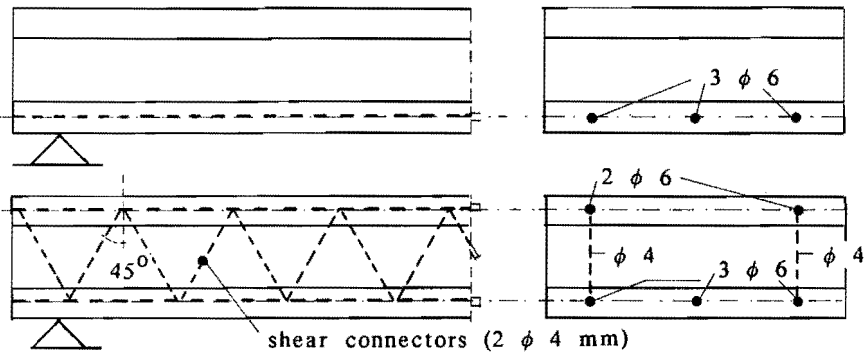


Fig. 7.1 Geometry of the samples

Table 7.2 Details of the test specimens

| Specimen no. | Type of testing | Series designation | Layer thickness [mm] | | | Details of reinforcement [mm] | | |
|--------------|-----------------|--------------------|----------------------|------|------------|-------------------------------|-------|------------------|
| | | | lower face | core | upper face | bottom face | top | shear connectors |
| 1,2,3,4 | ST | MR | 25 | 60 | 20 | 3 φ 6 | none | none |
| 9,10 | LT | | | | | | | |
| 5,6 | ST | SMR | 35 | 70 | 30 | 3 φ 6 | 2 φ 6 | 2 φ 4 |
| 7,8 | ST | | 30 | 60 | 30 | | | |
| 11,12 | LT | | | | | | | |

MR = Main Reinforcement

ST = Short Term

SMR = Shear and Main Reinforcement LT = Long Term

Three different techniques of beam manufacture were studied in preliminary tests on small sandwich beams [Appendix A7-1]. From the test results a typical cast order was preferred, with respect to the structural adhesion between concrete and foamed concrete.

In the first stage, the foamed concrete core was poured and covered with wet cloth and foil. In case of the beams provided with shear connectors, the complete reinforced cage was located in the mould before casting. After seven days, the moulded face was rubbed with sand-paper to remove the closed and shining cement film. In case of the samples from the series MR, the main reinforcement was located at the desired cover from the foamed concrete.

The lower concrete face was poured on a moisty foamed concrete and the samples were covered with wet cloth and foil. After two days, the samples were turned round and the upper concrete layer was cast and stored in the same way. None of the layers was vibrated after casting, in order to protect the brittle cellular structure of the foamed concrete. The beam was demoulded after two days and stored in a control room at a relative humidity of near 100% and a temperature of 20°C.

The proportions and properties of the concrete, foamed concrete and steel reinforcement used, are described in chapter 6.

7.3 Short-term tests

7.3.1 Test performance

Flexural tests were conducted on simply supported beams on a free span of 2400 mm. Seven out of eight specimens were tested in an approximately uniform distributed load condition, using a ten point loading system. One specimen (no.4) was studied under a four point bending test. The load was applied to the specimens by a hydraulic jack using a spreader beam. The jack was displacement controlled, operated by a function generator. The applied displacement rate of the jack was 0.002 mm/sec. A spherical head was placed between the rigid head of the testing machine and the load distribution beam. The effects of the horizontal thrusts were eliminated by roller bearings. At the loading and support points, 12 mm thick and 40 mm wide steel ribs are provided for an uniform load distribution. A schematic view of the testing rig and data acquisition system is given in Fig. 7.2.

The jack load was determined by means of a load cell. Deflections were registered using LVDTs at several locations along the axis of the beam as shown in Fig. 7.3. Besides deflections, one out of two types of strain measurements were performed. In the first type, designated as SR (Strain Readers), deformations at the outer surface of both the upper and lower face were recorded by means of strain readers (see Fig. 7.3). Notice that after cracking within the span of a strain reader, the crack width instead of the concrete strain was measured. The location of nine strain readers at the bottom face and two strain readers at the top face is shown in Fig. 7.3. The second type of strain measurements designated as SG (Strain Gauge) consists of strain gauges glued onto the reinforcement before casting.

The location of the strain gauges is shown in Fig. 7.3. All signals were recorded every two seconds.

7.3.2 Test results and discussion

Load-Deflection

The jack load versus midspan deflection curves for the similar test specimens are plotted in Figs. 7.4 to 7.7.

The structural behaviour of the sandwich beams is also numerically calculated by means of the finite difference analysis, presented in previous chapters. The material properties adopted are described in chapter 6. The numerical results are plotted in the same figures with dotted lines. Values of both the crack load and ultimate load are summarized in table 7.3.

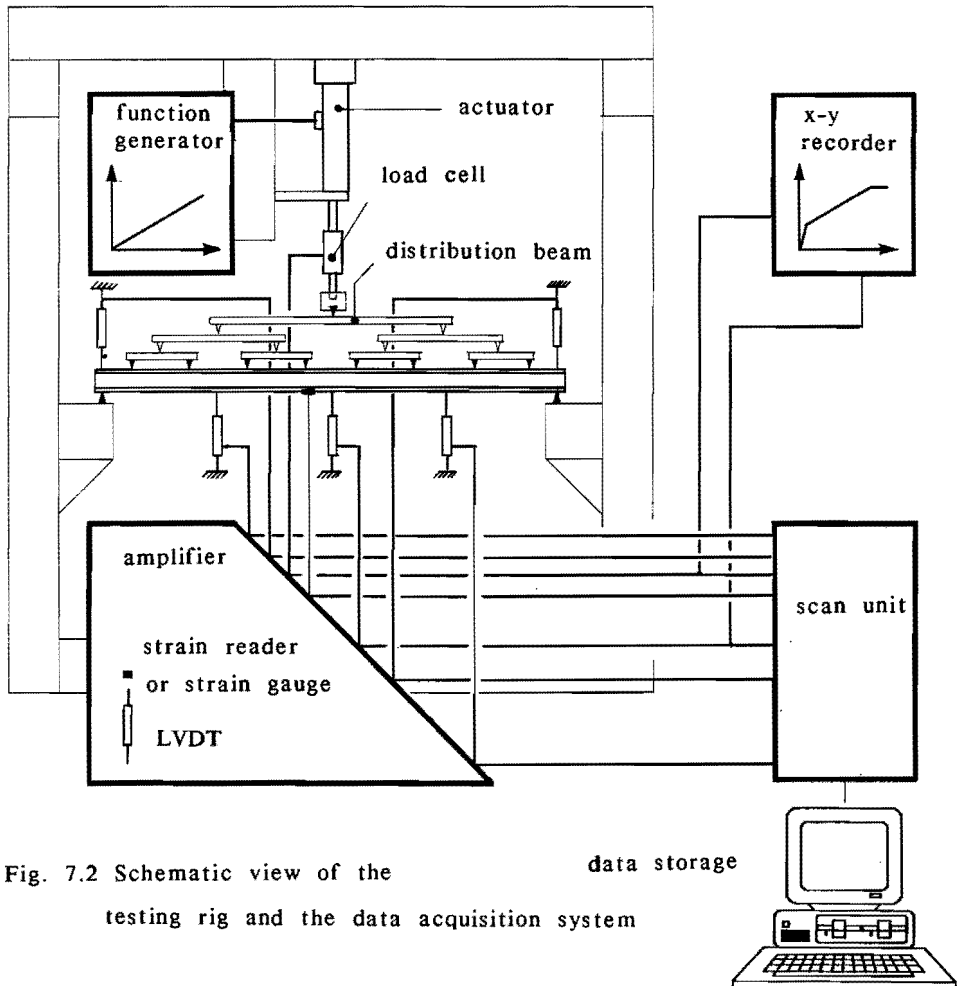
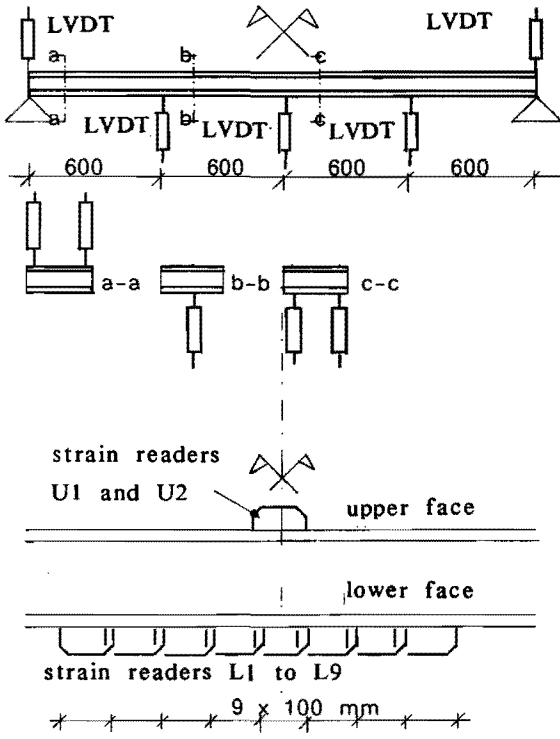


Fig. 7.2 Schematic view of the testing rig and the data acquisition system



| Beam no. | Measurement | | |
|----------|-------------|--------|----|
| | Deflection | Strain | |
| | | SR | SG |
| 1,2,5,6 | • | • | |
| 3,4,7,8 | • | | • |

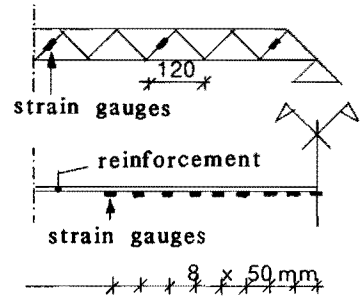


Fig. 7.2 Location of the measuring devices short-term tests

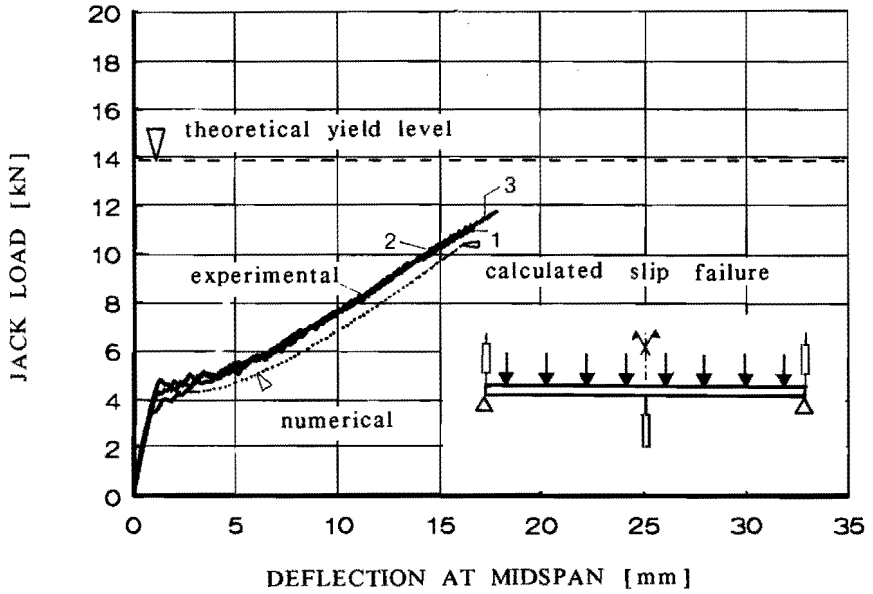


Fig. 7.4 Load-deflection relationships up to failure of the specimens 1,2 and 3 (series MR) and the result of the calculations.

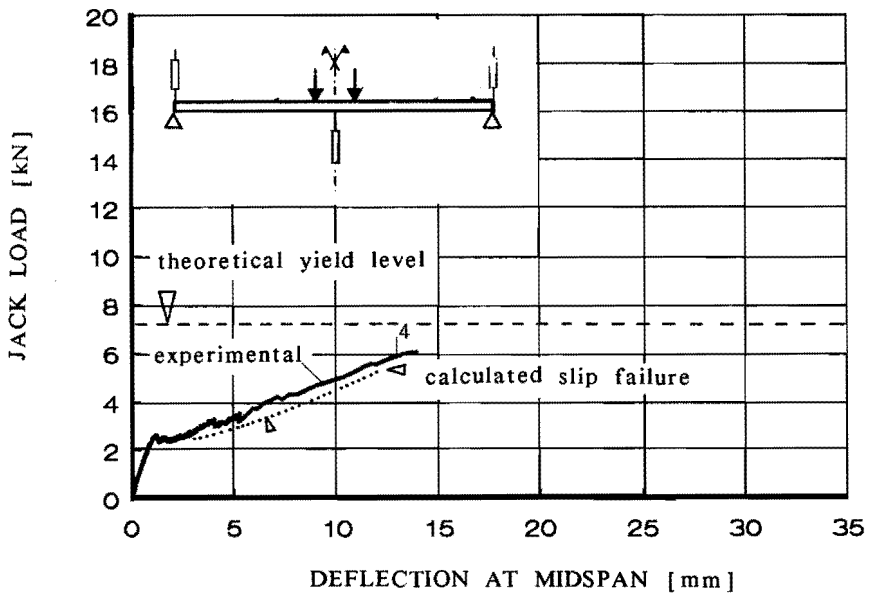


Fig. 7.5 Load-deflection relationship up to failure of specimen 4 (series MR) and the result of the calculations.

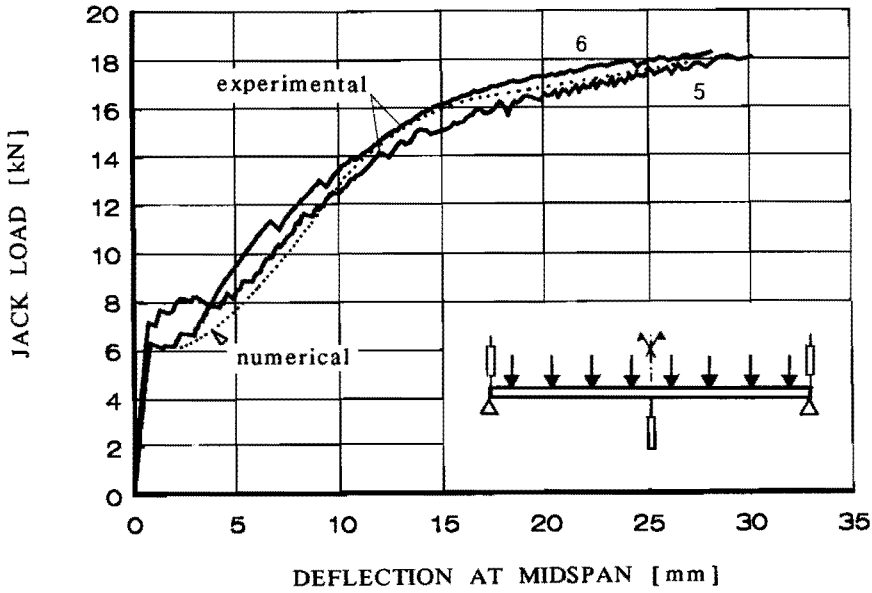


Fig. 7.6 Load-deflection relationship specimens 5 and 6 (series SMR) and the result of the calculations.

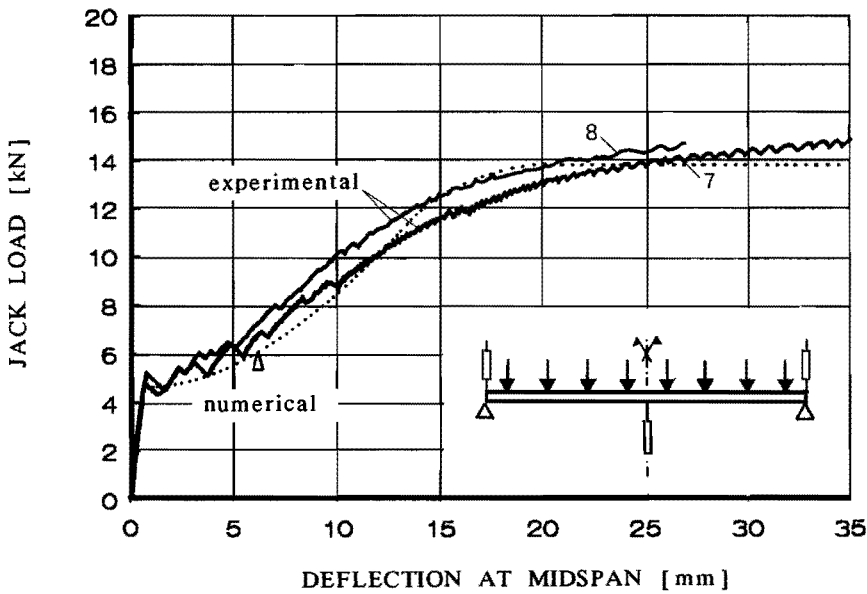


Fig. 7.7 Load-deflection relationship specimens 7 and 8 (series SMR) and the result of the calculations.

Table 7.3 Details of the experimental load-deflection relationships

| Specimen no. | Crack | | | Ultimate | | | Type of mode failure |
|--------------|-----------|--------------|-----------------|-----------|--------------|-----------------|--|
| | load [kN] | moment [kNm] | deflection [mm] | load [kN] | moment [kNm] | deflection [mm] | |
| 1 | 4.26 | 1.21 | 1.36 | 10.78 | 3.07 | 16.73 | horizontal slip failure |
| 2 | 4.79 | 1.37 | 1.34 | 10.16 | 2.90 | 14.50 | |
| 3 | 3.48 | 0.99 | 0.88 | 11.77 | 3.35 | 17.83 | |
| 4 | 2.63 | 1.34 | 1.23 | 6.09 | 3.10 | 13.97 | |
| 5 | 6.31 | 1.80 | 0.82 | ≥ 18.13 | ≥ 5.17 | ≥ 30.18 | yield of the reinforcement in the lower face |
| 6 | 7.13 | 2.03 | 0.72 | ≥ 18.31 | ≥ 5.22 | ≥ 28.20 | |
| 7 | 4.80 | 1.37 | 0.65 | ≥ 14.74 | ≥ 4.20 | ≥ 26.94 | |
| 8 | 5.24 | 1.49 | 0.73 | ≥ 14.98 | ≥ 4.27 | ≥ 35.79 | |

Bending moment capacities are included in order to facilitate comparison between the ten point and four point bending tests.

The experimentally tested specimens behave in an elastic manner during the early loading, continuing to the point of flexural cracking. In all cases cracking is followed by a large increase of deflection. The specimens from the same series behave very similar up to failure.

All specimens exhibit considerable post-cracking strength and ductility before final collapse. The load-deflection curves in the post-cracking zone however, vary significantly between the different types of specimens, dependent on the method of shear transfer (with or without shear connectors).

This difference is caused by the type of failure mode. In case of series MR, the specimens showed failure due to horizontal slip of the core, near the support. The full bending-moment capacity is not reached. In fact, a diagonal tension crack and a horizontal crack developed within the foamed concrete core near the interface between the core and the lower face. There was no bond failure. The typical failure of the specimens 1 to 4 is shown in Fig. 7.8.

The final failure of the beams provided with a shear connector was never reached in the tests. The tests were finished with a continuing increase of deflection together with no substantial increase of the registered jack load obtained from the x-y recorder. This typical load deflection behaviour was caused by yield of the main reinforcement.

The Fig. 7.4. to 7.7. show that the numerically calculated load versus deflection relationships are in close agreement with the experimental results. The failure mode observed in the samples provided with shear connectors (yield at the main reinforcement) is affirmed by the numerical calculation. In case of the samples without shear connectors, the failure due to horizontal slip is predictable by means of the simplified model described in chapter 5. If the slip failure had been left out of account, the beam would numerically fail in bending due to yield of the reinforcement and not by shear (see also Figs. 7.6. and 7.7.)

Strain readers of the lower face surface

Typical crack patterns are shown in Fig. 7.9. Details of the crack load, crack strain and crack width are given in Appendix A7-2, table A1 to A4. Typical load-strain relationships are plotted in Fig. 7.10.

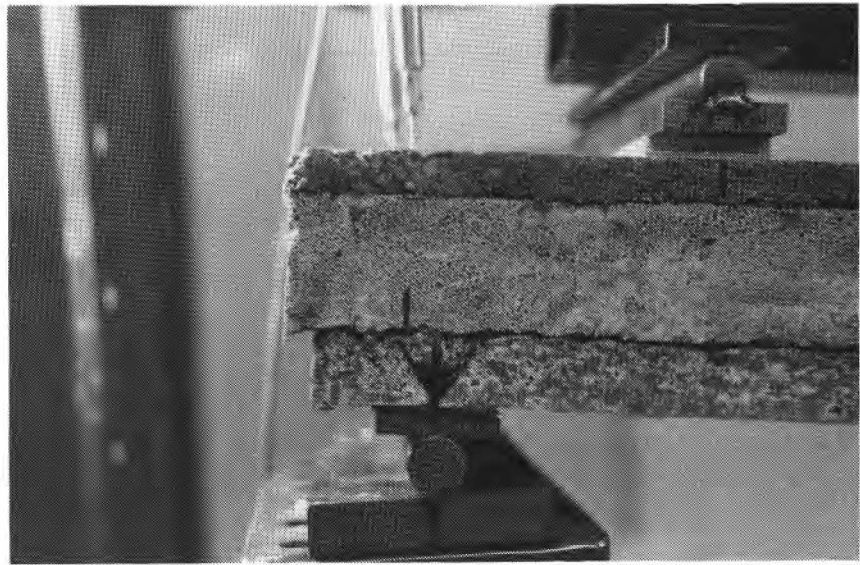
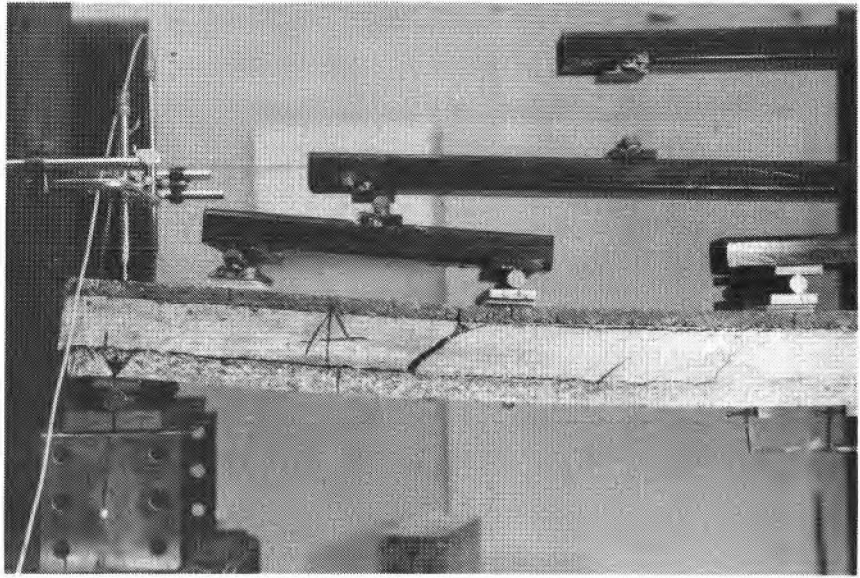
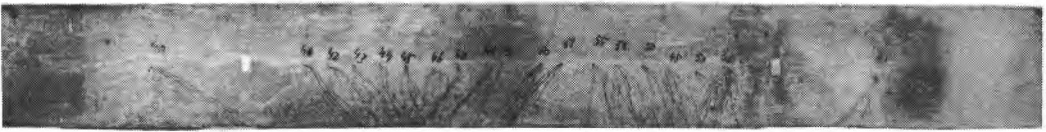


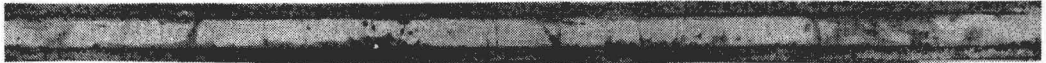
Fig. 7.8. Typical failure mode of the specimens without shear connectors (series MR)



Specimen no. 2 (series MR)



Specimen no. 4 (series MR)

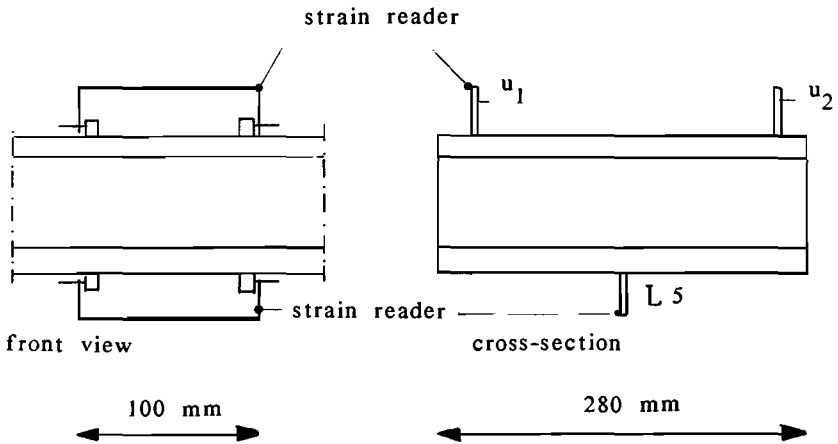
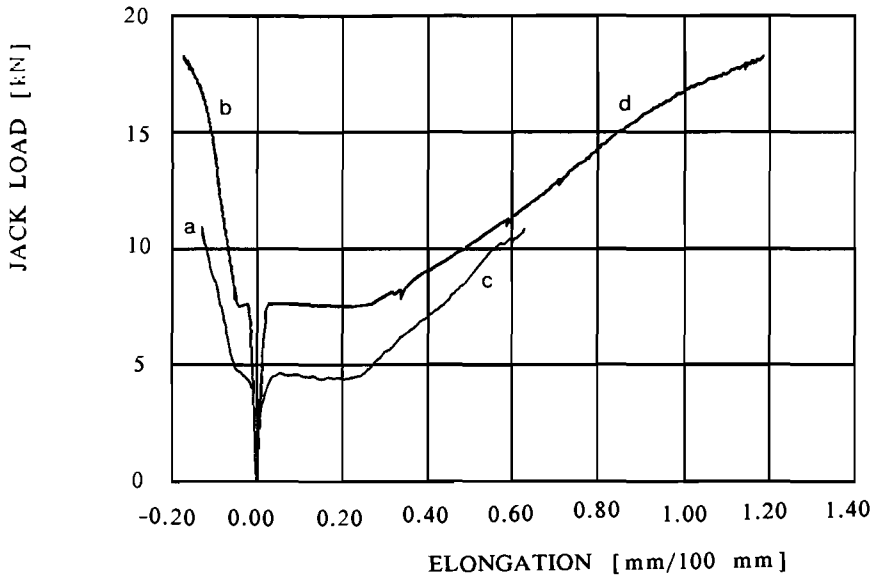


Specimen no. 6 (series SMR)



Specimen no. 7 (series SMR)

Fig. 7.9 Crack patterns of the lower faces and the distances between the cracks.



- a = average signal strain readers u_1 and u_2 (sample 2)
- b = average signal strain readers u_1 and u_2 (sample 6)
- c = signal strain reader L_5 (sample 2, MR)
- d = signal strain reader L_5 (sample 6, SMR)

Fig. 7.10 Typical load-strain relationships obtained from the strain readers at midspan.

All beams showed several cracks at regular distances, within the measuring zone (900 mm) of the reinforced concrete bottom face. The number of cracks and therefore the crack width (see appendix A7-2) depends on the percentage of reinforcement of the cracked lower face. The crack spacing is also numerically calculated by the discrete crack model described in chapter 3. The number of cracks in the reinforced concrete faces is numerically calculated with a parabolically distributed tensile load along the length. The material properties are given in table 6.4 while the following load-versus-slip relationship is adopted, i.e.

$$\tau = (0.07 + 0.32 \sqrt{\Delta u}) f_{co,tm} \quad [7.1]$$

Comparison between the results experimentally measured and calculated results are presented in table 7.4.

Table 7.4. The number of cracks calculated

| Specimen no. | percentage of reinforcement $\omega\%$ | number of cracks | | |
|--------------|--|------------------|-------|----------------|
| | | calculated | | experimental |
| | | measuring zone | total | measuring zone |
| 1/2/3 | 1,2 | 9 | 13 | 8 |
| 7/8 | 1,0 | 7 | 11 | 5,6 |
| 5/6 | 0,85 | 7 | 9 | 5,6 |

The load versus strain relationships obtained from the strain readers L_1 to L_9 , located at the lower face surface show that all cracks in a beam arose at an average concrete strain varying from 0.182 mm/m (specimen 5) to 0.240 mm/m (specimen 2). These strains are fairly high compared with the ultimate tensile strain of 0.15 mm/m measured on samples from the same cast (see chapter 6).

The last crack in each beam arose at less than 140% of the first crack load, with one exception.

* The adopted load-versus-slip relationship is the best fitting equations of the experimental results presented by Martin [1973] and Schiessl [1976]. See also Noakowsky [1978].

Strain readers upper face surface

Typical load-strain relationships are plotted in Fig. 7.10.

Details of the test results from the strain readers located on the upper face surface are given in table A5 (Appendix A7-2).

Strain gauges

A typical load-strain relation for various strain gauges is plotted in Fig. 7.11. A typical relation between the jack load and the tensile strain distribution along the main reinforcement in the lower face of the sandwich beam is shown in Fig. 7.12. The fluctuations in the strain demonstrate the origin of the cracks. No yield of the main reinforcement for the specimens of series MR is observed from the results.

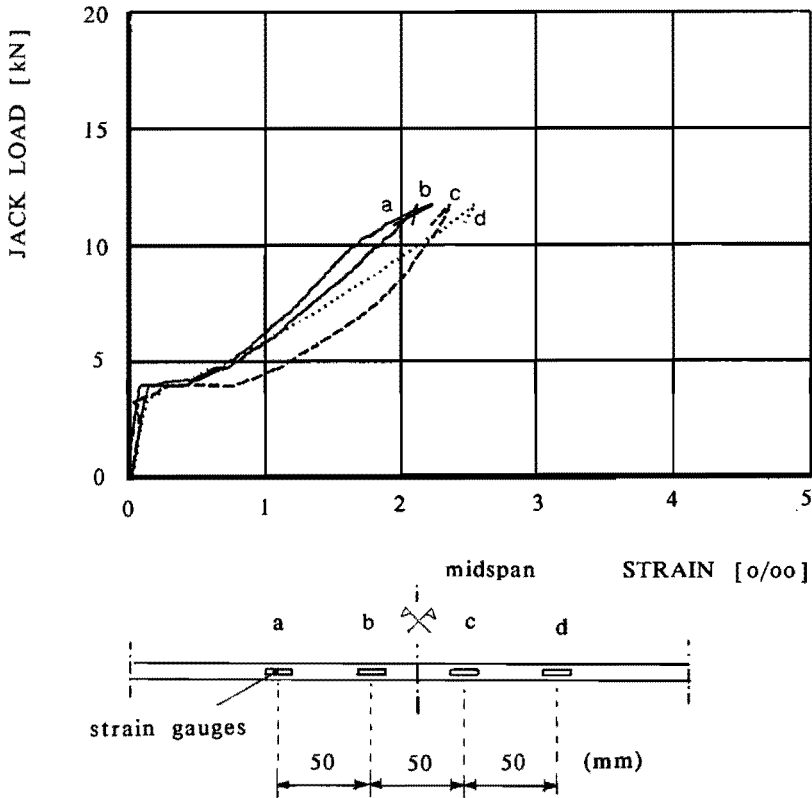
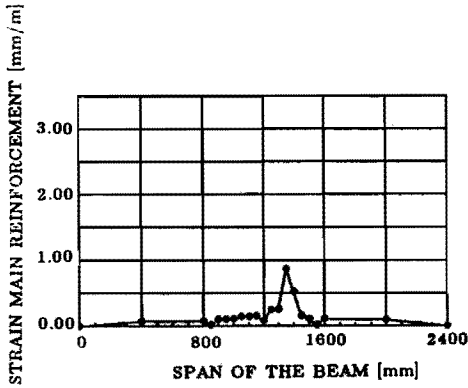
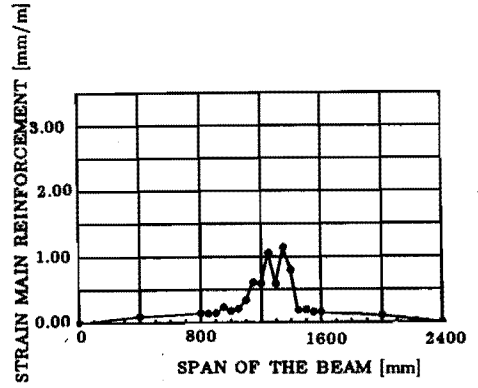


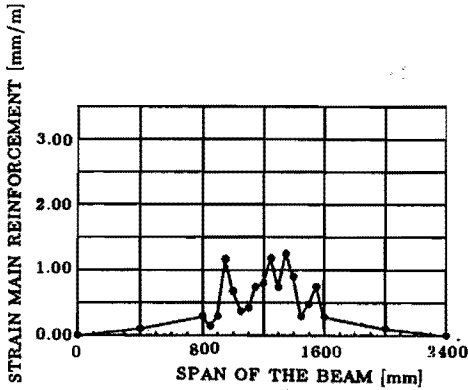
Fig. 7.11 Typical load-strain relationships obtained from the strain-gauges of sample no. 3 (without shear connectors).



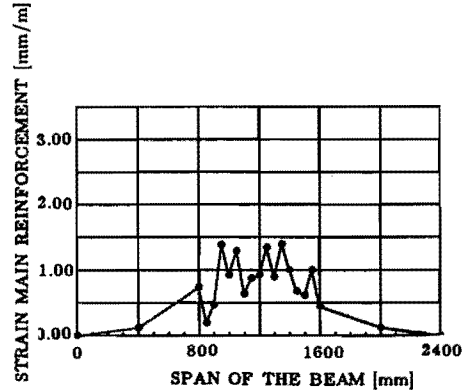
crack no. 1 (3819 N)



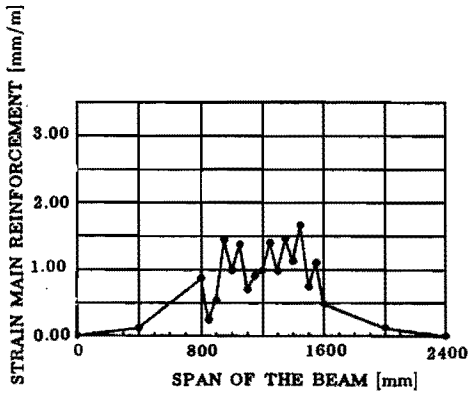
crack no. 2 (4674 N)



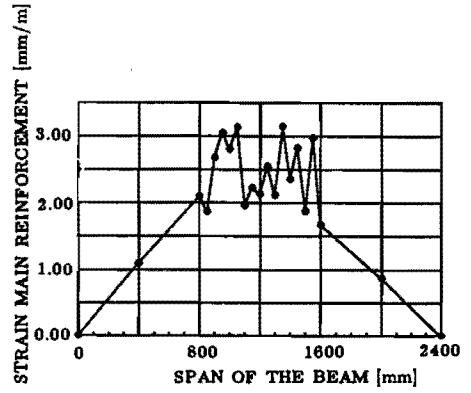
crack no. 3 and 4 (5020 N)



crack no. 5 and 6 (5577 N)



crack no. 7 and 8 (5834 N)



failure load

Fig. 7.12 Tensile strain distribution in the main reinforcement of specimen 3 (without shear connectors)

7.4. Long-term tests

7.4.1. Test performance

Long-term bending tests are conducted on 4 simply supported sandwich beams with reinforced concrete faces and a foamed concrete core. The dimension and the manufacture are described in section 7.2. The sides of the beams are provided with an epoxy coating in order to prevent the core from drying up through the sides. This is done in view of realistic conditions in case of wide slabs. Two out of four specimens are provided with shear connectors.

A ten-point loading system is used. The loading is applied by means of 8 separated weights of 400 N each, as shown in Fig. 7.13. Twenty-eight days after the last concrete face was poured the beams were stored in a control room at a relative humidity of 60% and a temperature of 20° C together with the control samples described in chapter 6. Four days later the beams were loaded. The beams were not cracked after loading. The deflections were measured by means of LVDTs at midspan and at the supports while the shear deformation of the core was registered using a digital pfender gauge. A schematic view of the tests and the measuring devices is shown in Fig. 7.13. The actually tested beams are shown in Fig. 7.14. The measurements started at the time of loading of the samples.

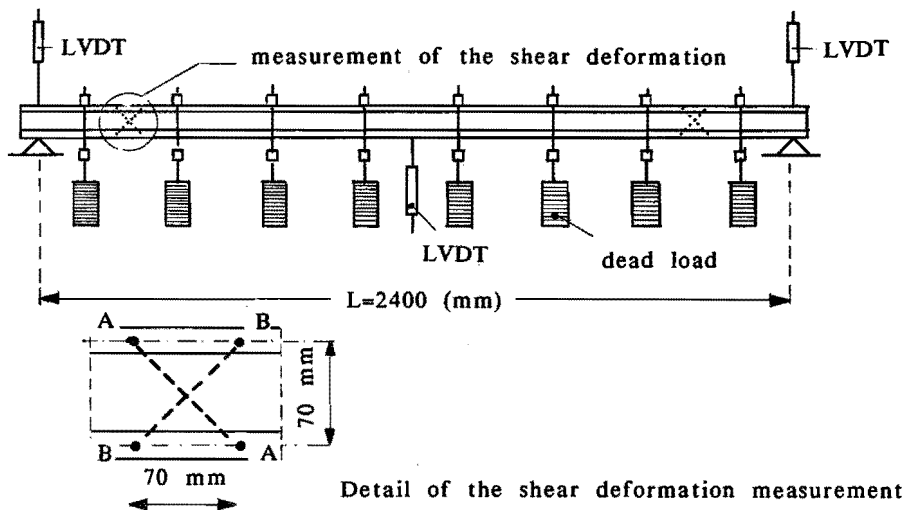


Fig. 7.13 Schematic view of the long-term tests and the measuring devices.

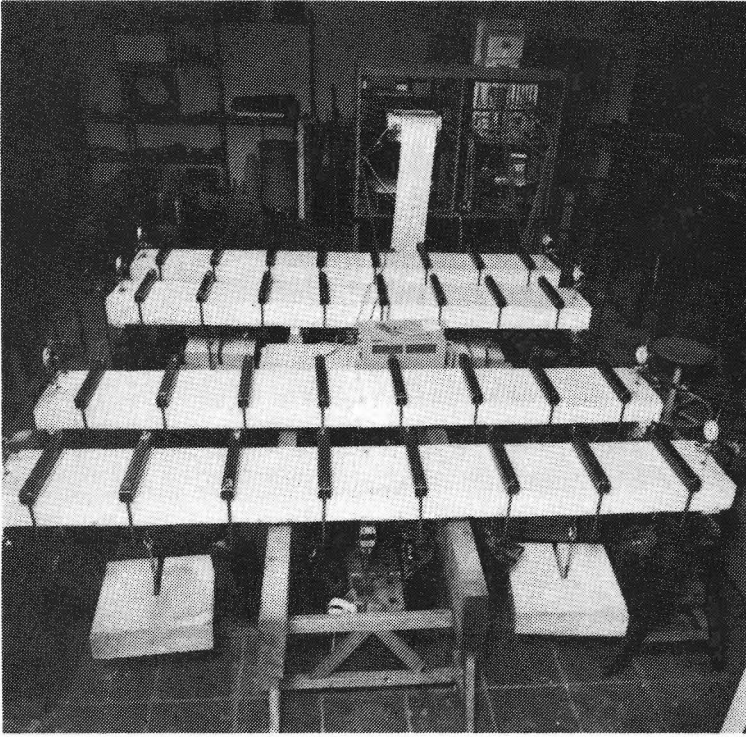


Fig. 7.14 Long-term tested sandwich beams

7.4.2. Test results

The time versus deflection relationships are shown in the Figs. 7.15 and 7.16 in case of sandwich beams without and with shear connectors respectively. The numerical results, obtained from the model described in chapter 4 and the material properties given in chapter 6, are included by the dotted lines.

The actual experimental results (denoted as c in the Figs 7.15 and 7.16) have been slightly adapted in order to allow comparison with the numerically calculated deflections. The adaptations are:

- (i) the immediate deflection ($t=0$) due to the dead-load of the beam (denoted with a in the Figs 7.15 and 7.16)
- (ii) the increase of deflection during the first four days of exposure in the control room due to shrinkage and creep caused by the dead-load only. (denoted with b in the Figs 7.15 and 7.16). The adaptations have been calculated by the numerical model.

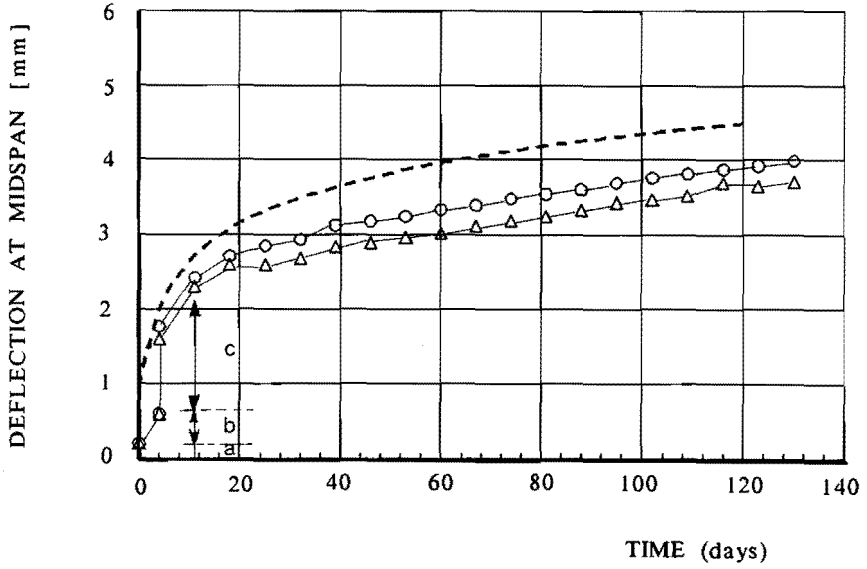


Fig. 7.15 Time versus deflection at midspan relationship of the beams without shear connectors (no. 9 and 10) (MR)

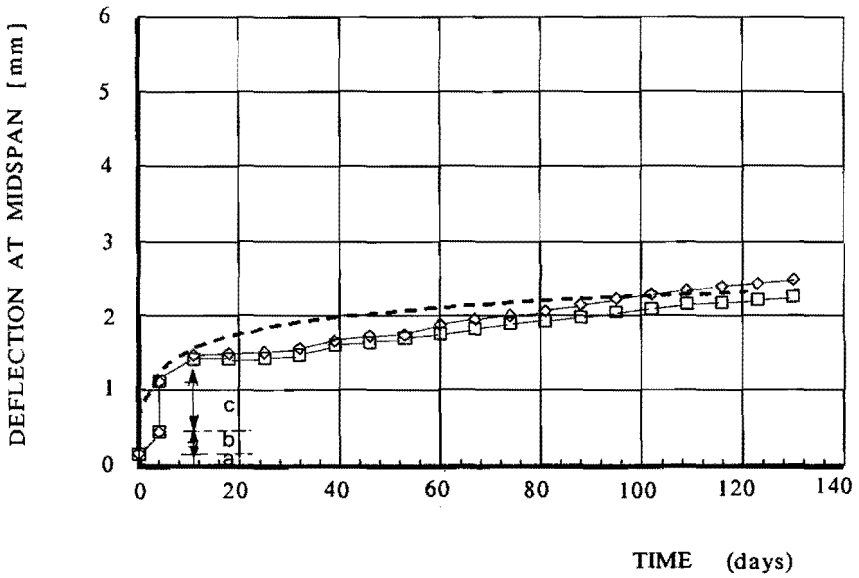


Fig. 7.16 Time versus deflection at midspan relationship of the beams with shear connectors (no. 11 and 12) (SMR)

The results show that the deflections calculated are of the same order of magnitude as the experimental results. In case the sandwich beams are not provided with the shear connectors, the numerically calculated and actually tested time versus deflection relationships are similar in shape. The shape of the time versus deflection relationship corresponds to the shape of the creep and shrinkage curves for both concrete and foamed concrete, described in the previous chapter. The beams provided with a shear connector show an irregular behaviour in the second and third week after loading ($t=7$ until $t=28$ days).

It is noticed that the deflections in case of sandwich beams provided with shear connectors are substantially smaller compared with the beams without shear connectors. This difference is caused by the following parameters:

- (i) the slightly different dimension of the upper and lower faces;
- (ii) the shear connector;
- (iii) the reinforcement in the upper face.

The influence of these parameters on the deflection at midspan is investigated by means of the numerical model. It is shown in table 7.5 that the different deflections are mainly caused by the dimensions of the faces and the shear connectors respectively. The presence of the adopted amount of reinforcement in the upperface is of minor importance.

Table 7.5 The influence of the shear connectors and reinforcement in the upper face, calculated by the numerical model.

| Duration of time (days) | Deflection at midspan (mm) | | | | |
|-------------------------|----------------------------|----------------------|------|------|------|
| | Beam no. 9/10 (MR) | Beam no. 11/12 (SMR) | | | |
| | | A | B | C | D |
| 0 | 0.98 | 0.63 | 0.66 | 0.65 | 0.64 |
| 121 | 4.50 | 2.33 | 3.25 | 3.00 | 2.58 |

A = with shear connectors and reinforcement in both faces (see section 7.2)
 B = without shear connectors and reinforcement in the upper face
 C = without shear connectors but with reinforcement in the faces
 D = with shear connectors but without reinforcement in the upper face.
 The differences between the deflections in the series MR and SMR-B are caused by the different dimensions of the faces.

The calculated results given in table 7.5 show that the deflections at $t=0$ are hardly affected by the presence of the shear connectors (compare A with C). Directly after loading, almost all the shear load T_s of the core is carried by the foamed concrete. This means that the core is relatively stiff immediately after loading compared with the shear connectors that are used. However, the foamed concrete core shows a large creep and shrinkage. The creep of the foamed concrete caused by the shear load, causes a larger shear deformation, and therefore a larger deflection of the beam. In case the sandwich is provided with a shear connector, the increase of shear deformation is partially prevented.

Therefore, the shear load T_s of the core is more and more carried by the shear connector. The shear stress in the core decreases and so does the creep. Fig. 7.17 shows the reduction of the shear stresses in the core, calculated by the numerical model. It is shown that all the shear load T_s of the core is carried by the shear connectors after only a few days. It is also shown in Fig. 7.17 that in case the sandwich beams are not provided with a shear connector, the shear stress and therefore the creep in the foamed concrete core also changes due to creep. In this case the shear load is partially transferred to the faces.

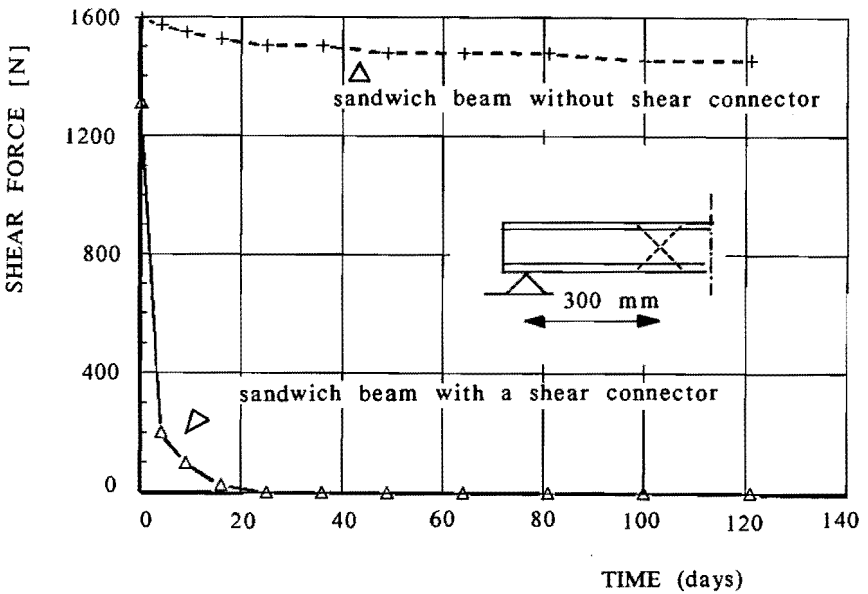


Fig. 7.17 Numerically calculated shear load in the foamed concrete core.

In the calculated results presented in this section, it is assumed that the creep and shrinkage behaviour of the core is similar to the prisms and hollow circular specimens described in chapter 6, despite the reinforced concrete frames and the epoxy coating at the sides. This means that the concrete faces are supposed to be moisture permeable. This statement is affirmed by comparison between the calculated and measured shear deformation, given in Table 7.6.

Table 7.6. Comparison between the shear deformations numerically calculated and actually measured (mm) *

| Duration of time (days) | Beams without shear connectors (MR) | | |
|-------------------------|-------------------------------------|-------------|-----------|
| | experimental | | numerical |
| | beam no.9 | beam no. 10 | |
| 0 | - | - | 0.01 |
| 28 | 0.03 | 0.04 | 0.10 |
| 121 | 0.10 | 0.09 | 0.13 |

* Average result of two measurements at each beam. (see also figure 7.10).

The comparison between the measured and calculated shear deformation shows that the creep and shrinkage of the core are not prevented but only delayed.

It is noticed that the foamed concrete core showed small cracks perpendicular to the span of the beam 21 days after loading at regular distances of about 150 mm. These cracks are caused by shrinkage of the foamed concrete.

7.5. Discussion and conclusions

Sandwich beams composed of reinforced concrete faces and a foamed concrete core with a density of 600 kg/m^3 were constructed and tested in bending. Both short-term test and long-term tests were performed. Generally, a close resemblance is observed between the test results of similar specimens.

Short-term tests

The samples, with an average weight reduction of 40% compared with a homogeneous concrete element of the same dimensions, actually showed composite action. The specimens behave in an elastic manner during the early loading continuing to the point of flexural cracking. The crack load was attended by a sudden increase of deflection. However, all beams exhibit considerable post-cracking strength and ductility before final collapse. The specimen provided with shear connectors, gradually failed in bending by yield of the main reinforcement. The specimen without shear connectors eventually showed failure induced by horizontal slip. This type of failure is marked by a horizontal crack in the foamed concrete core near the lower face and a large diagonal tensile-shear crack in the core. A number of 5 to 8 cracks are found to be evenly distributed along the measuring length of 900 mm round midspan, dependent on the percentage of reinforcement in the lower face. The increase of deflection after cracking is attended by an increase of all crack widths.

The numerically calculated load-versus deflection relationships are in close agreement with the experimental results. Although failure induced by horizontal slip is well predicted by means of a simplified model, further research into the actual method of shear transference in the cracked concrete is desirable.

Long-term tests

The time versus deflection relationships show an increase of deflection due to creep and shrinkage of the uncracked, loaded sandwich beams. In case the beams are provided with a shear connector, the immediate deflection at $t=0$ is enlarged 2 times at $t=121$ days, while this enlargement is 3 times in case of sandwich beams without shear connectors. The difference is caused by both the shear connector which partially prevents the shear deformation, and the slightly different dimensions of the faces.

Although final values have not yet been reached at $t=121$ days, it can be concluded that the deflections due to creep and shrinkage are small in case of an uncracked beam. The results show agreement between tests and calculations if creep and shrinkage data from non sealed prisms and cylindrical samples stored at the same temperature and relative humidity are used. This indicates that the concrete faces do not prevent shrinkage of the core despite sealing with epoxy coating along four sides. Therefore creep and shrinkage of the core must be taken into account.

The numerical results agree with the experimental results within engineering accuracy. In case the beams are not provided with a shear connector, the deflection caused by creep and shrinkage is overestimated at each point in time by about 20%.

In case the beams are provided with shear connectors, the numerical and experimental results are equal at $t=121$ days. However, there is a notable difference during the first few weeks after loading.

8. STRUCTURAL PARAMETERS

8.1. Introduction

The influence of the following parameters on the structural behaviour of sandwich beams can be studied with the numerical model * described in chapters 2 to 5.

- a. Geometry (span; cross-sectional dimensions of faces and core, main reinforcement in both faces and shear connectors; cross-sectional shape of the faces);
- b. Type of loading;
- c. Material properties (σ - ϵ relationships of the faces, core and reinforcements, τ - γ relationship of the core, creep and shrinkage of the faces and the core including creep of the core under sustained shear load).

In order to get a better understanding of the structural behaviour of a reinforced concrete sandwich beam, the influence of the quality of the foamed concrete core on the structural performance of the sandwich beams is analysed with respect to:

short-term loading

- (I) load-bearing capacity and the type of failure mode;
- (II) deflection;

sustained loading

- (iii) enlargement of the deflection caused by creep and shrinkage.

The following assumptions are made:

- a. The geometry of the beam is kept constant, as given in Fig. 8.1. Distinction is made between the type and amount of reinforcement.

*) Details of the input parameters of the numerical model are described in the manual [Salet and Vianen, 1990].

The sandwich beams subjected to a short-term loading are provided with a main reinforcement in the lower face, while in case of the sandwich elements under a sustained loading a reinforcement of $100 \text{ mm}^2/\text{m}$ in the upper face and shear connectors between the faces are also taken into account.

The main reinforcements are located in the centre of the faces. The shear connectors are located between the reinforcements in the upper and lower face, along the entire span.

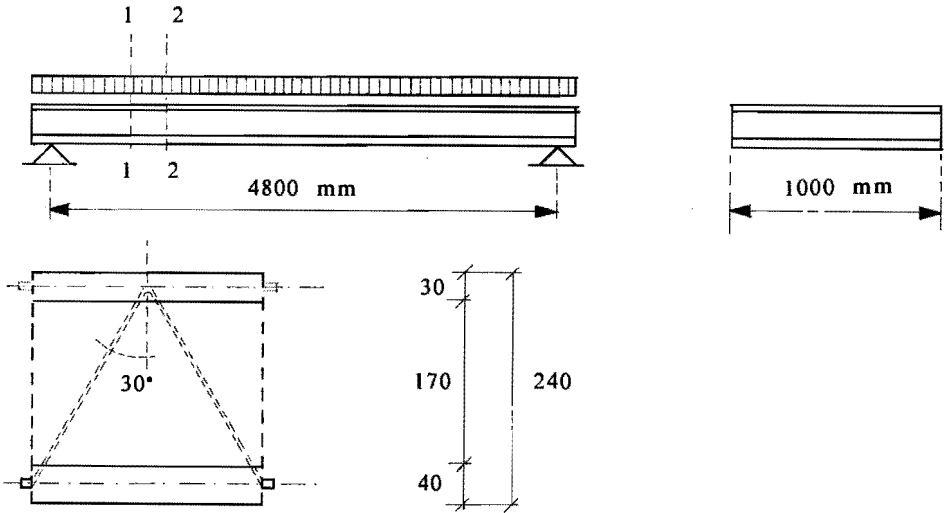


Fig. 8.1. Geometry of the sandwich beam.

- b. The beam is subjected to a uniformly distributed load. In case of the short-term type of loading, increments of 1 kN/m' are used. The long-term loading is taken as the sum of the dead load (2.7 kN/m'), based on $\rho_{\text{co}} = 2400 \text{ kg/m}^3$ and $\rho_{\text{fc}} = 600 \text{ kg/m}^3$, and 50% of an arbitrarily chosen service load ($0.5 * 4 \text{ kN/m'}$) of 2 kN/m' , together being 4.7 kN/m' .
- c. The material properties of the concrete faces and the steel reinforcements are kept constant. The material properties are given in the tables 8.1 and 8.2.

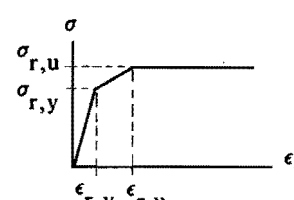
Table 8.1 Material properties of the concrete faces.

| Type of material property | Face no. | | |
|--|----------|----------------------|----------------------|
| | | 1 (lower face) | 2 (upper face) |
| stress-strain compression relationship $\sigma = a\epsilon + b\epsilon^2$ (3.5 o/oo) ¹⁾ | a | 32.500 | 28.000 |
| | b | $6.8 \cdot 10^6$ | $6.5 \cdot 10^6$ |
| | a | 32.500 | 28.000 |
| | b | $-8.9 \cdot 10^7$ | $-1.1 \cdot 10^8$ |
| shrinkage ²⁾ $\epsilon_{co}^{sh} = a \cdot \frac{1000 \cdot t}{1000 \cdot t + 9.3 \cdot 10^4}$ | a | $33.0 \cdot 10^{-5}$ | $40.0 \cdot 10^{-5}$ |
| | | | |
| creep ²⁾ $\phi_{co}^t = a \cdot \frac{1000 \cdot t}{1000 \cdot t + 9.3 \cdot 10^4}$ | a | 2.6 | 3.1 |
| | | | |

1) Ultimate strain capacity

2) Dutch practical code VB74/84, R.H. = 60%, $T = 20^{\circ}$ and $h_m = 175$.

Table 8.2 Material properties of the steel reinforcements in the faces and the shear connector.

| Stress [N/mm ²] | | Strain [mm/m] | |  |
|-----------------------------|----------------|------------------|------------------|---|
| $\sigma_{r,y}$ | $\sigma_{r,u}$ | $\epsilon_{r,y}$ | $\epsilon_{r,u}$ | |
| 500 | 550 | 2.5 | 5.0 | |

The sandwich beam is calculated with the following structural parameters and parameter values:

short-term loading

a. The amount of main reinforcement in the lower face (see Fig. 8.1);

$$A_{r,l} = 300, 400, 500, 600 \text{ (mm}^2\text{)};$$

b. The material properties of the foamed concrete core.

In order to reduce the weight of the structural element and in order to get sufficient thermal insulation, foamed concrete with a low density ($\leq 800 \text{ kg/m}^3$) is required. The structural properties of such a type of foamed concrete not only depend on the density but vary significantly due to the mix proportion, the way of manufacture, the type of foaming agent and the storing conditions.

The properties of the foamed concrete with $\rho \leq 800 \text{ kg/m}^3$, chosen from the scarce literature and the experiments described in chapter 6, are given in table 8.3.

sustained loading

- a. The amount of the cross-sectional area of the shear connectors between the faces (A_{sc}). $A_{sc} = 0, 125$ and ∞ (mm^2). $A_{sc} = \infty$ is used to gain insight into the order of magnitude of the shear deformation in the cases $A_{sc} = 0$ and $A_{sc} = 125$ (mm^2). In all cases the amount of reinforcement in the lower face is taken as 500 mm^2 and in the upper face as 100 mm^2 .
- b. The material properties of the foamed concrete core, as given in table 8.3.

Table 8.3 Properties of the foamed concrete core

| Type of property | | Designation of the foamed concrete | | | | |
|------------------|--|--|-------|-------|-------|-------|
| | | FC1.5 | FC2.0 | FC2.5 | FC3.0 | FC3.5 |
| short-term | $f_{fc,cm}$ [N/mm^2] | 1.5 | 2.0 | 2.5 | 3.0 | 3.5 |
| | E_{fc} [N/mm^2] | 600 | 900 | 1200 | 1500 | 1800 |
| | $f_{fc,tm}$ [N/mm^2] | $f_{fc,cm}/10$ | | | | |
| | G_{fc} [$\text{N/mm}^2 \text{ rad}$] | $E_{fc}/3$ | | | | |
| | Mohr's intrinsic curve | $\tau = (0.177 * f_{fc,cm}) - 1.24 * \sigma$ | | | | |
| long-term | ϵ_{fc}^{sh} [mm/m] | $-3.4*10^{-4} + 8.6*10^{-4}*\ln(t)$ | | | | |
| | $\phi_{\epsilon,fc}^t$ | 0.25 + $1.8*\ln(t)$ | | | | |
| | $\phi_{\gamma,fc}^t$ | 1.40 + $2.4*\ln(t)$ | | | | |

The beam is divided into 37 segments along the span and 10 fibres for each layer. The enlargement of the deflection under sustained load is calculated by the following polynomial series of the second order (in days): 1,4,9,....., 324,361.

8.2. Numerical results

Short-term loading

The load-bearing capacity of the beam and the type of failure mode are given in Fig. 8.2. with respect to the amount of reinforcement in the lower face and the tensile strength of the foamed concrete core. The following notations are used:

- A-A = Failure in bending due to yield of the main reinforcement
- B-B = Failure due to shear
- C-C = Failure due to horizontal slip

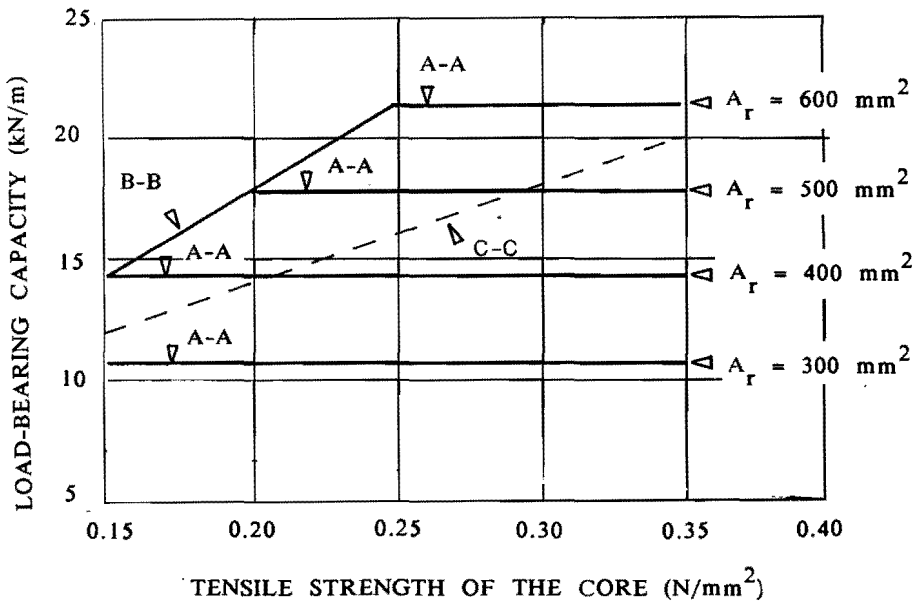


Fig. 8.2 The load-bearing capacity and the type of failure mode (t=0).

Fig. 8.2 shows that the load-bearing capacity in some cases is affected and in other cases is not affected (yield of the reinforcement, A-A) by the tensile strength of the foamed concrete core (shear failure, B-B). It is also shown by means of the dotted line, that the ultimate load-bearing capacity will not be reached in about 50% of the cases since failure is induced by horizontal slip, as calculated from the simplified model described in chapter 5.

Failure induced by horizontal slip is likely to be avoided in case of a sufficiently high tensile strength of the foamed concrete core, together with a relatively low amount of reinforcement.

Typical load versus deflection relationships of the sandwich beams for different types of foamed concrete cores are given in Fig. 8.3, in case of $A_{r,1} = 500 \text{ mm}^2$. The load versus deflection relationships are compared with a traditional fully concrete element and with a sandwich beam with a foamed plastic core. The properties of the foamed plastic core (polyurethane with a density of 50 kg/m^3) are given in table 8.4 [Salet, 1988]. In case of a fully concrete beam, the material properties of the 'core' are taken equal to the concrete of the upper face (see table 8.2). Details of the crack load, dead load and service load are given in table 8.5. The service load given in Table 8.5 is not the total service load but the load before cracking of the reinforced concrete lower face.

Table 8.4 Material properties of polyurethane with $\rho = 50 \text{ kg/m}^3$.

| Type of material property | | | |
|------------------------------------|--------------------------------------|---|------------------|
| stress-strain relationships | compression (4.0 %) ¹⁾ | a | 10 ²⁾ |
| | | b | 0 |
| $\sigma = a\epsilon + b\epsilon^2$ | tension (6.7 %) ¹⁾ | a | 15 |
| | | b | -111 |
| $\tau = a\epsilon + b\epsilon^2$ | shear (20 mm/m*rad) ¹⁾ | a | 3 |
| | | b | -7.5 |

1) Ultimate strain capacity

2) Linear elastic

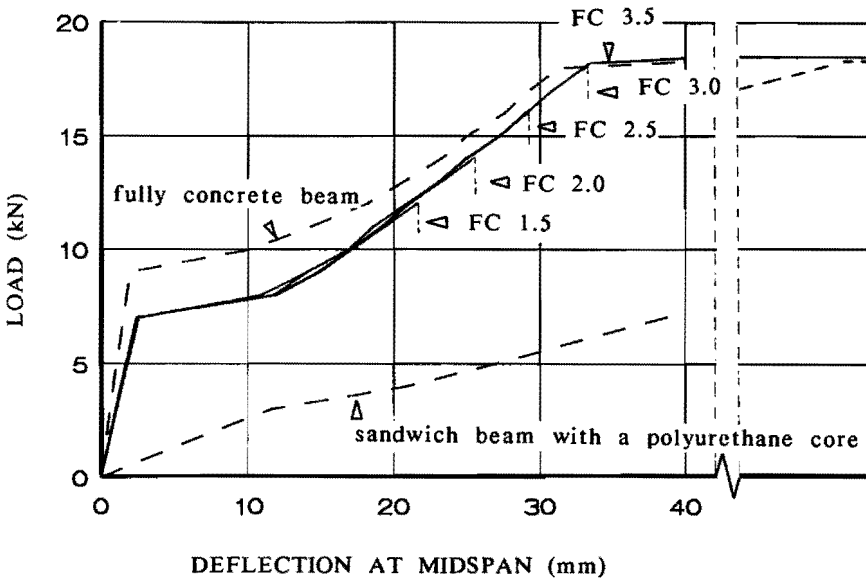


Fig. 8.3 Typical load versus deflection relationships $t = 0$ in case $A_{r,1} = 500 \text{ (mm}^2\text{)}$.

Table 8.5 Comparison of the service loads before cracking between different types of cores.

| Type of load | Type of core | | | |
|--------------------------------------|--------------|-----------------|-------|----------|
| | polyurethane | foamed concrete | | concrete |
| | | FC1.0 | FC2.5 | |
| crack load [kN/m'] | 3.7 | 7.2 | 7.3 | 9.5 |
| dead load [kN/m'] | 1.7 | 2.7 | 2.7 | 5.7 |
| service load [kN/m'] before cracking | 2.0 | 4.5 | 4.6 | 3.8 |

Sustained loading

The enlargement of the instantaneous deflection ($t=0$) at midspan (see Fig. 8.3) due to creep and shrinkage of the faces and the core after 361 days is given in Fig. 8.4. The structural parameters included are the shear modulus of the foamed concrete core and the total amount of cross-sectional area of the shear connectors A_{sc} . The results of the traditional fully concrete beam under the same sustained load as the sandwich beams have been included.

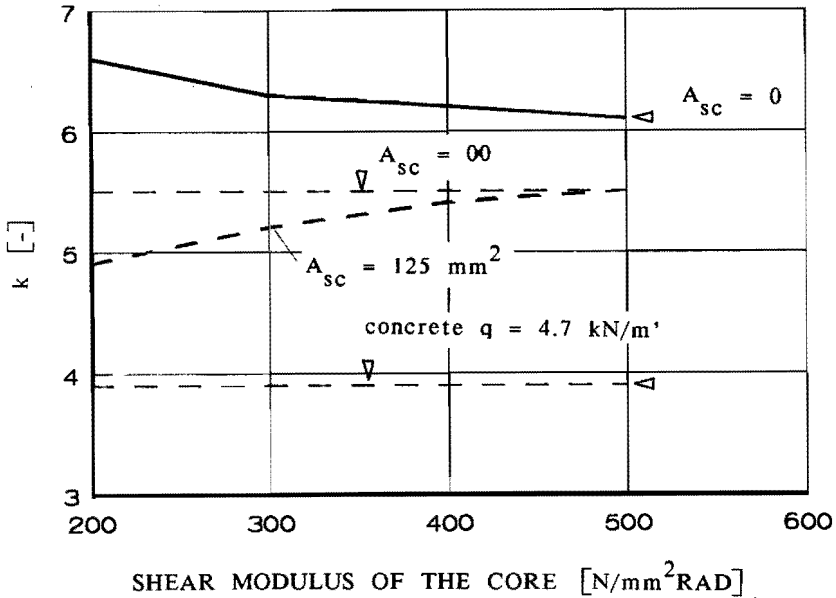


Fig. 8.4 Enlargement of the deflection at midspan at $t=361$ days compared with the immediate deflection at $t=0$; $k = w^{t=361} / w^{t=0}$.

Fig. 8.4 shows that in case of an infinite stiff shear connector ($A_{sc} = \infty$), the enlargement of the immediate deflection $w^{t=0}$ after 361 days ($w^{t=361}$) is not affected by the shear modulus of the core, since all the shear load is carried by the shear connectors. The comparison between the sandwich beams with $A_{sc} = \infty$ and $A_{sc} = 0$ shows that the deflection of the sandwich beam is indeed enlarged by the shear deformation of the foamed concrete core under a sustained shear load.

In case of $A_{sc} = 125 \text{ (mm)}$, the enlargement k increases together with the adopted shear modulus of the core. The reason for this is that the deflections after 361 days ($w^{t=361}$) are independent of the shear modulus of the foamed concrete core and only depend on the shear stiffness of the shear connector, while the immediate deflections ($w^{t=0}$) decrease with larger shear moduli of the foamed concrete core.

Time versus deflection relationships of the sandwich beams with foamed concrete cores are plotted in Fig. 8.5. Time versus deflection relationships of a fully concrete element under the same load as the sandwich beams, being 4.7 kN/m' , and a fully concrete element under the sum of actual dead-load (5.7 kN/m') and 50% of the service load ($0.5 \cdot 4 \text{ kN/m'}$), being 7.7 kN/m' are also included.

The sudden enlargement of the deflection in case of a traditional fully concrete beam ($q = 7.7 \text{ kN/m'}$) after 121 days, is caused by cracking of the lower face due to the redistribution of stresses.

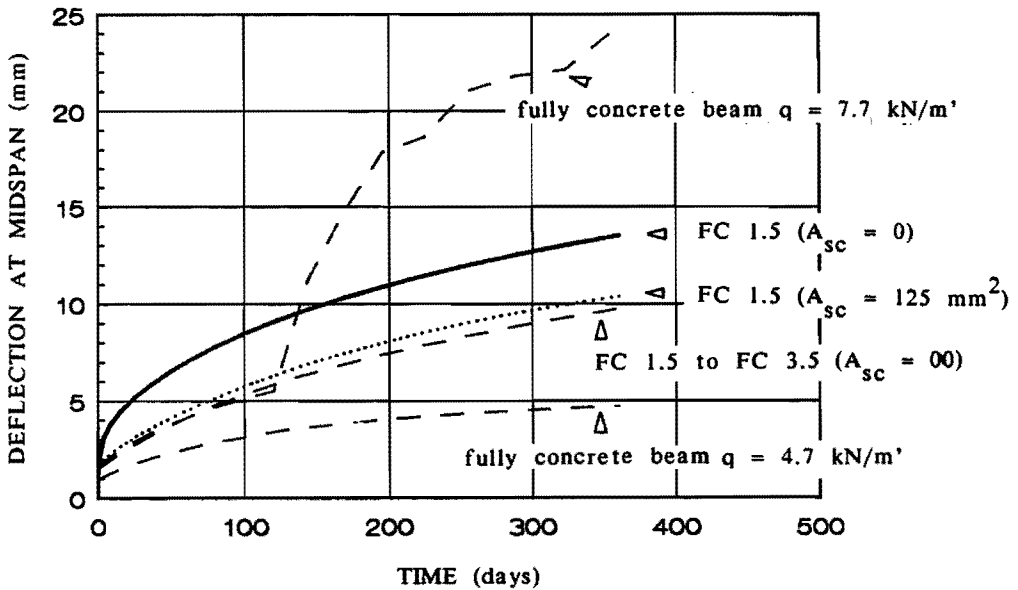


Fig. 8.5 Time versus deflection relationships

8.3 Conclusions

Short-term loading

In figure 8.2 it is shown that:

- (i) failure induced by horizontal slip is not likely to happen in case of a sufficiently high tensile strength of the foamed concrete core together with a relatively low amount of reinforcement; another, and by far the most certain method to avoid this kind of unwanted failure, is the use of shear connectors.

In figure 8.3 and in table 8.5 it is shown that:

- (ii) the deflection of a sandwich beam with a foamed plastic (polyurethane) core is strongly affected by the shear deformation; the shear deformation is of minor importance in case of sandwich beams with foamed concrete cores; the stiffness of sandwich beams with foamed cores is within the same order of magnitude with fully concrete beams;
- (iii) the crack load of sandwich beams with foamed concrete cores is relatively low compared with fully concrete beams; however, the crack load will generally not be reached since the dead load of the beam is even more reduced by the low density of the foamed concrete core.

Long-term loading

The following conclusions can be drawn from the figures 8.4 and 8.5:

- (iv) From the comparison between sandwich beams with only a foamed concrete core ($A_{sc} = 0$) and sandwich beams with an infinite stiff shear connector ($A_{sc} = \infty$), it can be concluded that the deflections are indeed enlarged by the shear deformation of the core due to the sustained shear load.
The deflection of the sandwich beams with foamed concrete cores is therefore affected by the type of foamed concrete;
- (v) In case the sandwich beam is provided with a shear connector ($A_{sc} = 125 \text{ mm}^2/\text{m}'$), the enlargement of the deflections is mainly caused by creep and shrinkage of the faces only. The shear deformation of the core under sustained load is of minor importance since the shear load is transferred from the foamed concrete to the shear connector (see also chapter 7, section 7.4.2);
- (vi) The time-dependent deflections of a fully concrete beam are smaller compared with the time-dependent deflections of a sandwich beam with a foamed concrete core, in case of the same permanent loading. The deflections of the concrete beam will increase largely in case the actual dead-load is taken into account due to cracking.

9. SUMMARY AND CONCLUSIONS

A structural sandwich element is a particular type of composed structure. The cross-section consists of two strong and stiff sheets (faces) connected by a weak core commonly consisting of insulation material. The favourable stiffness to weight ratio, combined with the good thermal insulation have promoted the use of sandwich elements. In a structural sense, the bending moment is carried by the stiff faces and the shear load by the core. The shear deformation of sandwich elements must emphatically be taken into account, since the transverse shear rigidity is provided by the relatively weak core. Bernouilli's law of plane-cross sections is therefore no longer valid.

In this study, the advantages of sandwich elements are to be combined with the typical advantage of concrete by developing a fully cement-based sandwich. The aim of the study is to analyse the structural behaviour of sandwich beams, particularly composed of reinforced concrete faces and a foamed concrete core. Both short-term loading and sustained loading are taken into account. Foamed concrete is a very lightweight concrete, consisting of cement, water, fine sand and a foaming agent. Contrary to aerated autoclaved concrete, foamed concrete hardens under normal atmospherical conditions. Compared with normal concrete ($\rho = 2400 \text{ kg/m}^3$), the density can be lowered to about 400 kg/m^3 , depending on the amount of foam. The lower density considerably improves the thermal insulation properties but at the expense of the structural properties like strength and stiffness.

The study described in this thesis is concerned with the structural behaviour of simply supported sandwich beams, subjected to a symmetric and static type of load. Normal load and instability phenomena are left out of account.

The structural behaviour of fully concrete sandwich beams is affected by a number of effects which are not or insufficiently considered in the classical analysis of sandwich beams. These effects are:

- (i) the bending stiffness of the core;
- (ii) the physical nonlinear behaviour, including cracking of reinforced concrete;
- (iii) the creep and shrinkage of the faces and the core, including creep of the core under a sustained shear load.

After a short introduction and some explanatory notes in chapter 1, a numerical model is described in the chapters 2 to 5, for the calculation of the load versus deflection relationship and the time versus deflection relationship of sandwich beams. The special purpose computer program that has been developed, based on the numerical model, is suitable for a PC environment.

In chapter 2, generalized differential equations are described, taking the shear stiffness as well as the bending stiffness of the core into account. It is demonstrated that in case of various stiffnesses of the core, the theory of plane cross-sections (Bernoulli, $G_c = \infty$) fades into the classical theory of sandwich beams ($E_c = 0$) with the equations presented. The differential equations are numerically solved by means of the finite difference method.

It is demonstrated that the finite difference analysis presented:

- is suitable for a large range of both geometrical and physical input data, without numerical problems;
- converges fast.

Physical nonlinearity, including a nonlinear τ - γ relationship, is taken into account by means of an iterative algorithm based on the secant modulus method. Cracking of reinforced concrete is calculated by means of a smeared-out concept, since the adopted finite difference approach is not suitable to take discrete cracks into account. The application of the smeared-out concept is supported by a separated discrete crack analysis considering a reinforced concrete bar (the face of a sandwich beam) subjected to a nonuniformly distributed tensile load along the length. This study has shown that:

- in case of a uniformly distributed load acting on a beam, the calculated deflection depends on the chosen number of segments in which the beam is divided in view of the finite difference analysis; a number of segments of about $n = L/h$ is needed, in order to avoid casual failures;

- application of the fictitious stress versus strain relationships by which the tension stiffening is taken into account, can result in a considerable overestimation of the stiffness of cracked reinforced concrete in case the relationship is based on a reinforced concrete bar subjected to a uniformly distributed tensile load along the entire bar;
- caused by the nature of a uniformly distributed load acting on a beam, cracks arise at relatively short distances compared with e.g. a pure bending moment; generally the tension stiffening is small and can be left out of account.

The numerical model is extended in the fourth chapter by the time-dependent behaviour caused by creep and shrinkage. Creep and shrinkage are taken into account by means of a generalized relaxation method, by which the initial strains due to creep and shrinkage are counterbalanced by means of dummy restraints. The so-called step-by-step analysis is based on the superposition principle of McHenry, and takes the stress-history into account. The method has the additional advantage that it provides insight into the problem under consideration. It is demonstrated that:

- in case other solutions are available, the results are in close agreement;
- the deflections and stress-redistribution due to shrinkage of the faces are not affected by the shear stiffness of the core;
- the deflections and stress-redistribution due to creep of the faces are only affected by the shear stiffness of the core in case of sandwich beams with bending stiff faces;
- the outcome of the creep of the core under sustained shear load depends on the stiffness of the core; both in case of stiff and weak cores the increase of deflection and redistribution of stresses are small.

The description of the numerical model is finished in chapter 5 by means of a reflection on the possible failure modes.

The application of the numerical model in order to predict the structural performances of the sandwich beams composed of reinforced concrete faces and a foamed concrete core, has been verified by means of experimental research described in the chapters 6 and 7.

The experimental research into the mechanical properties of the concrete faces and the foamed concrete core is described in chapter 6.

Special attention has been paid to the structural properties of the foamed concrete ($\rho = 600 \text{ kg/m}^3$) subjected to both a short-term and a sustained shear load. Torsion tests have been developed for this purpose. The properties of the foamed concrete are characterized by the low (tensile) strength and stiffness and the large creep and shrinkage. A summary of the test results is presented at the end of the chapter. Both short-term tests and long-term tests on sandwich beams composed of reinforced concrete faces and a foamed concrete core are described in chapter 7. One out of two beams were provided with additional shear connectors. Preliminary research, described in appendix 7.1 to chapter 7, showed that the quality of the structural adhesion between foamed concrete and normal concrete depends on the method of manufacture. In the sandwich beams tested, the concrete of the faces is poured on already hardened foamed concrete, ensuring a good structural adhesion. The tests on the sandwich beams showed:

- actual composed action resulting in a stiff element;
- a considerable load-bearing capacity and post-cracking ductility in the elements with and without shear connectors;
- failure induced by a typical kind of shear failure in case of the sandwich beams without additional shear connectors, marked by a large diagonal tensile-shear crack and a horizontal crack in the foamed concrete core near the lower face (= horizontal slip);
- failure induced by yield of the main reinforcement in case of the elements provided with additional shear connectors;
- an enlargement of the immediate deflection by a factor 2 or 3 after 121 days in case of elements with and without shear connectors, respectively; the concrete faces are not a damp-proof course; creep of the foamed concrete core under sustained load is not prevented, resulting into a contribution to the enlargement of the deflection;
- close resemblance to the results calculated numerically.

The sensitiveness of the structural behaviour of the sandwich beams for various types of foamed concrete is traced by means of the numerical model (chapter 8). It is demonstrated that:

- failure induced by the so-called horizontal slip is not likely to happen in case of a sufficiently high tensile strength of the foamed concrete core together with a relatively low amount of reinforcement in the lower face; however, application of an additional shear connector is advisable for the time being with a view to safe structural failure mode;
- the structural performance of the sandwich beams is comparable with familiar fully concrete elements; the shear deformation of the foamed concrete core is neglected in case of a short-term loading; in case of a long-term loading the enlargement of the deflection due to the shear deformation must be taken into account, although it does not affect the serviceability of the sandwich beams; generally, the crack load will not be reached, thanks to the low dead load.

Supplementary research into the structural behaviour of sandwich beams composed of reinforced concrete faces and a foamed concrete core under temperature and non static types of load is recommended.

Appendix A2-1 Elaboration of the equations [2.13a] and [2.13b]

Expressing the centre-line of the sandwich beam as the reference-line [z_{ref} - zp_s] (see section 2.2.6.) equation [2.11] is given by means of

$$\begin{aligned}
 M = & (E_1 a_1^2 A_1) \Phi' + [E_1 A_1 a_1 (z p_1 - h_1)] (\Phi' + w'') - (E_1 I_1) w'' \\
 & + (E_2 a_2^2 A_1) \Phi' + [E_2 A_2 a_2 (h_1 + h_c + z p_s - a_2)] (\Phi' + w'') - (E_2 I_2) w'' \\
 & + (E_c a_c^2 A_c) \Phi' + (E_c I_c) (\Phi' + w'') - (E_c I_c) w'' \quad [2.11*]
 \end{aligned}$$

The substitution of the equations [2.11* and 2.12] into the equation of equilibrium [2.6b]:

$$\begin{aligned}
 & (E_1 a_1^2 A_1) \Phi'' + [E_1 A_1 a_1 (z p_s - h_1)] (\Phi'' + w''') - (E_1 I_1) w''' \\
 & + (E_2 a_2^2 A_1) \Phi'' + [E_2 A_2 a_2 (h_1 + h_c - z p_s - a_2)] (\Phi'' + w''') - (E_2 I_2) w''' \\
 & + (E_c a_c^2 A_c) \Phi'' + (E_c I_c) (\Phi'' + w''') - (E_c I_c) w''' \\
 & [-E_1 I_1 w''' - E_2 I_2 w''' + [G_c b (a_1 + a_2)] (\Phi + w')] = 0
 \end{aligned}$$

Rearranging of this equation results in:

$$\begin{aligned}
 & (E_1 a_1^2 A_1 + E_2 a_2^2 A_2 + E_c a_c^2 A_c) \Phi'' \\
 & (E_1 I_1 + E_2 I_2 + E_c I_c) w''' \\
 & + \\
 & (E_1 A_1 a_1 (z p_1 - h_1) + E_2 A_2 a_2 (h_1 + h_c - z p_s - a_2) + E_c I_c) (\Phi'' + w''') \\
 & + \\
 & (E_1 I_1 + E_2 I_2) w''' \\
 & - \\
 & [G_c b (a_1 + a_2)] (\Phi + w') = 0
 \end{aligned}$$

*) with reference to the centre-line

With

$$B_s = (E_1 a_1^2 A_1 + E_2 a_2^2 A_2 + E_c a_c^2 A_c);$$

$$B_1 = E_1 I_1; \quad B_2 = E_2 I_2; \quad B_c = E_c I_c$$

$$R = E_1 A_1 a_1 (z p_1 - h_1) + E_2 A_2 a_2 (h_1 + h_c + z p_s - a_2)$$

$$K = G_c b (a_1 + a_2)$$

the former equation can be written as,

$$\begin{aligned} B_s \Phi'' - (B_1 + B_2 + B_c) w''' + R (\Phi'' + w''') + B_c (\Phi'' + w''') \\ + (B_1 + B_2) w''' - (K) (\Phi + w') = 0 \end{aligned}$$

and therefore

$$(B_s + B_c) \Phi'' + R (\Phi'' + w''') - (K) (\Phi + w') = 0 \quad [2.13a]$$

Substitution of the equation [2.12] into the equation of equilibrium [2.6c]:

$$\begin{aligned} (-E_1 I_1) w'''' - (E_2 I_2) w'''' + [G_c b(a_1 + a_2)] (\Phi' + w'') \\ + q = 0 \end{aligned}$$

So, with the stiffness definition given before,

$$- (B_1 + B_2) w'''' + (K) (\Phi' + w'') + q = 0 \quad [2.13b]$$

Appendix A2-2. Elaboration of the equations [2.15a] and [2.15b]

Rearranging equation [2.13n] results in:

$$(B_s + B_c + R) \gamma_c'' - (B_s + B_c) w''' - (k) \gamma_c = 0 \quad [2.13b]$$

The first order derivative of equation [2.13b] is therefore given by:

$$(B_s + B_c + R) \gamma_c''' - (B_s + B_c) w'''' - (k) \gamma_c' = 0$$

The first order derivative of the shear deformation γ_c' is given by equation [2.14b]:

$$\gamma_c' = \frac{(B_1 + B_2)}{k} w'''' - \frac{q}{k}$$

The third order derivative of the shear deformation γ_c''' follows from the second order derivative of equation [2.14b]:

$$\gamma_c''' = \frac{(B_1 + B_2)}{k} w'''''' - \frac{q''}{k}$$

Substitution of the former equations into the first derivative of equation [2.13*b] results in:

$$\begin{aligned} (B_s + B_c + R) \left[\frac{(B_1 + B_2)}{k} w'''''' - \frac{q''}{k} \right] \\ - (B_s + B_c) w'''' \\ - \left[(B_1 + B_2) w'''' - q \right] = 0 \end{aligned}$$

and therefore,

$$\begin{aligned} \frac{(B_1 + B_2)}{k} w'''''' - \left[\frac{B_1 + B_2 + B_c + B_s}{B_s + B_c + R} \right] w'''' \\ - \frac{q''}{k} + \frac{q}{(B_s + B_c + R)} = 0 \end{aligned}$$

From this equation [2.15a] is calculated by means of two times integration.

Appendix A3-1 Numerical modelling of the shear connectors

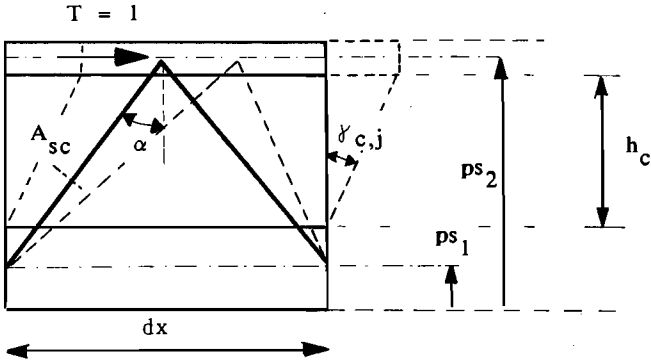


Figure A1 Geometry of the shear connectors and the correlation with the segmentary length dx.

In order to link on to the sandwich analysis, the shear stiffness of the shear connectors is translated into a fictitious shear modulus $G_{sec_sc,c,j}^*$. The fictitious shear modulus is calculated from:

$$G_{sec_sc,c,j}^* = \frac{T=1}{b*(ps_2-ps_1)*\gamma_{c,j}} \quad [A1]$$

with

$$\gamma_{c,j} = 2*dL_{sc,c,j}*\sin(\alpha) / h_c \quad [A2]$$

$$dL_{sc,c,j} = \left(\frac{dx}{2\sin^2(\alpha)} \right) / \left(E_{sec_sc,j} * A_{sc} \right) \quad [A3]$$

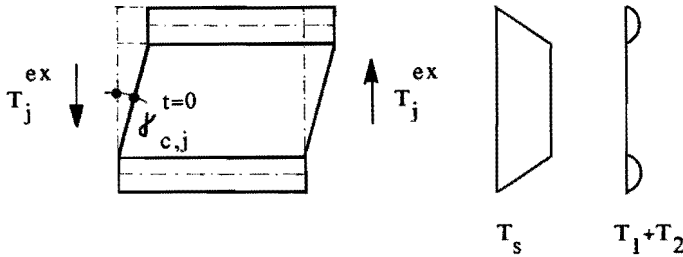
$$\epsilon_{sc,c,j} = \left[\left(\gamma_c * h_c \right) / \left(2 * \sin(\alpha) \right) \right] / L_{sc} \quad [A4]$$

The normal stresses in the shear connector follow from the stress-strain relationship. The shear load in the shear connectors is therefore given by,

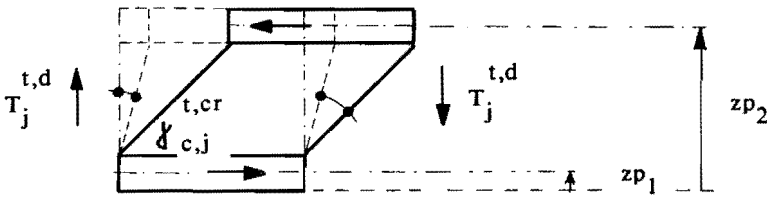
$$T_{sc,c,j} = \sigma_{sc,c,j} * A_{sc} * 2\sin(\alpha) \quad [A5]$$

Appendix A4-1 Application of the relaxation method to creep of the core under shear load.

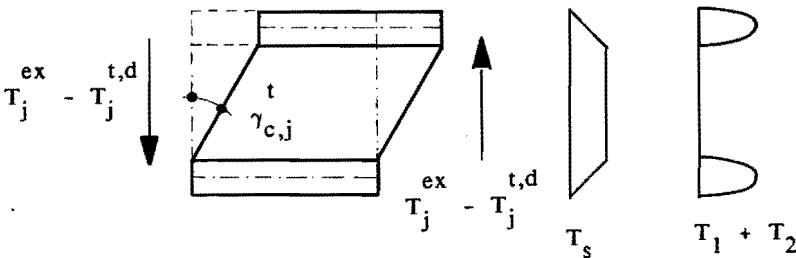
In the first stage of the analysis the external shear load T_j^{ex} is resisted by both facing and core.



The creep strain of the core $\gamma_{c,j}^{t,cr}$ (equation [4.9]) is prevented by a dummy restraint $T_j^{t,d}$ is given in equation [4.10c].



In the second stage of the analysis, the actual shear deformation of the core is calculated from the sum of the external force T_j^{ex} and the dummy restraint $T_j^{t,d}$ (equation [4.11b]).



The shear stress in the core is calculated from the sum of the actual strain calculated in the second stage of the analysis and the time-dependent relaxation strain, i.e. $\gamma_{c,j}^t - \gamma_{c,j}^{t,cr}$

Appendix A6-1 Elaboration of the torsion test

The torsional moment M_t is calculated from

$$M_t = \frac{F_v}{2\cos\alpha} * D \quad (\text{see Fig. 6.4 and Fig. 6.5}) \quad [6.1]$$

The rotation is calculated from

$$\frac{d\Phi}{dx} = \frac{\text{Arctan} [(d_LVDT1a - d_LVDT1b) + (d_LVDT2a - d_LVDT2b)]}{2r_m dx} \quad [6.2]$$

(see Fig. 6.4 and Fig. 6.5)

From these test results the stress-strain relations were calculated. The effects of both a non-uniform stress distribution and a physical nonlinear response were analytically modelled.

The basic equations are (see Fig. 6.4):

$$\gamma = r \frac{d\Phi}{dx} \quad (\text{deformation-strain relation}) \quad [6.3]$$

$$\tau = \Sigma b_n \left(r \frac{d\Phi}{dx} \right)^n \quad (\text{stress-strain relation}) \quad [6.4]$$

$$M = \int_F \tau r dF \quad (\text{equation of equilibrium}) \quad [6.5]$$

Substitution of equation [6.4] into equation [6.5] gives

$$M = \int_F \Sigma b_n \left(r \frac{d\Phi}{dx} \right)^n r dF,$$

$$\text{so } M = 2\pi \Sigma b_n \frac{d\Phi}{dx} \left[\frac{r^{n+3}}{n+3} \right]_{r1}^{r2} \quad [6.6]$$

If both the moment-rotation curve and the shear stress-strain are fitted by the n^{th} order polynomial functions

$$M = \Sigma a_n \left(\frac{d\Phi}{dx} \right)^n$$

$$\tau = \Sigma b_n \gamma^n,$$

$$\text{respectively, then } b_n = \frac{a_n * (n+3)}{2\pi (r_1^{n+3} - r_2^{n+3})} \quad [6.7]$$

APPENDIX A7-1 Four point bending tests on small sandwich beams composed of concrete faces and a foamed concrete core

Introduction

With a view the requirements to be set for a proper and reliable adhesion between concrete and foamed concrete, an experimental study was established. Four points bending tests were performed on sandwich beams composed of concrete faces (without reinforcement) and a foamed concrete core with a small ratio of slenderness. The parameter in this study was the cast order of the faces and the core.

Specimens and material properties

The dimensions of the specimens are shown in figure A1.

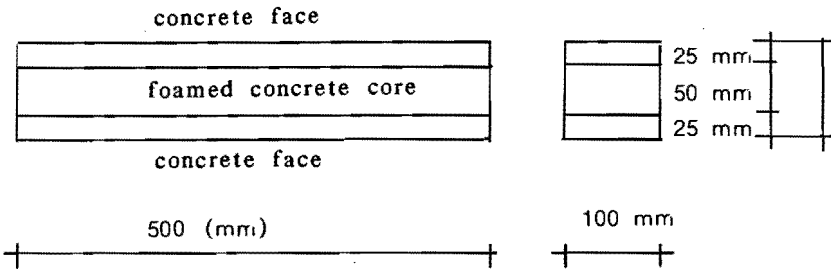


Figure A1 The dimensions of the small concrete sandwich beams.

Three series of six samples each were casted. The cast orders used are given in table A1. The duration of time between each cast was 48 hours.

Table A1

| series no. | cast 1 | cast 2 | cast 3 |
|------------|--|---------------------|---------------------|
| 1 | lower concrete face | foamed concrete | upper concrete face |
| 2 | foamed concrete | lower concrete core | upper concrete face |
| 3 | lower concrete face + foamed on the fresh concrete | upper concrete face | |

APPENDIX A7-1 Continued

The specimens were covered with foil after each cast and stored at a temperature of 20°C and a relative humidity of near 100%. Twenty-eight days after the last layer was poured, the samples were demoulded and tested.

The mix proportions of both concrete and foamed concrete conform to the descriptions given in table 6.2 and table 6.3. The material properties closely correspond with the data summarized in table 6.4.

Test performance

A schematic view of the test is given in figure A2 and figure A3. The tests were deformation controlled at a rate of 0.05 mm/min measured at the hydraulic jack. Although the objective of the test is only concerned with the failure load, deformations were measured by means of six LVDTs. The deflections at midspan are compared with the numerical model (see chapters 2 and 3).

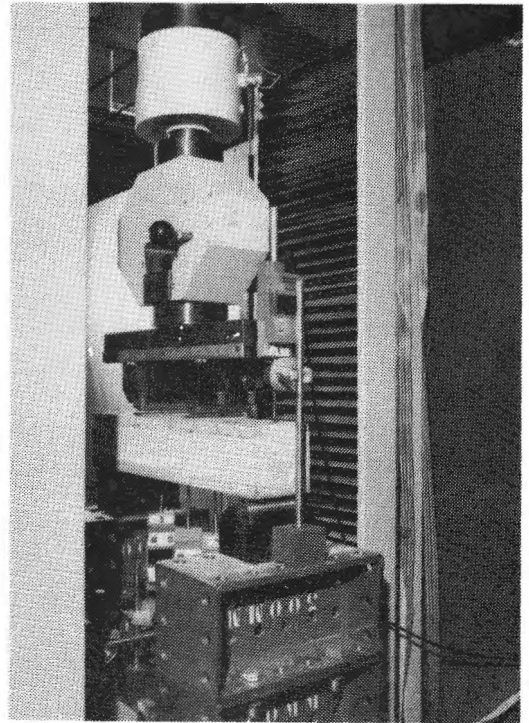
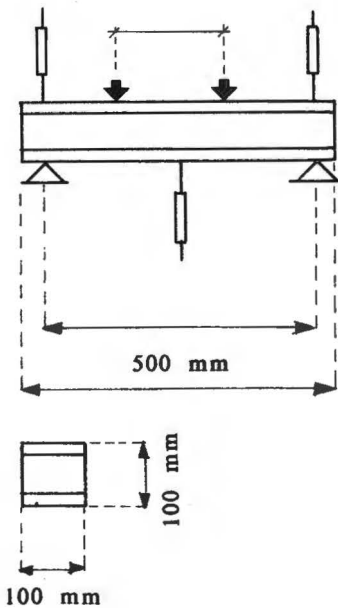


Figure A2 Schematic view of the testing equipment.

APPENDIX A7-1 Continued

Test results

The ultimate load bearing capacity is given in table A2.

Table A2 The jack loads (P) (N) at failure.

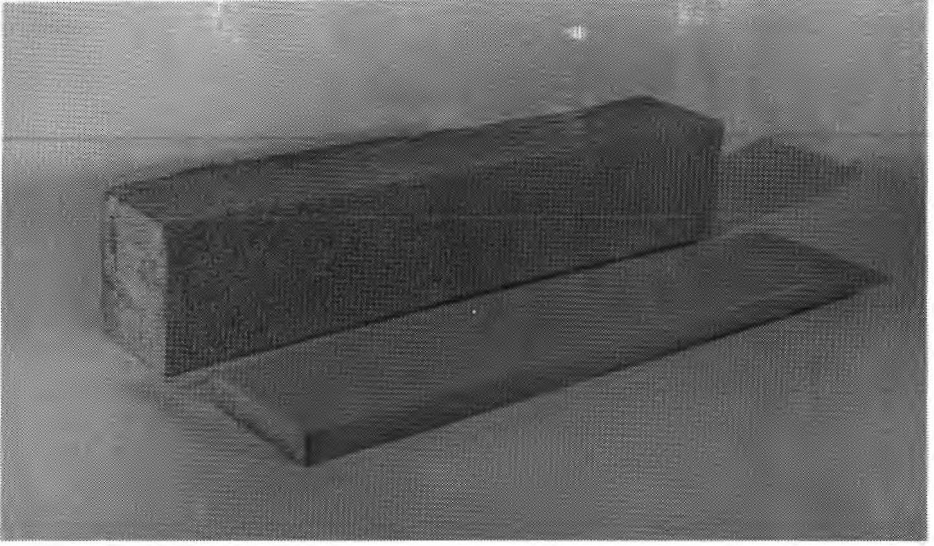
| specimen no. | series no. | | |
|---------------------------|------------|------|------|
| | 1 | 2 | 3 |
| 1 | 0 | 6415 | 3366 |
| 2 | 4922 | 6385 | 4560 |
| 3 | 2926 | 6985 | 3377 |
| 4 | 5292 | 6520 | 1966 |
| 5 | 1988 | 7120 | 6250 |
| 6 | 5110 | 5812 | 0 |
| mean | 3373 | 6546 | 3088 |
| standard deviation factor | 63% | 7% | 61% |

The samples from cast no. 1 and cast no. 3 showed failure caused by horizontal slip in the core near the lower face. A thin film of foamed concrete (± 1 mm) present at the separate concrete lower face, makes it believable that failure has been caused by a substantial shrinkage of foamed concrete during hardening. Since remainders of foamed concrete remain on the separated concrete face it is believed that the adhesion is sufficient.

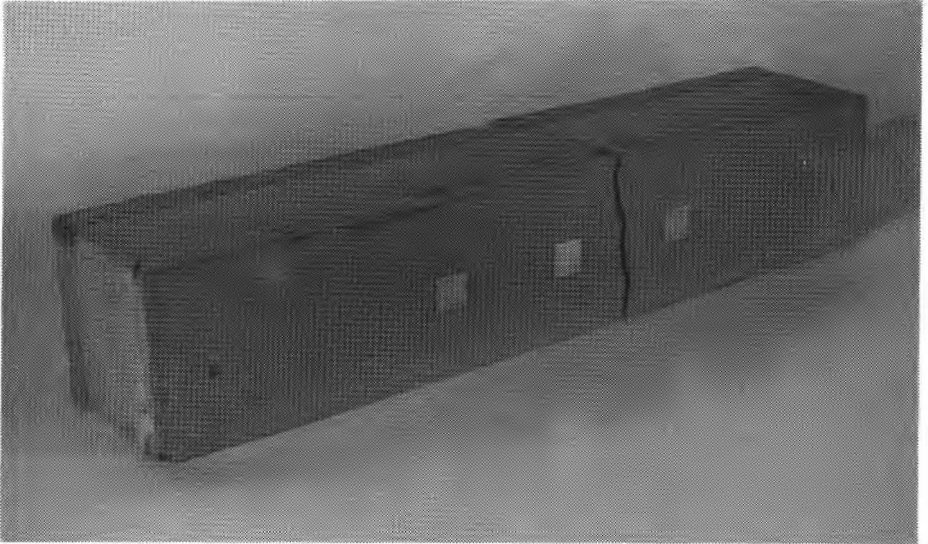
The samples from cast no. 2 failed in bending without any damage to the concrete - foamed concrete adhesion. The typical failure modes are shown in figure A3.

The jack load P versus the average deflection at midspan is shown in figure A4 for three typical measurements, together with the numerically calculated result. The linear material properties used in the numerical analysis are:

$$E_{co} = 34.000 \text{ N/mm}^2; E_{fc} = 1350 \text{ N/mm}^2; G_{fc} = 400 \text{ N/mm}^2 \text{ rad.}$$



failure due to horizontal slip



failure due to bending

Figure A3 Typical failure modes

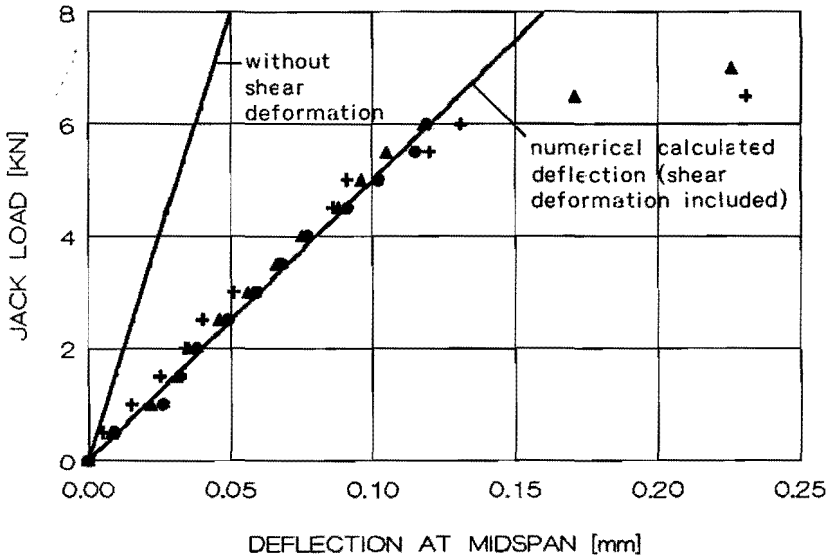


Figure A4 Actual deflection at midspan and comparison with the numerical results.

Conclusions

From the test results, cast order no. 2 foamed concrete core \Rightarrow concrete lowerface \Rightarrow concrete upperface is preferred. The actual deflection measured shows that in case of specimens with a small ratio of slenderness the shear deformation contributes substantially to the total deflection. The numerical results are in close agreement with the experimentally determined deflection if the shear deformation of the core is taken into account.

APPENDIX A7-2 Details of the crack patterns

Table A1 Details crack pattern specimen no. 1 (without a shear connector)

| Crack no. | Jack Load [kN] | Moment at mid-span [kNm] | Concrete strain before cracking [mm/m] | Crack width after cracking [mm] | Ultimate crack width [mm] |
|-----------|----------------|--------------------------|--|---------------------------------|---------------------------|
| 1 | 4.10 | 1.17 | 0.129 | 0.081 | 0.245 |
| 2 | 4.24 | 1.21 | 0.144 | 0.043 | 0.234 |
| 3 | 4.44 | 1.27 | 0.184 | 0.090 | 0.341 |
| 4 | 4.61 | 1.33 | 0.247 | 0.091 | 0.337 |
| 5 | 5.04 | 1.44 | 0.221 | 0.103 | 0.328 |
| 6 | 5.52 | 1.57 | 0.221 | 0.096 | 0.260 |
| 7 | 5.75 | 1.64 | 0.363 | 0.068 | 0.230 |

Remark: strain reader L5 was defective

Table A2 Details crack pattern specimen no. 2 (without a shear connector)

| Crack no. | Crack Load [kN] | Moment [kNm] | Concrete strain before cracking [mm/m] | Crack width after cracking [mm] | Ultimate crack width [mm] |
|-----------|-----------------|--------------|--|---------------------------------|---------------------------|
| 1 | 4.58 | 1.30 | 0.297 | 0.138 | 0.620 |
| 2 | 4.70 | 1.34 | 0.287 | 0.061 | 0.307 |
| 3 | 4.73 | 1.35 | 0.233 | 0.087 | 0.385 |
| 4 | 4.90 | 1.40 | 0.220 | 0.051 | 0.186 |
| 5 | 4.97 | 1.42 | 0.204 | 0.040 | 0.284 |
| 6 | 5.01 | 1.43 | 0.221 | 0.092 | 0.391 |
| 7 | 5.10 | 1.45 | 0.226 | 0.084 | 0.295 |
| 8 | 5.21 | 1.48 | 0.234 | 0.101 | 0.389 |

APPENDIX A7-2 Continued

Table A3 Details crack pattern specimen no. 5 (with a shear connector)

| Crack no. | Crack Load [kN] | Moment [kNm] | Concrete strain before cracking [mm/m] | Crack width after cracking [mm] | Ultimate crack width [mm] |
|-----------|-----------------|--------------|--|---------------------------------|---------------------------|
| 1 | 6.17 | 1.76 | 0.086 | 0.091 | >1.003 |
| 2 | 6.17 | 1.76 | 0.151 | 0.063 | >0.699 |
| 3 | 6.31 | 1.80 | 0.155 | 0.200 | >1.458 |
| 4 | 6.71 | 1.91 | 0.191 | 0.190 | >0.978 |
| 5 | 7.86 | 2.24 | 0.221 | 0.140 | >0.499 |
| 6 | 16.27 | 4.63 | 0.289 | 0.300 | >0.369 |

Remark: strain reader L5 was defective

Table A4 Details crack pattern specimen no. 6 (with a shear connector)

| Crack no. | Crack Load [kN] | Moment [kNm] | Concrete strain before cracking [mm/m] | Crack width after cracking [mm] | Ultimate crack width [mm] |
|-----------|-----------------|--------------|--|---------------------------------|---------------------------|
| 1 | 7.13 | 2.03 | 0.130 | 0.101 | >1.355 |
| 2 | 7.66 | 2.18 | 0.277 | 0.169 | >1.188 |
| 3 | 8.14 | 2.32 | 0.227 | 0.068 | >0.654 |
| 4 | 8.22 | 2.34 | 0.167 | 0.109 | >1.278 |
| 5 | 8.22 | 2.34 | 0.219 | 0.169 | >2.084 |

Table A5 Details concrete strains upper layer surface at midspan

| Specimen no. | Crack load [kN] | Concrete strain [mm/m] | | |
|--------------|-----------------|------------------------|----------------|----------|
| | | before cracking | after cracking | ultimate |
| 1 | 4404 | - 0.175 | - 0.321 | - 1.154 |
| 2 | 4765 | - 0.231 | - 0.491 | - 1.317 |
| 5 | 6307 | - 0.161 | - 0.342 | - 2.028 |
| 6 | 7662 | - 0.223 | - 0.461 | - 1.736 |

REFERENCES

Chapter 1

- [1] Karl, S.,
Leichtzuschlag-Schaumbeton als Konstruktionsleichtbeton mit abgeminderter Rohdichte, Thesis TH Darmstadt, 1979
- [2] Jaegermann, C.H., Karl, S., Weigler, H.,
Konstruktionsleichtbeton mit abgeminderter Rohdichte - Möglichkeiten und Eigenschaften, Betonwerk und Fertigteil-Technik, no. 11, 1976.
- [3] Weigler, H., Karl, S., Jaegermann, C.,
Leichtzuschlag-Beton mit hohem Gehalt an Mortelporen, Deutscher Ausschuss für Stahlbeton, no. 321, 1981.
- [4] Shendy-El-Barbary, M.E.,
The properties of concrete sandwich beams with polystyrene concrete cores, Thesis University of Durham, 1981.
- [5] Jungbluth, O.,
Verbund und Sandwichtragwerke, Springer-Verlag, 1986.
- [6] Zerjeski, B.,
Zum Tragverhalten von Stahlprofilblech Verbundplatten mit anorganischen Schichtwerkstoffen unter Berücksichtigung ihrer bauphysikalischen Eigenschaften, Thesis TH Darmstadt, 1981.
- [7] Delsing, E.J.F.,
Sandwich elements of steel and aluminium for use in building, Technical University Eindhoven, report BKO-KO-88.001, 1988.

Chapter 2

- [1] Habip, L.M.,
A survey of modern developments in the analysis of sandwich structures, Applied Mechanics Review, vol. 18, no. 2, 1965.
- [2] Plantema, F.J.,
Sandwich Construction, J. Wiley and Sons, New York/London/Sydney, 1966
- [3] Allen, H.G.,
Analysis and design of structural sandwich panels, Pergamon Press Ltd., 1969
- [4] Hartsock, J.A.,
Design of foamed-filled structures, Technomic Publishing Co., Stanford, Conn., 1969
- [5] Stamm, K., Witte, H.,
Sandwichkonstruktionen - Berechnung, Fertigung, Ausführung, Springer-Verlag, 1974
- [6] Dundrova, V.
Biegungstheorie der Sandwich-platten, Academia Prag, 1970

- [7] Wiedeman, J.M.
Leichtbau band 1: Elementen, Berlin, 1986
- [8] Drysdale, R.G., Betancourt-Angel, F., Haddad, B.,
Thick skin sandwich beam columns with weak cores,
Journal of the Struct. Div., Vol.105, No. ST12, 1979, pp. 2601-2619
- [9] Sharma, S.R. and Rao, D.K.,
Static deflections and stresses in sandwich beams under various
boundary conditions, Journal mechanical engineering science, Vol. 24,
No. 1, 1982, pp. 11-20.
- [10] Berner, K.,
Stahl/Polyurethan-Sandwichtragwerke unter Temperatur und
Brandbeanspruchung, Thesis, Technische Hochschule Darmstadt, 1978.
- [11] Linke, K.P.,
Zum Tragverhalten von Profilsandwichplatten mit Stahldeckschichten
und einem Polyurethan-Hartschaum-Kern bei kurz- und langzeitiger
Belastung, Thesis, TH Darmstadt, 1978.
- [12] Vogel, W.,
Verbundflachertragwerke mit anorganischen Deck- und Kernschichten,
Thesis, TH Darmstadt, 1983.
- [13] Bergfelder, J.,
Näherungsverfahren zur Berechnung allgemeiner zusammengesetzter
hölzerner Biegeträger mit elastischem Verbund, Der Bauingenieur
Vol. 49, No. 9, 1974 pp. 350-357.
- [14] Jungbluth, O.,
Verbund- und Sandwichtragwerke, Springer Verlag, 1986.
- [15] Blaauwendraad, J., de Groot, A.K.,
Progress in research on reinforced concrete plane frames,
Heron, vol. 28, no. 2, 1983.
- [16] Davies, J.M.,
The analysis of sandwich panels with profiled faces, proceedings
eight international conference on cold-formed steel structures, 1986,
pp. 351-369.
- [17] Sharifi, P.,
Nonlinear analysis of sandwich structures, Thesis University of
California, 1970
- [18] Kraus, H.D.,
Eine finite Elementen Methode zur Berechnung Sandwichballen und
orthotropen Sandwichplatten unter Berücksichtigung der
Eigenbiegesteifigkeit der Deckhaute, Thesis TU, München, 1974
- [19] Monforton, G.,
Stiffness matrix for sandwich beams with thick anisotropic
laminated faces, Computer and Structures, Vol. 10 , no. 10, 1979,
pp. 547-551.

- [20] Al-Querra
Finite deflections of sandwich beams and plates by finite element method, *Journal of Engineering Mechanics*, Vol. 115, No. 6, 1989, pp. 1318 - 1335.
- [21] Hussein, R.M.
Composite panels/plates: Analysis and Design, Technomic Publishing, 1986.

Chapter 3

- [1] Noakowski, P.,
Verbundorientierte, kontinuierliche Theorie zur Ermittlung de Rißbreite, *Beton und Stahlbetonbau*, No.7/1985, pp. 185-190, No. 8/1985, pp.215-221.
- [2] König, G., Fehling, E.,
Zur Rißbreitenbeschränkung im Stahlbetonbau, *Beton und Stahlbetonbau*, Vol. 83, No.6/1988, pp. 161-167, Vol. 83, No.7/1988, pp. 199-204.
- [3] Somayaji, S., Shah, S.P.,
Bond stress versus slip relationship and cracking response of tension members, *ACI Journal*, Proceedings Vol. 78, No. 3, May-June 1981, pp. 206-216.
- [4] Shungsheng Yang, Jiakui Chen,
Bond slip and crack width calculations of tension members, *ACI Struc. Journal*, No. 4, July-August 1988, pp. 414-422.
- [5] Rizkalla, S.H., Hwang, L.S.,
Crack prediction for members in uniaxial tension, *ACI Journal*, No. 6, Nov.-Dec. 1988, pp. 572-579
- [6] Hartl, G.,
Die Arbeitslinie Eingebetteter Stähle unter Erst- und Kurzzeitbelastung, *Beton und Stahlbetonbau*, Vol. 78, No. 8, 1983, pp. 221-224.
- [7] Tassios, T.P., Yannopoulos, P.J.,
Analytical studies on reinforced concrete members under cyclic loading based on bond-slip relationships, *ACI Journal*, No. 3, May-June 1981, pp. 206-216.
- [8] Lee, S.L., Mansur, M.A., Tan, K.H., Kasiraju, K.,
Cracking behaviour of concrete tension members reinforced with welded wire fabric, *ACI Struc. Journal*, No. 6, Nov.-Dec. 1987, pp. 481-491.
- [9] Beeby, A.W.,
The prediction of crack widths in hardened concrete, *Struc. Eng.*, Vol. 57A, No. 1, 1979, pp. 9-17.
- [10] Braam, C.R.,
The cracking behaviour of reinforced concrete structures, *Annual-Report Progress in concrete research*, Delft University of Technology, V. 1, 1990, pp. 1-17.

- [11] Bruggeling, A.S.G.,
Structural concrete: Science into practice, Heron, V. 32, No. 2,
1987, pp. 1-67.
- [12] Martin, H.,
Zusammenhang zwischen Oberflächenbeschaffenheit, Verbund und
Sprengwirkung von Bewehrungsstählen unter Kurzzeitbelastung,
Deutscher Ausschuss für Stahlbeton, No. 228, 1973, pp. 1-50.
- [13] Noakowski, P.,
Die Bewehrung von Stahlbetonbauteilen bei Zwangbeanspruchung
infolge Temperatur, Deutscher Ausschuss für Stahlbeton, No. 296,
1978, pp. 144.
- [14] Rehm, G.,
Über die Grundlagen des Verbundes zwischen Stahl und Beton,
Deutscher Ausschuss für Stahlbeton, No. 138, 1961.
- [15] Hamelink, S.A.,
Ontwikkeling van een trekstaaf-analogie. Report BKO-KO-89.17,
Eindhoven University of Technology, 1989
- [16] Martin, H.,
Zusammenhang zwischen Oberflächenbeschaffenheit, Verbund und
Springwirkung von Bewehrungsstählen unter Kurzzeitbelastung, DA/St
228, 1973.
- [17] Schiessl, P.,
Beschränkung der Rißbreiten bei Zwangbeanspruchung, Betonwerk und
Fertigteil-Technik, Vol. 42, No. 6, 1976, pp. 269-274
- [18] Noakowski, P.,
Die Bewehrung von Stahlbetonbauteilen bei Zwangbeanspruchung
infolge Temperatur, Deutsche Ausschuss für Stahlbeton, Vol. 296,
1978

Chapter 4

- [1] Hartsock, J.A.,
Design of foamed-filled structures, Technomic Publishing Co., 1969.
- [2] Ploos van Amstel, H.,
Mechanisch gedrag van sandwichpanelen, Bouwwereld, Vol. 83, No.
12, 1987, pp. 37-39 (in Dutch)
- [3] Wölfel, E.,
Nachgiebiger Verbund: Eine Näherungslösung und deren
Anwendungsmöglichkeiten, Stahlbau, Vol. 56, No. 6, 1987, pp. 173-180.
- [4] O'Dell, W.W., Graham, P.L.,
Structural behaviour of sandwich panels with foamed-plastics cores,
proceedings, Plastics in building structures, Bradley and Sons, 1966,
pp. 221-231.
- [5] Hummel, R.L.,
Structural building panels with expanded polystyrene cores, Plastics
in building structures, proceedings, Bradley and Sons, 1966, pp.
243-252.

- [6] Chung-Gon Kim, Chang-Sun Hong,
Visco elastic sandwich plates with cross ply faces, Journal of the
Str. Eng., Vol. 114, No. 1, 1988, pp. 150-164.
- [7] Stamm, K., Witte, H.,
Sandwichkonstruktionen - Berechnung, Fertigung, Masföhrung, Springer
Verlag, 1974.
- [8] Stamm, K.,
Sandwichelemente mit metallischen Deckschichten als Dachbauteile
im Bauwesen, Stahlbau, Vol. 53, No. 8, 1984, pp. 231-236.
- [9] Zerjeski, B.,
Zum Tragverhalten von Stahlprofilblech Verbundplatten mit
anorganischen Schichtwerkstoffen unter Berücksichtigung ihrer
Bauphysikalischen Eigenschaften, Thesis, TH-Darmstadt, 1981.
- [10] Vogel, W.,
Verbundflächentragwerke mit anorganischen Deck- und Kernschichten,
Thesis, TH-Darmstadt, 1983.
- [11] Lee, S.L., Mansur, M.A., Paramasirrom, P., Ong, K.C.G., Tan, C.T.,
A study of sandwich wall panels, Journal of Ferrocement, V.16,
No.3, 1986, pp. 295-313.
- [12] Linke, K.P.,
Zum Tragverhalten von Profilsandwichplatten mit Stahldeckschichten
und einem Polyurethan - Hartschaum - Kern bei kurz- und
langzeitiger Belastung, Thesis, TH-Darmstadt, 1978.
- [13] Burkhardt, S.,
Zeitabhängige Verformungen von Sandwichelementen, Bauingenieur,
V.64, No. 7, 1989, pp. 327-331.
- [14] Just, M.,
Ergebnisse experimenteller Untersuchungen zum Langzeitverhalten
von PUR - Hartschaumstoff - Stützkernbauteilen und
Schlussfolgerungen für die Anwendung, Ifl. - Mitt. Technische
Universität Dresden, V. 22, No. 3, 1983
- [15] Cartade, R.H., Hamelin, P.,
Sandwich structures with a foamed core - some results on their
viscoelastic behaviour, Proceedings of the IPC/RILEM/IBK
Symposium, June 1981, Elsevier, 1982.
- [16] Ackermann, G.,
Ergebnisse aus Berechnung des Zeitabhängigen Tragverhaltens
dreischichtiger durchlaufender Träger, Wiss. Z. Hochsch. Archit.
Bouwes. Weimar, Vol. 30, No. 5, 1984, pp. 307-311.
- [17] Ackermann, G., Mohand-Said Brenti,
Anwendung der elastisch-viscoelastischen Analogie zur Berechnung
des Zeitabhängigen Tragverhaltens dreischichtiger Träger, Wiss. Z.
Hochsch. Arch. Bouw., Weimar, Vol. 29, No.2, 1983, pp. 179-188.
- [18] Ackermann, G.,
Zum zeitabhängigen Tragverhalten dreischichtiger Träger unter Quer-
und Längsbelastung, Bauplanung, Bautechnik, Vol. 39, No. 7, 1985,
pp. 319-324.

- [19] Ackermann, G.,
Des zeitabhängige Tragverhalten von dreischichtigen Trägern mit
Querbelastung und Längsdruckkräften nach der Theorie II. Ordnung,
Wiss. Zeitsch. Hochsch. Archit. Bouw. Weimar, Vol.30, No.4, 1984,
pp. 234-243.
- [20] Hausdörfer, C.,
Aufstellung eines Rechenprogramma zur zeitabhängigen Berechnung
von dreischichtigen Zweifeldträgern, Diplomarbeit Hochsch. Arch.
Bouw. Weimar, 1982.
- [21] Branti, M.S.,
Untersuchungen zum zeitabhängigen Tragverhalten von dreischichtigen
Konstruktionen mit dünnen, ebenen Deckschichten, Diplomarbeit
Hochsch. Arch. Bouw. Weimar, 1980.
- [22] Vianen, H.P.C.A., Salet, T.A.M.,
Handleiding voor het programmapakket SANDI, BKO-KO-90.06,
University of Eindhoven (in Dutch), 1990.
- [23] Neville, A.M.,
Creep of concrete: plain, reinforced and prestressed; North Holland
Publ. Co., Amsterdam 1970.
- [24] Neville, A.M., Dilger, W.H. and Brooksm J.J.,
Creep of plain and structural concrete, Construction Press, 1983,
361 pp.
- [25] Gilbert, R.I.,
Time effects in concrete structures, Elsevier, 1988, 321 pp.
- [26] Rüsçh, H., Jungwirth, D. and Hilsdorf, H.K.,
Creep and Shrinkage (Their effect on the behaviour of concrete
structures), Springer-Verlag, 1983.
- [27] Smërda, Z., Kristek, V.,
Creep and shrinkage of concrete elements and structures, Elsevier,
1988, pp. 296.
- [28] McHenry, D.,
A new aspect of creep in concrete and its application to design,
Proc. ASTM, Vol. 43, 1943, pp. 1069-1084.
- [29] Faber, O.,
Plastic yield, shrinkage and other problems of concrete and their
effects on design, Minutes of Proc. of the Inst. of civil eng., Vol.
225, part 1, London 1927, pp. 27-73.
- [30] Whitney, C.S.,
Plain and reinforced concrete arches, ACI-journal, Vol. 28, 1932, pp.
479-519.

Chapter 6

- [1] CUR-report no. 86-3, Literatuurstudie schuimbeton, 1986 (in Dutch)
- [2] Hermann, V., Schubert, P. and Wesche, K.,
Korrosions- und Verformungsversuche an Hostaporbeton,
Betonsteinwerk und Fertigteile-Technik, no. 2, 1975
- [3] Thiede, H.,
Die Druck und Biegezug-festigkeit von glasfaserverstärktem
Schaumbeton, Thesis TU Berlin, 1978
- [4] Thiede, H.,
Glasfaserverstärkter Schaumbeton, Beton, no. 12, 1979
- [5] Untersuchungsbericht B 446
Schaumbeton, Forschungsinstitut des Vereins der Österreichischen
Zementfabrikanten, Wien, Juni 1981
- [6] Untersuchungsbericht B 446/1
Festigkeit und Schwinden von Schaumbeton, Forschungsinstitut des
Vereins der Österreichischen Zementfabrikanten, Wien, Mai 1982
- [8] Taylor, W.H.,
The production, properties and uses of foamed concrete, Precast
Concrete, no. 2, 1974.
- [9] Valore, R.C.,
Insulating concretes, Journal of the American Concrete Institute, no.
11, 1956
- [10] Bastgen, K., Wesche, K.,
Kürzzeitverhalten von extrem leichten Betonen, Druckfestigkeit und
Formänderungen, Deutscher Ausschuss für Stahlbeton, no. 314, 1980
- [11] Schuimbeton, Betoniek no. 5/26, June 1982, (in Dutch).
- [12] Hordijk, D.A., Salet, T.A.M.
Experimental investigation into the tensile properties of a foamed
concrete, report 25.5-89-03/VFA, Delft University of Technology,
1989.
- [13] Mier, J.G.M. van,
Strain-softening of concrete under multiaxial loading conditions,
thesis TUE, 1984.

Chapter 7

- [1] Jungbluth, O.,
Verbund- und Sandwichtragwerke,
Springer-Verlag, 1986
- [2] Lee, S.L., Mansur, M.A., Paramasivam, P., Ong, K.C.G. and Tam,
C.T.,
Study of sandwich wall panels,
Journal of Ferr. Cement, Vol. 16, no. 3, 1986

- [3] Pathan, I.A.,
Flexural behaviour of lightweight sandwich panels of glass fibre reinforced high alumina cement skins and polystyrene core,
Mehran Univ. Res. J. Eng. Technol, vol. 1, no. 2, april 1982, pp. 9-15
- [4] Pfeifer, D.W., Hanson J.A.,
Precast concrete wall panels: flexural stiffness of sandwich panels,
Precast wall panels, symposium, publication SP-11,
American concrete institute, Detroit, Mich., 1965, pp. 67-86
- [5] Shendy-El-Barbary, M.E.,
The properties of concrete sandwich beams with polystyrene concrete cores,
Thesis department of Engineering, University of Durham, 1981
- [6] Vogel, W.,
Verbundflächentragwerke mit anorganischen Deck- und Kernschichten,
Thesis TH Darmstadt, 1983
- [7] Wright, C.,
The properties of expanded steel reinforced sandwich beams,
Honours degree project report presented to the department of Engineering, University of Durham, 1977
- [8] Zerjeski, B.,
Zum Tragverhalten von Stahlprofilblech Verbundplatten mit anorganischen Schichtwerkstoffen unter Berücksichtigung ihrer Bauphysikalischen Eigenschaften. Thesis, TH Darmstadt, 1982
- [9] Annamalai, G., Parameswaran, V.S. and Shanmugasundaram, J.,
Flexural behaviour of ferrocement-celcrete sandwich panels, Indian concrete journal, Vol. 51, no. 7, 1977, pp. 206-211
- [10] Saglam, B.,
The properties of fibre reinforced cement based sandwich beams,
Thesis University of Durham, 1979
- [11] Parton, G.M. and Shendy-El-Barbary, M.E.
Polystyrene concrete sandwich beams: stiffness and ultimate load analysis, International journal of composites and lightweight concrete, Vol. 4, no. 4, 1982, pp. 199-208

Chapter 8

- [1] Salet, T.A.M.,
De mechanische eigenschappen van kunststofschuimen (Een oriënterende literatuurstudie), Eindhoven, University of Technology, BKO-KO-88.07, 1988. (in Dutch).
- [2] Vianen, H.P.C.A., Salet, T.A.M.,
Handleiding bij het rekenprogramma SANDI (SANDwich Displacements), Eindhoven University of Technology, BKO-KO-90.06, 1990 (in Dutch).

SAMENVATTING

Een sandwich element is een samengestelde constructie waarvan de doorsnede is opgebouwd uit twee stijve huidplaten die onderling zijn verbonden door een slappe kern van isolatiemateriaal. Een sandwich wordt gekenmerkt door de bijzondere combinatie van een laag eigen gewicht en een hoge stijfheid, tesamen met een goede thermische isolatie. In konstruktieve zin wordt het buigend moment door de stijve huidplaten en de dwarskracht door de relatief slappe kern opgenomen. De dwarskracht opname door de kern gaat, gezien de geringe stijfheid van de gebruikelijke isolatie materialen, gepaard met dwarskracht vervormingen. Hierdoor blijft de doorsnede van een sandwich element niet meer vlak en is de stelling van Bernouilli derhalve niet meer toepasbaar.

In deze studie worden de voordelen van sandwich elementen gecombineerd met de specifieke voordelen van beton constructies door de ontwikkeling van een volledig cement-gebonden sandwich element. Doel van het onderzoek is het beschrijven van het konstruktieve gedrag van sandwich elementen met gewapend betonnen huidplaten en een schuimbeton kern onder zowel een korteduur- als een permanente belasting.

Schuimbeton is een extreem licht beton vervaardigd uit cement, water, zand en een schuimmiddel. Schuimbeton verhardt, in tegenstelling tot gasbeton, onder normale atmosferische omstandigheden. In vergelijking tot grindbeton ($\rho = 2400 \text{ kg/m}^3$) kan de volumieke massa, afhankelijk van de toegepaste hoeveelheid schuim, tot ongeveer 400 kg/m^3 worden teruggebracht. De afname van de volumieke massa komt enerzijds ten goede aan de thermische isolatie waarde maar gaat anderzijds ten koste van de konstruktieve eigenschappen.

Het onderzoek beschreven in deze dissertatie beperkt zich tot het gedrag van liggers over twee steunpunten met een statische en symmetrische belasting. Belasting in de richting van de overspanning en instabiliteit zijn niet beschouwd.

Bij het konstruktieve gedrag van de betonnen sandwich elementen speelt, naast de genoemde dwarskracht vervorming, een aantal aspecten een rol waarmee in de 'klassieke' sandwich theorie geen of in onvoldoende mate rekening wordt gehouden. Deze aspecten zijn:

- (i) de buigstijfheid van de kern;
- (ii) fysisch niet-lineair gedrag, inclusief scheurvorming;
- (iii) krimp en kruip van de huid en de kern, inclusief kruip van de kern onder permanente schuiflast.

Na een inleiding en een toelichting op de gemaakte keuze in hoofdstuk 1, wordt in de hoofdstukken 2 tot en met 5 een computer programma beschreven, waarmee last-vervormings relaties en tijd-vervormings relaties van sandwich elementen bepaald kunnen worden. Het 'special purpose' programma is geschikt voor een pc-omgeving.

In hoofdstuk 2 worden gegeneraliseerde differentiaal vergelijkingen opgesteld, waarmee naast de schuifstijfheid ook de buigstijfheid van de kern in rekening kan worden gebracht. De differentiaal vergelijkingen worden numeriek opgelost met de eindige differentie methode.

Fysische niet-lineariteit, waaronder ook een niet-lineaire τ - γ relatie voor de kern, wordt in hoofdstuk 3 in rekening gebracht met een iteratief algoritme (successieve substitutie) gebaseerd op de secant-modulus. Aangezien met de eindige differentie analyse geen discrete scheuren kunnen worden beschouwd, is scheurvorming in rekening gebracht met een uitgesmeerd concept. De toepassing van het uitgesmeerde concept is met een afzonderlijke discrete scheur analyse, voor een gewapend betonnen staaf onder een niet uniform verdeelde trek belasting, onderbouwd. In het vierde hoofdstuk is het model uitgebreid met de tijdsafhankelijke invloedsgrootheden krimp en kruip, zonder dat de differentiaalvergelijkingen hiervoor zijn aangepast. Hierdoor wordt een zo groot mogelijke vrijheid voor het invoeren van krimp en kruip relaties gewaarborgd. Het model waarmee krimp en kruip in rekening worden gebracht is gebaseerd op de relaxatiemethode, waarbij optredende initiële vervormingen worden gecompenseerd door vasthoudkrachten. Hierbij wordt gebruik gemaakt van het superpositie beginsel van McHenry. Door middel van een 'step-by-step' analyse wordt rekening gehouden met de spannings historie als gevolg van optredende herverdelingen. Het numerieke model wordt in hoofdstuk 5 afgesloten met een bespreking van de mogelijke bezwijkvormen van de sandwich.

De toepassing van het numerieke model op de betonnen sandwich elementen is geverifieerd met experimenteel onderzoek dat wordt beschreven in de hoofdstukken 6 en 7.

In hoofdstuk 6 wordt het onderzoek naar de eigenschappen van de toegepaste materialen beschreven. Bijzondere aandacht is hierbij besteed aan de eigenschappen van het schuimbeton ($\rho = 600 \text{ kg/m}^3$) onder zowel korteduur- als langeduur schuifbelasting. Hiervoor zijn torsieproeven ontwikkeld.

Korteduur en langeduur proeven op de sandwich elementen samengesteld uit gewapend betonnen huidplaten en een schuimbeton kern zijn beschreven in hoofdstuk 7. Zowel elementen met als zonder een additionele dwarskracht wapening zijn onderzocht. De proeven tonen aan dat er daadwerkelijk sprake is van een goede samenwerking, resulterend in een sterk en stijf element. Uit de vergelijking van de proefresultaten met de resultaten van de numerieke berekening blijkt een goede overeenkomst.

In hoofdstuk 8 is met het computerprogramma, aan de hand van een voorbeeld, de gevoeligheid van de sandwich elementen voor variaties in de wapening en de kwaliteit van het schuimbeton onderzocht.

In hoofdstuk 9 worden de conclusies, die per hoofdstuk zijn gegeven, samengevat.

CURRICULUM VITAE

- 1962 Geboren in Nijmegen op 8 juni en opgegroeid in
Ravenstein (vanaf 11 juni)
- 1974 - 1980 VWO-B aan het Maasland College in Oss
- 1980 - 1986 Studie Bouwkunde aan de Technische Universiteit Eindhoven
- 1984 - 1985 Student-lid van de faculteitsraad Bouwkunde
- 1986 - 1990 Wetenschappelijk assistent bij de vakgroep Konstruktief
Ontwerpen, Faculteit Bouwkunde, aan de Technische
Universiteit Eindhoven
- 1989 - Junior-lid van de studievereniging voorgespannen beton
(STUVO)

STELLINGEN

behorende bij het proefschrift

STRUCTURAL ANALYSIS OF SANDWICH BEAMS COMPOSED OF REINFORCED CONCRETE FACES AND A FOAMED CONCRETE CORE

1. Betonnen sandwich elementen met een schuimbeton kern kunnen door de gunstige verhouding tussen het eigen gewicht en de stijfheid een aantrekkelijk alternatief bieden voor de gangbare betonelementen bij toepassing in hoge gebouwen.
2. Toepassing van dwarskracht wapening leidt als gevolg van kruip van de kern onder een voortdurende belasting op afschuiving, tot een geleidelijke afname van de konstruktieve functie van het schuimbeton.
- Dit proefschrift, hoofdstuk 7.
3. Indien bezwijken op slijp in het grensvlak tussen de kern en de huid wordt voorkomen zijn de konstruktieve prestaties van de sandwich elementen, samengesteld uit gewapend betonnen huidplaten en een schuimbeton kern, voor het korteduur gedrag praktisch gelijk en voor het langeduur gedrag bij goede benadering gelijk aan die van volledig betonnen elementen. Bezwijken op slijp kan worden voorkomen door de combinatie van een laag wapenings percentage en een relatief grote treksterkte of door toepassing van een dwarskracht wapening.
- Dit proefschrift, hoofdstuk 8.
4. Toepassing van fictieve spannings- ϵ relaties voor het in rekening brengen van de tension stiffening die zijn gebaseerd op het model van een gelijkmatig verdeelde trek langs een gewapend betonnen staaf, leiden tot overschatting van de stijfheid van gewapend betonkonstrukties onder een gelijkmatig verdeelde belasting.
- Dit proefschrift, hoofdstuk 3.
5. De invloeden van krimp en kruip op het gedrag van de sandwich elementen met betonnen huidplaten en een schuimbeton kern, kunnen op een inzichtelijke wijze met behulp van het in dit proefschrift beschreven model in rekening worden gebracht.
- Dit proefschrift, hoofdstuk 4.

6. Zolang de krimp en kruip eigenschappen van beton over de volledige hoogte van de konstruktie gelijk worden gesteld en derhalve geen rekening wordt gehouden met de aanwezige vochtgradient, dienen nauwkeurige berekeningen en beschouwingen over krimp en kruip grootheden met de nodige scepsis te worden beschouwd.
7. De krimp en kruip van een schuimbeton kern ingesloten door twee dunne betonnen huidplaten wordt niet verhinderd, wel vertraagd.
- Dit proefschrift, hoofdstuk 7.
8. De kwaliteit van de hechting tussen beton en schuimbeton is afhankelijk van de gekozen produktiemethode.
- Dit proefschrift, hoofdstuk 7.
9. De term 'skating' in de langlaufsport impliceert ten onrechte een overeenkomst in techniek met het schaatsen en dient derhalve slechts als onderscheid op de traditionele diagonaal-pas te worden beschouwd.
10. Een deel van het toegenomen vandalisme en de daaruit voorkomende financiële schade voor de samenleving, kan worden voorkomen door een verhoogde aandacht van de gemeentelijke politiek voor een actief jongerenbeleid.
11. De sterke toename van de wereldbevolking noopt tot de vraag of we niet gebaat zouden zijn bij een vervaging van de idee van individualiteit.
(Vrij naar Oek de Jong, cirkel in het gras)
12. Een van de maatregelen die zouden kunnen bijdragen aan een stimulans voor het reizen per openbaar vervoer (ook voor studenten), is het invoeren van stille coupes in treinen (ook 2e klas).
13. In het verhaal 'brommer op zee' van J.M.A. Biesheuvel wordt helaas ten onrechte gesuggereerd dat bij zorgvuldig gestuurd belasten het draagvermogen van water (oppervlakte spanning) onbegrensd is.